2007

Characterizing the heme binding properties of the iron regulated surface determinant proteins of Staphylococcus aureus

Mark Christopher Pluym
Western University

Characterizing the heme binding properties of the iron regulated surface determinant proteins of *Staphylococcus aureus*

(Spine title: *S. aureus* Isd heme binding properties)

(Thesis format: Integrated-Article)

by

Mark Christopher Pluym

Graduate Program in Chemistry

A thesis submitted in partial fulfillment
of the requirements for the degree of
Master of Science

Faculty of Graduate Studies
The University of Western Ontario
London, Ontario, Canada

THE UNIVERSITY OF WESTERN ONTARIO
FACULTY OF GRADUATE STUDIES

CERTIFICATE OF EXAMINATION

Supervisor	Examiners
Dr. Martin J. Stillman	Dr. Brian H. Shilton
Supervisory Committee	Dr. Richard J. Puddephatt
Dr. Melvyn C. Usselman	Dr. Nathan D. Jones
Dr. Ronald R. Martin	

The thesis by

Mark Christopher Pluym

entitled:

Characterizing the heme binding properties of the iron regulated surface determinant proteins of *Staphylococcus aureus*

is accepted in partial fulfillment of the
requirements for the degree of
Master of Science

Date _____

_____
Chair of the Thesis Examination Board

ABSTRACT

Staphylococcus aureus infection is becoming a widespread threat in both hospitals and communities worldwide, resulting in substantial treatment costs and numerous patient deaths. Bacterial survival is largely dependant on the organism's ability to scavenge iron from a host via specialized pathways. The recently identified cell wall- and membrane-associated Iron regulated surface determinant (Isd) proteins are one such pathway. They serve to transport iron-containing heme, from hemoglobin, from the environment into the bacterial cell for nourishment. To date very little is known about the heme binding properties of these proteins and the overall Isd heme scavenging mechanism.

Through the use of UV-visible absorption and magnetic circular dichroism spectroscopies, mass spectrometry, and mutational analysis, the heme-binding properties of IsdA, IsdC, and IsdE have been characterized. Recombinant IsdA (rIsdA) was found to bind a single high-spin ferric heme, coordinated by tyrosine 166 of the IsdA near abc transporter (NEAT) domain. Recombinant IsdC (rIsdC) was purified bound primarily to protoporphyrin IX, with traces of high-spin ferric heme and an unidentified ligand of approximately 320 Da. Recombinant IsdE (rIsdE) was purified bound to two heme molecules and an unidentified ligand of approximately 320 Da. One heme is ferric and is bound near the edge of a heme binding pocket through the imidazole group of histidine 229. The other is low-spin ferrous and is inaccessible to small ligands. The ferrous heme binding amino acid residue(s) remain unknown but it appears to be bound deep within the heme binding pocket of rIsdE.

Key words

Iron regulated surface determinants, Gram-positive bacteria, *Staphylococcus aureus,* heme, heme proteins, bacterial iron transport, UV-visible absorption spectroscopy, magnetic circular dichroism spectroscopy, electrospray ionization mass spectrometry, heme-iron spin states, NEAT domain, charge states.

Dedication

This thesis is dedicated to my parents,
whose endless support and guidance have helped me achieve my goals.
I cannot thank you enough.

Acknowlegements

First and foremost I would like to thank my supervisor Dr. Martin Stillman for all his guidance, support, encouragement, allowing me to go to Rome (and World Cup 2006), and for picking up the bar tab once in a while.

I would like to thank Dr. David Heinrichs and Christie Vermeiren for their help and the endless supply of protein. Without their expertise and support none of this would have been possible.

Thanks to NSERC for funding both myself and my research.

Many thanks to:

~ All my London friends and those back home for all the laughs, nights out, and trips over the years.

~ My friends in the chemistry department for all the poker nights, sporting events, and good times at the Grad Club.

~ Dr. John Mack for lending his expertise and assistance to everything from experimental setup to publications.

~ My lab girls: Kelly, Amanda Junior, Dr. Gina (or maybe it was Jayna?), Dr. Maria, Dr. Maureen (now that you're getting paid, where's my stew?), and Mad-Thanh. Good luck to all of you in the future.

~ The departmental technical experts, Warren, John, Jon, Barakat, and Doug, who've kept our equipment running.

~ Dr. Richard Puddephatt for the generous use of his mass spectrometer.

~ Chris Kirby and Kyle Pollard for allowing us to "piggyback" on their helium deliveries.

~ Mary-Lou, Sherry, and Marty in ChemStores for their help over the years.

TABLE OF CONTENTS

List of Tables

List of Figures

List of Abbreviations and Definitions

Abs	Absorption
B band	Heme absorption band appearing between 380 and 430 nm
DNA	Deoxyribonucleic acid
E. coli	*Escherichia coli*
ESI-MS	Electrospray ionization mass spectrometry
F#A	Phenylalanine (number) mutated to alanine
Fe-PPIX	Iron-protoporphyrin IX or heme-*b*
Ferric	3+ oxidation state of iron
Ferrous	2+ oxidation state of iron
FhuD	Ferrichrome uptake protein D
Fur	Ferric uptake repressor
GST	Glutathione S-transferase
H#A	Histidine (number) mutated to alanine
HarA	Haptoglobin receptor A
HOMO	Highest occupied molecular orbital
IsdX	Iron regulated surface determinant protein X
LCAO	Linear combination of atomic orbitals
LUMO	Lowest unoccupied molecular orbital
MALDI	Matrix assisted laser desorption ionization
MCD	Magnetic circular dichroism
MRSA	Methicillin resistant *Staphylococcus aureus*
NAM	N-acetyl-muramine
NAG	N-acetyl-glucosamine
NEAT	NEAr abc Transporter
PBS	Phosphate buffered saline
PPIX	Protoporphyrin IX
PPIX-DME	Protoporphyrin IX dimethyl ester
Q_{00}, Q_{vib}	Heme absorption bands appearing 500 and 600 nm
S. aureus	*Staphylococcus aureus*

ShuA	*Shigella dysenteriae* heme uptake protein A
SrtA	Sortase A
SrtB	Sortase B
TEV	Tobacco etch virus
TOF	Time of flight analyzer
UV	Ultraviolet
Y#A	Tyrosine (number) mutated to alanine

Chapter 1: General introduction

1.1 *Staphylococcus aureus* threat

Staphylococcus aureus (*S. aureus*) is an gram-positive human pathogen (Figure 1.1) that has been implicated in a number of illnesses ranging from moderate, superficial skin lesions to severe, life-threatening infections including pneumonia, meningitis, urinary tract infections, osteomyelitis, and septicemia (*1-3*). It is commonly found in the nose and on the skin of humans and is more prevalent in areas where personal hygiene is suboptimal. *S. aureus* is often referred to as an opportunistic bacterium, due to its pathogenicity when located within an environment rich in resources, such as an open wound. With access to a nourishing blood supply the bacteria can flourish, rapidly leading to serious illness and in many cases death. For the past few decades, *S. aureus* infections, or "Staph" infections, have received much attention due to their role in causing nosocomial infections in hospitals (*4*). The severity has now escalated as community acquired *S. aureus* infections are now commonplace (*5*).

The cause for concern over *S. aureus* infection lies in our inability to combat infection with current antibiotics (*2, 6-9*). In 1943, 15 years after its discovery by Sir Alexander Fleming, penicillin was first introduced to fight bacterial infections. Its

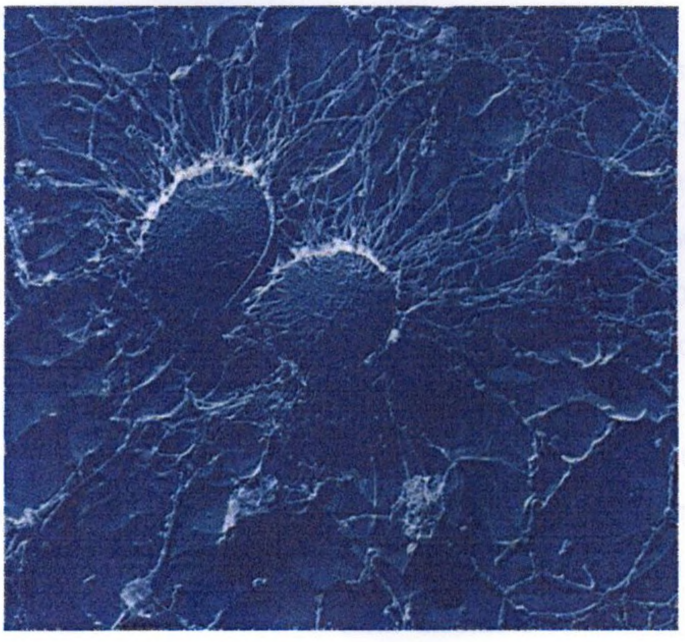

Figure 1.1. Transmission electron micrograph of *S. aureus* cells at 50,000x magnification (*3*).

success was tremendous, however, in 1944 the first reports of penicillin resistant *S. aureus* had already emerged (*6, 9*). Today, nearly all known strains of *S. aureus* are resistant to penicillin. Due to their overuse, particularly in hospitals, the rise in antibiotic resistant bacteria has become a common theme for virtually all antibiotics. Methicillin was first released in North America in 1961 to combat drug resistant bacterial strains, however, reports of methicillin resistant *Staphylococcus aureus* (MRSA) appeared as early as 1968 (*10*). Currently, serious MRSA infections are primarily treated with the glycopeptide antibiotic vancomycin (Vancocin), however, resistance to this drug has also been reported (*11*). Vancomycin resistant *S. aureus* was first reported in the United States in 2002 (*8*). Strict control over the use of vancomycin and other MRSA effective antibiotics has now been implemented, only being used in severe cases where other less-toxic antibiotics are ineffective.

The statistics concerning Canadian society are quite alarming. Upwards of $100 million is spent annually on treating antibiotic resistant *S. aureus* infection and in many cases treatment is unsuccessful, resulting in 8000 Canadian deaths each year (*12*). Similar statistics can be found throughout the world (*13, 14*) and have helped spark a great interest into developing new methods to fight bacterial infections.

1.2 Iron biochemistry

Iron is an essential mineral in nearly all living systems. It plays a major role in vital processes such as energy production, detoxification, and oxygen transport and storage. Iron exists primarily in the +2 (ferrous) and +3 (ferric) oxidation states (*15*). Compounds containing iron in the +4, +5, and +6 oxidations states also exist, but, are quite rare. In living systems, free iron is also extremely scarce due to the low solubility of ferric iron, and the potential for oxidative damage with ferrous iron. In aqueous solution, ferric iron coordinates with water to form $[Fe(H_2O)_6]^{3+}$. Three water molecules then deprotonate, and three are lost, to form insoluble $Fe(OH)_3$ ($K_{sp} = 2.64 \times 10^{-39}$). The smaller positive charge on ferrous iron lowers this deprotonation effect and as a result ferrous iron is quite soluble in aqueous solution at physiological conditions. However, ferrous iron readily undergoes oxidation to form insoluble ferric iron via the Fenton

reaction (shown below) (*16*), resulting in the additional production of hydroxyl radicals, that can damage biological macromolecules.

Fenton reaction: $Fe^{2+} + H_2O_2 \rightarrow Fe^{3+} + OH^- + OH^{\cdot}$

To avoid the problems with solubility and oxidative damage, all of the iron in mammals is sequestered by a variety of molecules (Table 1.1). The vast majority of iron in mammals is bound to protoporphyrin IX (PPIX) to form heme-*b* (Fe-PPIX) (Figure 1.2), a vital cofactor found in proteins such as hemoglobin and myoglobin. A variety of

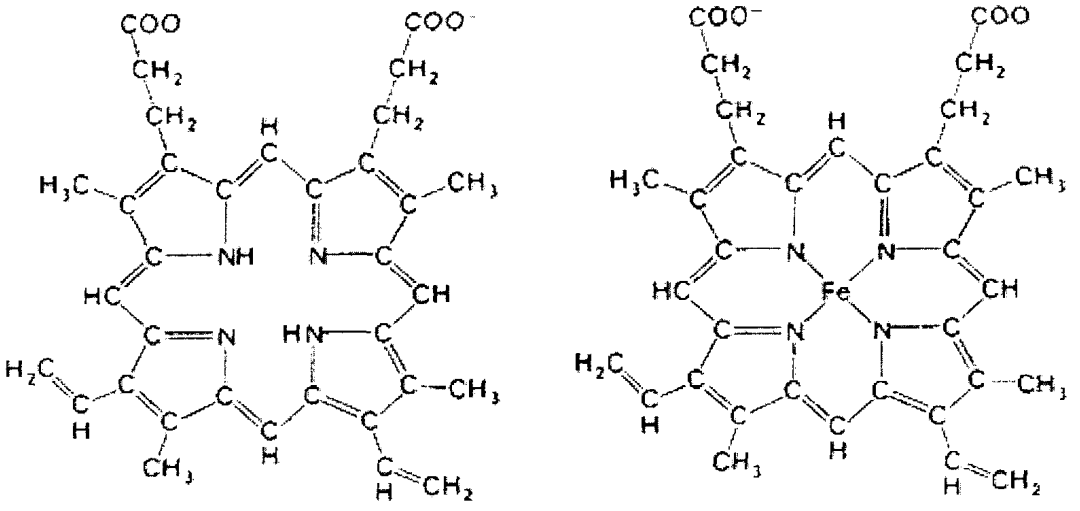

Figure 1.2. Structures of PPIX and heme (Fe-PPIX)

other porphyrins also complex iron to form different heme cofactors (for example heme-*a* in cytochrome c oxidase, heme-*c* in cytochrome c, and heme-*d* in the catalases) (*17*). In mammals, following ingestion and absorption in the intestine, iron is bound by the transport protein transferrin and delivered to tissues in need or to storage sites (*18*). The largest storage site for iron is in the liver, where it is bound by ferritin, an intracellular protein approximately 450 kDa in size. Within the hollow core of ferritin, up to 4500 iron atoms are stored as iron (III) hydroxyphosphate (*18*). Bodily demands dictate the action of ferritin, accepting or releasing iron as required.

Iron sequestration results in a minimal level of free iron in mammalian systems (approximately 10^{-24} M). In addition to the prevention of oxidative damage and precipitation of ferric iron, this also acts as an innate defense mechanism against invading

Table 1.1. List of the major iron containing molecules in mammals and their percentage of the total iron pool.

Iron containing molecules	% of total human iron pool
Heme (hemoglobin)	~ 70 %
Heme (myoglobin)	~ 5 %
Ferritin	~ 25 %
Transferrin	< 1 %
Heme enzymes	< 1 %
Other heme/iron containing molecules	< 1%

pathogens. The lack of free iron hinders pathogenic growth, allowing the host's immune system to destroy infection. However, bacteria have evolved accordingly. Numerous iron acquisition systems have been characterized that utilize a number of the iron containing molecules listed in Table 1.1. One example is the use of siderophores, low molecular weight iron binding molecules (usually 400-1000 Da) that are secreted by bacteria into their extra-cellular environments (*19*). Due to their high affinity for iron, siderophores are capable of removing iron from transferrin. Iron bound siderophores are then transported into the bacterial cytoplasm, via transport proteins, nourishing the cell. Figure 1.3 shows ferri-enterochelin, a siderophore secreted by *E. coli* under low iron conditions. Numerous heme-iron scavenging systems have also been identified, which use heme as the iron source to feed growing bacteria. When referring to heme

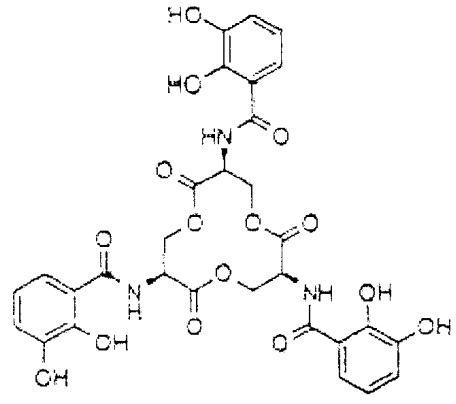

Figure 1.3. Structure of the ferri-enterochelin siderophore of *E. coli*.

scavenging systems, it is assumed that heme-*b* is being scavenged, since hemoglobin and haptoglobin (a serum hemoglobin binding protein (*20*)) are believed to be the primary targets for heme extraction (*21-23*).

1.3 Iron regulated surface determinant protein heme-iron transport system

In 2003, a series of bacterial proteins expressed only under iron limiting conditions were identified in *S. aureus* (Figure 1.4) (*22*). Referred to as the iron regulated surface determinant (Isd) proteins, this system is associated with the cell wall and membrane of *S. aureus* as well as other bacterial species, such as *Listeria monocytogenes* and *Bacillus anthracis*. Controlling the protein expression are regulatory regions found on the bacterial chromosome referred to as ferric uptake repressor (fur) boxes (Figure 1.4B). Under heightened iron concentrations the protein fur binds to these upstream regulatory regions, preventing the transcription of the Isd proteins. This inhibitory mechanism ensures that valuable bacterial resources are not consumed if not required.

Under low iron conditions, fur dissociates from DNA, allowing the synthesis of the Isd proteins. Once translated in the bacterial cytoplasm, each protein is transported to its respective location via signal sequences present within the proteins. IsdA, IsdB, IsdC, and HarA (also referred to as IsdH) are directed to the cell wall, IsdD, IsdE, and IsdF to the cell membrane, and IsdG and IsdI remain in the cytoplasm (*21, 22*). HarA/IsdH and IsdB have been shown to bind hemoglobin, as well as haptoglobin in the case of HarA/IsdH, and are, therefore, believed to interact and possibly extract heme from these sources (*24*). Although hemoglobin and heme concentrations are extremely low in the direct bacterial environment, *S. aureus* is known to secrete hemolysins which act to disrupt the cell membranes of erythrocytes (*25*). The large stock of hemoglobin is then released and is susceptible for uptake by bacterial heme scavenging systems. IsdA has also been shown to bind heme and transferrin as well as act as a multi-adhesion, capable of binding fibronectin, a component of the mammalian extra-cellular matrix (*26*). The adhesion function is believed to aid bacteria in the early stages of infection (*27*). Concealed within the cell wall is IsdC, a covalently anchored protein of unknown function. Based on its location, IsdC has been proposed to function as a heme transfer

protein, accepting heme from the surface proteins IsdA, IsdB, HarA/IsdH, and delivering it to the membrane proteins IsdD, IsdE, and IsdF (*21, 22, 27*). IsdE (a lipoprotein), IsdF (a permease), and IsdD (a predicted membrane protein), have been shown to bind heme and due to their location and homology to other iron transport proteins, are believed to shuttle heme across the cell membrane and into the bacterial cytoplasm (*21, 22*). Once inside the cell, IsdG and IsdI, members of the monooxygenase family of proteins, act to cleave the PPIX ring, releasing the central iron atom (*28*). This scheme illustrates the proposed heme transport mechanism, however, direct evidence to support it is lacking. The functions, structures, heme binding characteristics, and roles in the transport mechanism of each of the Isd proteins remain largely unknown. This thesis will examine the heme binding characteristics of three of the proteins, namely, IsdA, IsdC and IsdE, and will provide insight into the overall Isd heme scavenging mechanism of *S. aureus*.

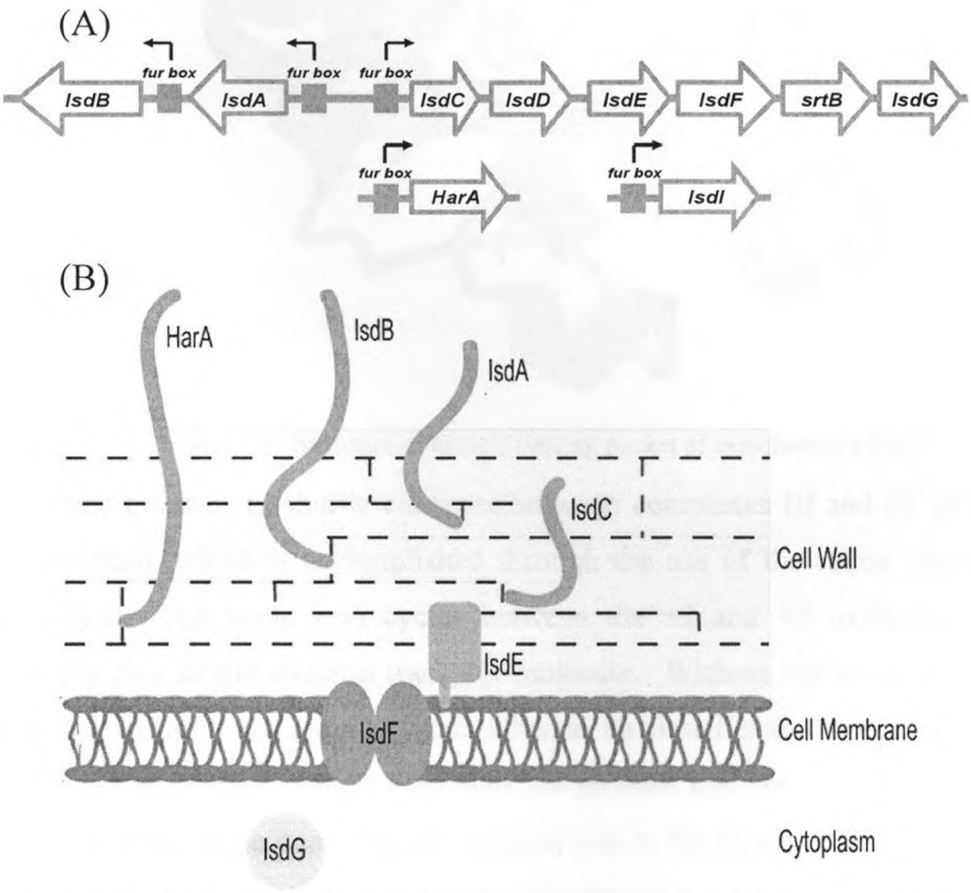

Figure 1.4. Overview of the Isd heme scavenging system of *S. aureus*. (A) Schematic depicting the orientation and organization of the Isd locus in the *S. aureus* chromosome. (B) Schematic representation of the predicted localization of the Isd proteins at the bacterial cell surface.

1.4 Heme proteins and heme binding proteins

It is important to distinguish between heme proteins and heme binding proteins, since the two classifications imply very different functions. A heme protein is a protein containing a heme cofactor, which plays an essential chemical role in the proper functioning of the protein. For example, cytochrome c is a heme protein found in the inner mitochondrial membrane. Heme is bound to the protein through a methionine and a histidine residue, as well as peripherally through two cysteine residues (Figure 1.5) (*29*).

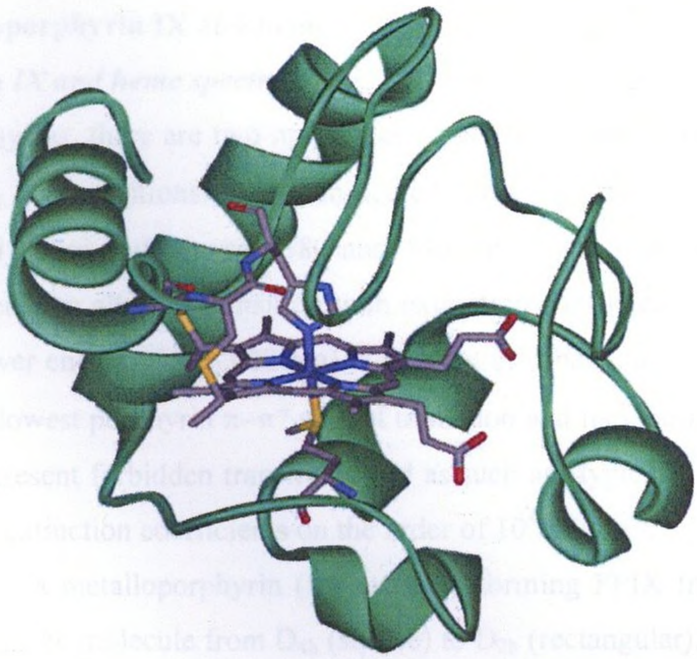

Figure 1.5. Structure of heme c binding pocket of cytochrome c *(29)*.

Cytochrome c serves to shuttle electrons between complexes III and IV of the electron transport chain, which is accomplished through the use of the redox chemistry of the heme group. The heme iron cycles between the +2 and +3 oxidation states, thus, functioning as a single electron transport molecule. Without the heme cofactor present cytochrome c cannot perform its function, hence, its classification as a heme protein.

Conversely, heme binding proteins are proteins that are capable of binding heme molecules but the heme does not play a direct role in the functioning of the protein. For example, hemopexin is a heme binding protein that ensures the level of heme in serum is kept very low (*30*). This helps to prevent the loss of iron from mammalian systems, mainly following the lysis of erythrocytes. In the absence of heme, the proper

functioning of the protein is not affected, simply because its role is to bind heme. Numerous heme binding proteins are associated with bacterial heme scavenging systems that serve to transport heme into the bacterial cell where the central heme-iron atom can be recycled, nourishing the bacterium. An example is the ShuA protein of *Shigella dysenteriae (31),* a receptor protein that transports heme across the bacterial outer cell membrane. The Isd proteins also fall under the category of heme-binding proteins, as their function is to scavenge heme for its iron content.

1.5 Studying protoporphyrin IX and heme

1.5.1 Protoporphyrin IX and heme spectroscopy

In metalloporphyrins, there are two major electronic bands and a strong vibronic band arising from $\pi \rightarrow \pi^*$ transitions of the conjugated 18π e^- system (Figure 1.6). At higher energy (typically observed between 380 and 430 nm) is the very intense B (or Soret) band. It represents an allowed transition with extinction coefficients on the order of 10^5 $M^{-1}cm^{-1}$. At lower energy (500 - 600 nm) is the Q_{00}, or α band, and the Q_{vib}, or β band, arising from the lowest porphyrin π–π^* singlet transition and its vibronic envelope, respectively. They represent forbidden transitions and as such are typically weaker than the B band, possessing extinction coefficients on the order of 10^4 $M^{-1}cm^{-1}$.

Demetallation of a metalloporphyrin (for example forming PPIX from heme-*b*) reduces the symmetry of the molecule from D_{4h} (square) to D_{2h} (rectangular). As a result a splitting of the doubly degenerate Q bands is observed. The Q_{00} band splits into x and y components ($Q_{x,\,00}$ and $Q_{y,\,00}$) as does the Q_{vib} band ($Q_{x,\,vib}$ and $Q_{y,\,vib}$). The result is a visible region absorption spectrum consisting of four peaks (Figure 1.7).

The three metalloporphyrin bands (B, Q_{00} and Q_{vib}) vary considerably in band maximum and relative intensity. These variations are characteristic of the oxidation and spin state of the central iron. Overlaid on the 3 bands are charge transfer transitions between the central metal and the ring, which occur in the same spectral region. Charge transfer transitions are particularly sensitive to the oxidation and spin state of the central iron, being observed at different, but characteristic wavelengths in the visible region for all but the diamagnetic low spin ferrous iron. The combination of π–π^* and charge transfer transitions produces a very complex UV-visible absorption spectrum. In some

instances this leads to a masking of important spectroscopic information. For this reason, magnetic circular dichroism (MCD) spectroscopy has often been utilized in the study of heme-containing proteins (refer to section 2.1.2).

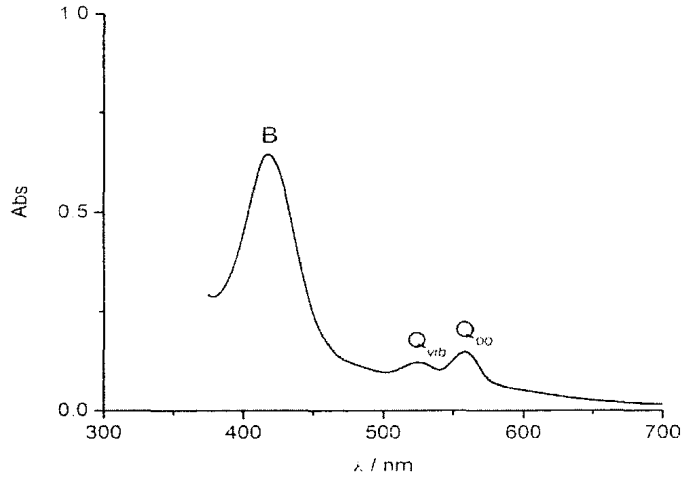

Figure 1.6. UV-visible absorption spectrum of ferrous heme with pyridine axial ligands.

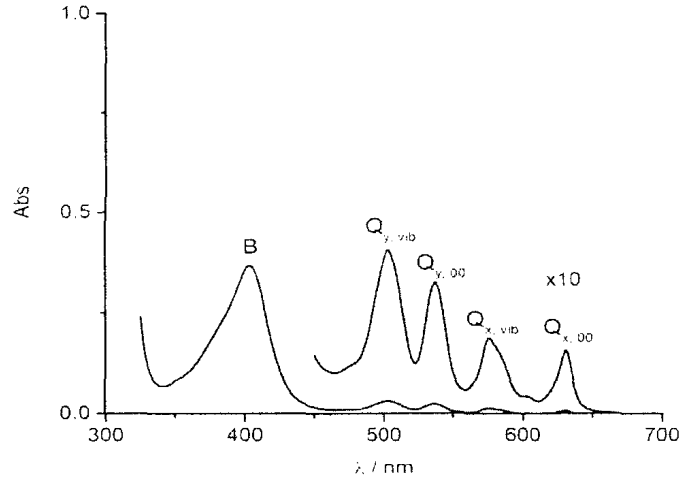

Figure 1.7. UV-visible absorption spectrum of PPIX-dimethyl ester in 2-butanone.

1.5.2 Gouterman's 4-orbital LCAO model

The spectroscopy of porphyrins is conveniently explained using Gouterman's four orbital Linear Combination of Atomic Orbital (LCAO) model. The HOMO to LUMO transitions occur between the states with ± 4 (e_u) to ± 5 (e_g) units of angular momentum (Figure 1.8). These porphyrin orbitals contain 4 and 5 nodes respectively. Transitions

between the HOMO and LUMO gives rise to the B and Q bands previously described. The B band corresponds to a change in angular momentum (ΔM_L) of ± 1 and is an allowed transition and, therefore, very intense. The Q band corresponds to a change in angular momentum of ΔM_L ± 9 and is therefore forbidden. As predicted by Hund's rule, the lower energy state corresponds to ΔM_L ± 9, satisfying the observation that the Q bands are much less intense than the B band.

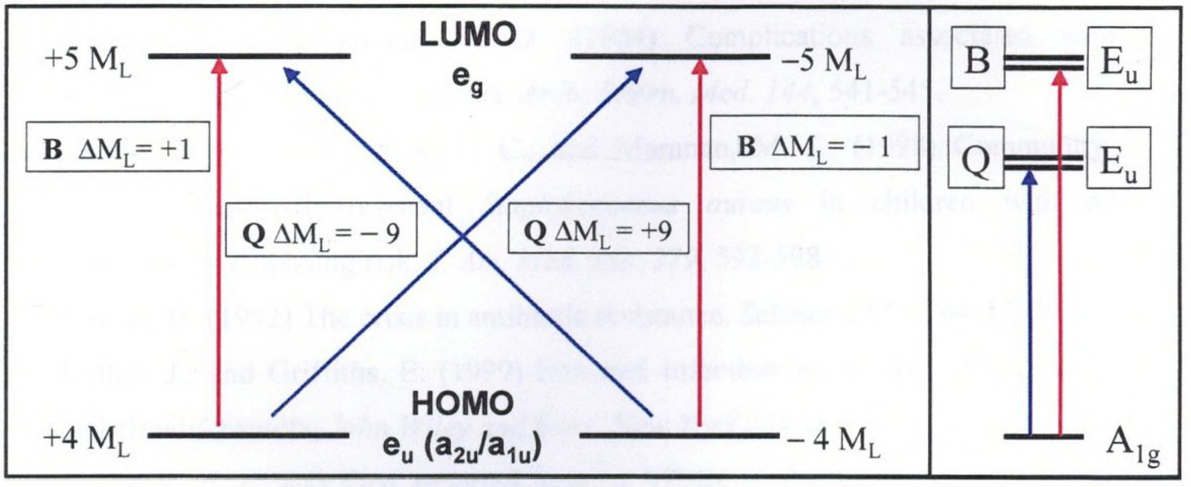

Figure 1.8. Gouterman's 4 orbital LCAO model

1.6 Scope of the thesis

Limiting the availability of iron has been shown to effectively inhibit bacterial growth (*7, 19*). Furthermore, studies inhibiting the Isd heme-scavenging system, through Isd gene knockout, have shown its importance to *S. aureus* cells trying withstand a host's defenses (*21, 22, 32, 33*). This suggests that chemical interruption of the Isd system would be an effective method of fighting *S. aureus* infection. Before this can be accomplished knowledge of the Isd heme-scavenging system is required.

The goals of this research were to explore the heme binding properties of the individual Isd proteins and, in doing so, shed light on the overall heme-scavenging mechanism. Chapter 2 provides the protocols and background into the specialized techniques used to investigate the heme binding properties of the Isd proteins. Chapters 3, 4, and 5 describe heme binding in IsdA, IsdC, and IsdE, respectively. Chapter 6 gives some general conclusions and provides insight into the overall heme scavenging mechanism.

1.7 References

1. Bullen, J. J., Rogers, H. J., Spalding, P. B., and Ward, C. G. (2006) Natural resistance, iron and infection: a challenge for clinical medicine, *J. Med. Microbiol. 55*, 251-258.
2. Tenover, F. C., and Gorwitz, R. J. (2006) Gram-positive pathogens, *ASM Press, Washington, D. C.*, 526-534.
3. (2007) *Staphylococcus aureus*, Wikipedia.
4. Libman, H., and Arbeit, R. D. (1984) Complications associated with *Staphylococcus aureus* bacteremia, *Arch. Intern. Med. 144*, 541-545.
5. Herold, B. C., Immergluck, L. C., and Maranan, M. C. (1998) Community-acquired methicillin-resistant *Staphylococcus aureus* in children with no identified predisposing risk, *J. Am. Med. Ass. 279*, 593-598.
6. Neu, H. C. (1992) The crisis in antibiotic resistance, *Science 257*, 1064-1073.
7. Bullen, J., and Griffiths, E. (1999) Iron and Infection: molecular, physiological and clinical aspects, *John Wiley and Sons, New York 2*, 409-415.
8. Goldrick, B. (2002) First reported case of VRSA in the United States, *Am. J. Nursing 102*, 17.
9. Rice, L. B. (2006) Antimicrobial resistance in gram-positive bacteria, *Am. J. Infec. Cont. 34*, 11-19.
10. Barrett, F. F., McGehee, R. F., and Finland, M. (1968) Methicillin-resistant *Staphylococcus aureus* in US hospitals, *N. Engl. J. Med. 279*, 441-448.
11. Bamberger, D. M., and Boyd, S. E. (2005) Management of *Staphylococcus aureus* infection, *Am. Fam. Phys. 72.*
12. (2005) 'Superbug' infections spiraling in Canadian hospitals, CBC News.
13. Perovic, O., Koornhof, H., Black, V., Moodley, I., Duse, A., and Galpin, J. (2006) *Staphylococcus aureus* bacteraemia at two academic hospitals in Johannesburg, *S. Afr. Med. J. 96*, 714-717.
14. Moet, G. J., Jones, R. N., Biedenbach, D. J., Stilwell, M. G., and Fritsche, T. R. (2007) Contemporary causes of skin and soft tissue infections in North America, Latin America, and Europe, *Diagn. Microbiol. Infect. Dis. 57*, 7-13.

15. Housecroft, C. E., and Sharpe, A. G. (2005) *Inorganic chemistry*, Vol. 2, Pearson Education Limited, Essex, England.

16. Fenton, H. J. H. (1894) Oxidation of tartaric acid in the presence of iron., *J. Chem. Soc. 65*, 899-910.

17. (1999) Haem proteins, *Metalloscripps*.

18. Hinzmann, R. D. (1999) Ferritin and Transferrin: Iron deficiency and overload, *Immunodiagnostics 12*.

19. Sutak, R., Tachezy, J., Camadro, J. M., and Lesuisse, E. (2004) Siderophore and haem iron use by *Tritrichomonas foetus*, *Microbiology 150*, 3979-3987.

20. Wassell, J. (2000) Haptoglobin: function and polymorphism, *Clin. Lab. 46*, 547-552.

21. Skaar, E. P., and Schneewind, O. (2004) Iron-regulated surface determinant (Isd) of *Staphylococcus aureus*: stealing iron from heme, *Microb. Infect. 6*, 390-397.

22. Mazmanian, S. K., Skaar, E. P., Gaspar, A. H., Humayun, M., Gornicki., P., Jelenska, J., Joachmiak, A., Missiakas, D. M., and Schneewind, O. (2003) Passage of heme-iron across the envelope of *Staphylococcus aureus*, *Science 299*, 906-909.

23. Baker, H. M., Anderson, B. F., and Baker, E. N. (2003) Dealing with iron: Common structural principles in proteins that transport iron and heme, *Proc. Nat. Acad. Sci. U.S.A. 100*, 3579-3583.

24. Torres, V. J., Pishchany, G., Humayun, M., Schneewind, O., and Skaar, E. P. (2006) *Staphylococcus aureus* IsdB is a hemoglobin receptor required for heme iron utilization, *J. Bacteriol. 188*, 8421-8429.

25. Wiseman, G. M. (1975) The Hemolysins of *Staphylococcus aureus*, *Am. Soc. Microbiol. 39*, 317-344.

26. Clarke, S. R., Wiltshire, M. D., and Foster, S. J. (2004) IsdA of *Staphylococcus aureus* is a broad spectrum iron-regulated adhesin, *Mol. Microbiol. 51*, 1509-1519.

27. Maresso, A. W., and Schneewind, O. (2006) Iron acquisition and transport in *Staphylococcus aureus*, *Biometals 19*, 193-203.

28. Skaar, E. P., Gaspar, A. H., and Schneewind, O. (2005) *Bacillus anthracis* IsdG, a Heme-Degrading Monooxygenase, *J. Bacteriol. 188*, 1071-1080.

29. (2007) Cytochrome C, Wikipedia.

30. Tolosano, E., and Altruda, F. (2002) Hemopexin: Structure, function and regulation, *DNA Cell Biol. 21*, 297-306.

31. Eakanunkul, S., Lukat-Rodgers, G. S., Sumithran, S., Ghosh, A., Rodgers, K. R., Dawson, J. H., and Wilks, A. (2005) Characterization of the periplasmic heme-binding protein ShuT from the heme uptake system of *Shigella dysenteriae*, *Biochemistry 44*, 13179-13191.

32. Maresso, A. W., Chapa, T. J., and Schneewind, O. (2006) Surface protein IsdC and Sortase B are required for heme-iron scavenging of *Bacillus anthracis*, *J. Bacteriol. 188*, 8145-8152.

33. Mazmanian, S. K., Ton-That, H., Su, K., and Schneewind, O. (2002) An iron-regulated sortase anchors a class of surface protein during *Staphylococcus aureus* pathogenesis, *Proc. Nat. Acad. Sci. U.S.A. 99*, 2293-2298.

Chapter 2: Techniques

2.1 Spectrometric and spectroscopic techniques

2.1.1 Protein mass spectrometry

Mass spectrometry (MS) has become a widely used tool in both academic fields and industry due to its ability to identify, through mass analysis, different components in suitable samples (*2, 3*). The basic principle underlying mass spectrometry is the ability of electric and magnetic fields to influence the trajectory of charged particles within a vacuum. Simple mass spectrometers consist of three main components, an ionization source, an analyzer and a detector. More complicated arrangements can arise if using techniques such as tandem mass spectrometry, which contain a collision cell where sample ions are fragmented. In order to analyze a sample it must first be vaporized at the ionization source. The two most common methods of ionization used in protein mass spectrometry are matrix-assisted laser desorption ionization (MALDI) and electrospray ionization (ESI). Since only ESI data will be reported in this thesis, a brief description of only this technique will be given.

The application of ESI mass spectrometry (ESI-MS) to large biological molecules was initially developed by John B. Fenn, who was awarded the 2002 Nobel Prize in Chemistry for his contributions to this field (*4, 5*). In ESI-MS sample flowing through a capillary is dispersed into very small droplets through the use of high positive or negative voltages applied to the capillary tip (Figure 2.1A). Depending on the polarity of the voltage, droplets with excess positive or negative charge are formed. Evaporation and charge-driven breakup of the droplets eventually leads to desolvated, charged protein molecules (Figure 2.1C) (*2*), which then enter the mass analyzer and are ultimately measured at the detector. One of the most common mass analyzers, and the type used to measure the data presented here, is a time of flight (TOF) analyzer. TOF analyzers use an electric field to move charged sample molecules within the analyzer. The principle is that light, highly charged molecules will travel faster than heavy molecules possessing few charges. Sample ions are timed between a shutter and the detector and a mass to charge ratio (m/z) is measured by the instrument. The m/z ratio is then plotted against the relative intensities of all ions detected to produce a charge state spectrum.

(A)

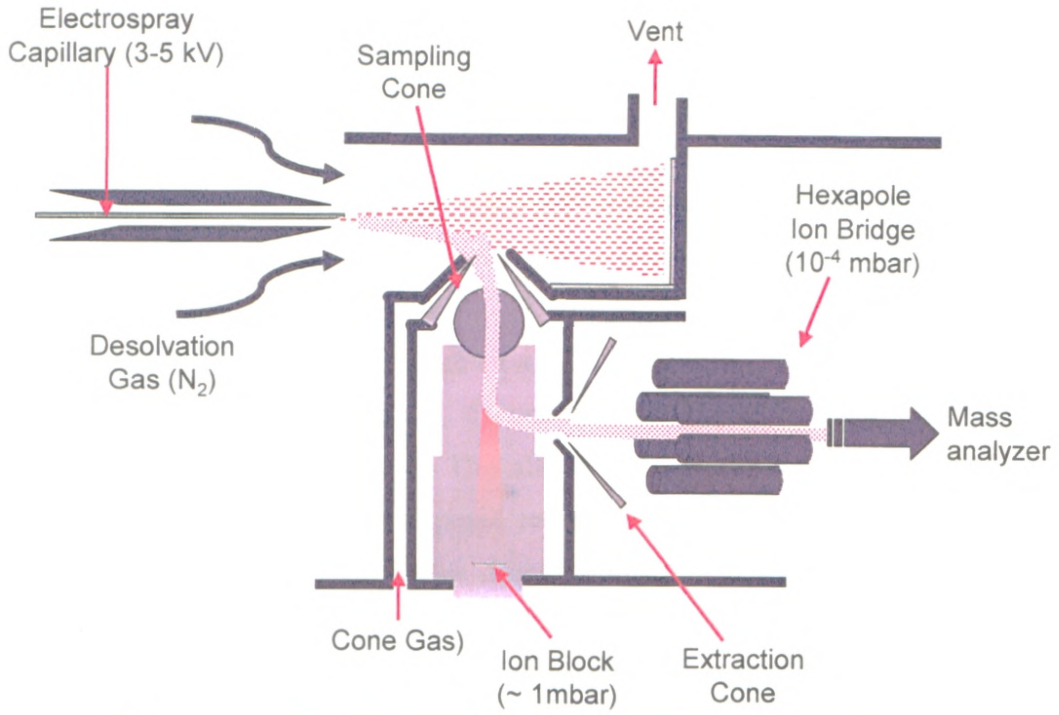

(B)

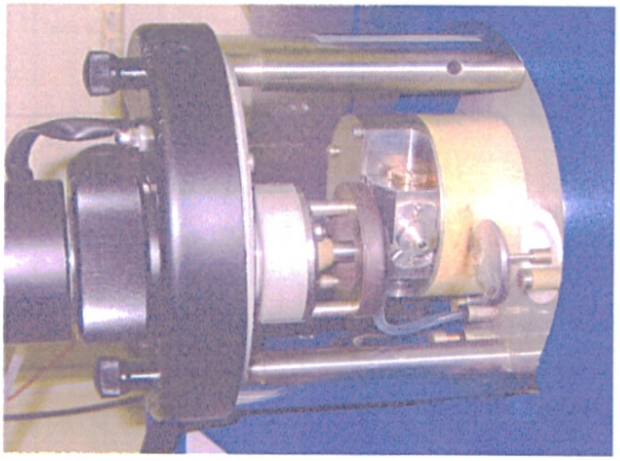

(C)

Figure 2.1. Overview of the ESI process. (A) Schematic diagram of an electrospray ionization source. (B) Photograph of the Micromass LCT-MS ionization source. (C) Charge residue model illustrating the formation of charged, gas phase protein molecules.

Either negatively or positively charged analyte molecules can be produced at the ionization source and be detected by the instrument, depending on the user's selection. All of the spectra presented in this thesis were recorded in positive ion mode, which is the common method for studying proteins. Nucleic acids on the other hand are commonly studied in negative ion mode due to the presence of numerous phosphate groups in a polynucleotide backbone (*2*). In protein mass spectrometry, sample ions arise from the protonation of basic amino acid residues (lysine and arginine) or deprotonation of acidic residues (aspartic acid and glutamic acid). Depending on the number of exposed acidic/basic residues, the amount of charge on a protein molecule can vary, producing a number of charge states (Figure 2.2) (*1, 6*), unlike MALDI which typically produces analyte molecules with a single charge. This allows ESI-MS to be used to monitor the extent of folding of a protein. The exposed residues will be protonated/deprotonated before those residues that are buried in the structure, so that if the structure changes for example, as a function of heme binding or denaturation, then the number of residues exposed will change. Denatured proteins will show higher charge states than the properly

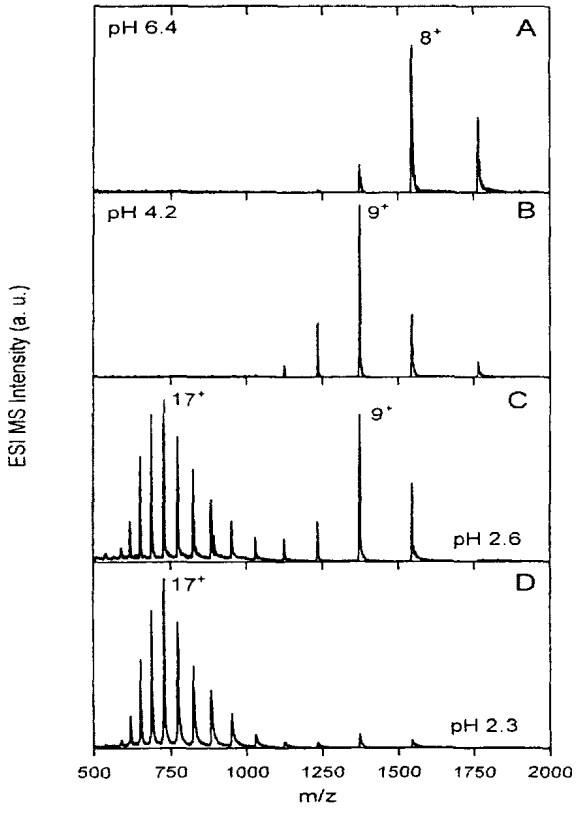

Figure 2.2. ESI mass spectra of cytochrome c at pH 6.4, pH 4.2, pH 2.6 and pH 2.3 (*1*).

folded protein due to the increase in exposure of accessible sites (Figure 2.3D). An observation that the center of the charge state distribution shifts to higher numbers is strong evidence that the structure has become less folded or more open (*1, 6, 7*).

ESI is a soft ionization source, meaning that even weak intramolecular interactions within a protein and intermolecular interactions between a protein and its ligand(s) can be studied. From the charge state spectra the masses of present molecules are calculated using computer programs (for example Masslynx), which use sophisticated algorithms to account for isotopic mass differences. The resulting mass spectrum can then readily identify components of an injected sample, such as a protein and its ligand(s). Occasionally minor mass discrepancies can arise between the expected and observed masses. Monocation and monoanion adducts can displace protons along the peptide chain resulting in adduct spectra. For example, sodium adducts are commonly observed and result in an increase in mass of 22 Da (23 Da from Na – 1 Da from H). If examination of the deconvoluted mass spectrum reveals multiple peaks at consistent increments, this is strong evidence for the presence of adduct species.

2.1.2 MCD spectroscopy

MCD spectroscopy has been widely used to study heme-containing proteins for several decades (*8-13*). Key to the analysis MCD spectroscopic data is that MCD bands lie at the same energy and have the same approximate band width as the corresponding absorption bands (section 1.5). The need for MCD spectroscopy arises from the complexity of the heme UV-visible absorption spectrum due to the overlapping of the $\pi-\pi^*$ bands (B, Q_{00}, and Q_{vib}) with the charge transfer bands between the iron center and the PPIX ring (*14*). In MCD spectroscopy these bands resolve into finer components, thus providing additional spectroscopic information. MCD spectroscopy typically provides information about the ground and excited state orbital degeneracies of high symmetry complexes based on the Faraday A, B, and C terms (Figure 2.3) (*14*). From this, the oxidation and spin states of the iron, as well as identification of axial ligands can be determined (*9, 10, 12, 15, 16*).

Faraday A terms arise from splitting of degenerate excited states, which absorb either left- or right-handed circularly polarized light. A terms are typically seen in

molecules with a high degree of symmetry, such as metalloporphyrins with D_{4h} or square symmetry. In the presence of a magnetic field, degenerate states split according to their magnetic moments. Transitions from the non-degenerate ground state to the split excited state then absorb either left or right handed circularly polarized light (lcp or rcp) depending on the selection rule that the transition with $\Delta M_L = +1$ absorbs lcp, and transition with $\Delta M_L = -1$ absorbs rcp. The corresponding increase or decrease in energy of the excited states in the presence of a magnet field also results in a slight displacement of the two bands, producing a derivative shaped peak. For species with degenerate excited states and nondegenerate ground states, positive A terms (positive lobe to high

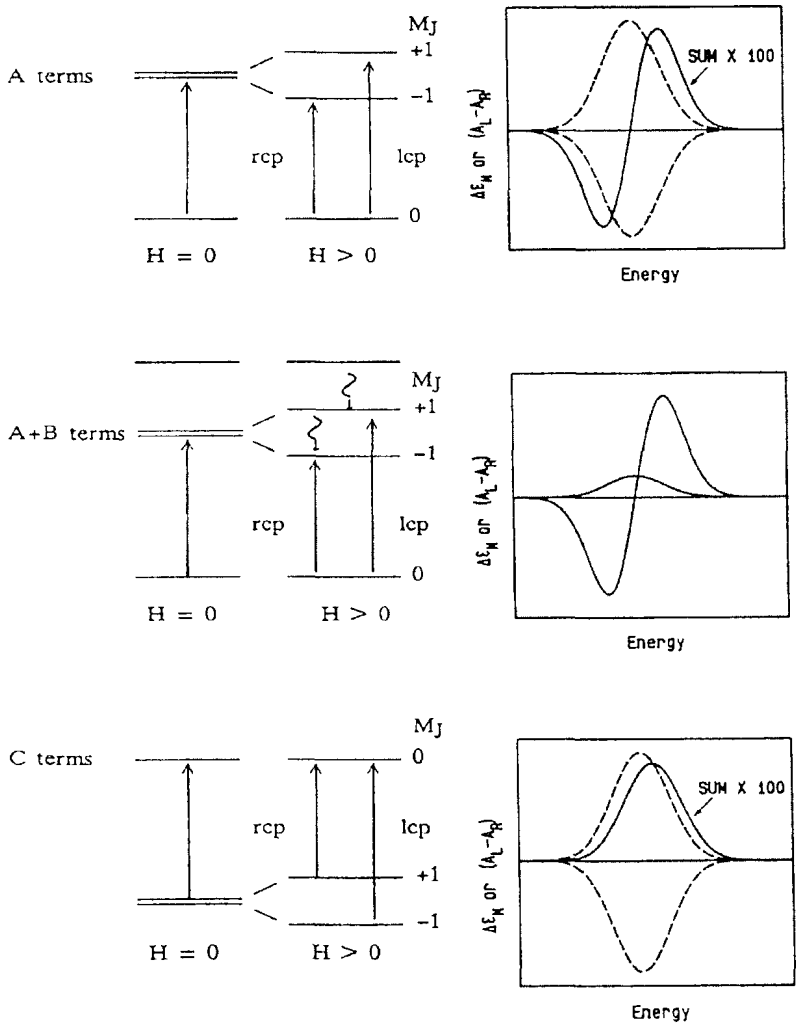

Figure 2.3. State splitting diagrams showing the origins of Faraday A (top), B (middle, showing the combination of an A and a B term) and C (bottom) terms.

energy of the cross-over energy) are observed. This will be the case for low spin ferrous hemes (*12*). Due to the non-degenerate ground state, A terms are temperature independent, and as such are studied using room temperature experiments.

Faraday B terms arise from a mixing of excited states and are predominant in molecules with low symmetry, such as D_{2h} (rectangular) in PPIX. Within a magnetic field, fluctuations in the energies of the excited states may result in mixing. The result is a preference to absorb either left or right handed circularly polarized light, depending on the nature of the mixed states. Thus, B terms are Gaussian shaped and can be of either sign. Like A terms, B terms are also temperature independent due to their non-degenerate ground state.

Faraday C terms arise from a splitting of degenerate ground states and are Gaussian shaped. According to the Boltzman distribution, these levels are relatively equally occupied at room temperature. The overall result is that the split states cancel one another out, producing a weak signal. However upon reducing the temperature, using liquid nitrogen or liquid helium, the lower ground state becomes more highly populated, resulting in the temperature dependence of C terms. Variable temperature experiments can therefore be used to identify C terms. In iron porphyrins, ground state degeneracy is found for high spin ferrous and all spin states of the ferric oxidation state. In addition, pseudo-A terms may be seen when two, oppositely-signed C terms exist closely in energy. These pseudo-A terms may be of either sign. In the heme proteins, the MCD spectrum of 5-coordinate, high spin ferrous heme provides an example of a B band (not to be confused with a B term) region characterized by a distorted negative pseudo-A term (*12*).

Despite this apparent complexity, the MCD spectral bands are diagnostic of the axial ligand identity, spin state, and oxidation state allowing in many cases unambiguous determination of each of these parameters. This diagnostic sensitivity has been used widely and successfully to interrogate the spin, oxidation and ligation state of the heme in a wide range of heme proteins, including hemoglobin, myoglobin (*12, 17*), the cytochromes (*18, 19*) and catalase (*8*).

2.2 General sample preparation procedures

Table 2.1 provides a list of the chemicals used in this thesis and their suppliers.

Table 2.1. Biological and chemical reagents used

CHEMICAL	SUPPLIER
2-butanone ($C_2H_5COCH_3$)	Sigma Aldrich
AcTEV protease	Amersham
Ammonium formate (NH_4COOH)	Fisher
Ammonium hydroxide (NH_4OH)	BDH
Ampicillin	Sigma Aldrich
Bovine hemin ($C_{34}H_{32}ClFeN_4O_4$)	Sigma Aldrich
Carbon monoxide (CO)	L-TEC
Formic acid ($HCOOH$)	Caledon
Glutathione ($H_2NCH(CO_2H)CH_2CH_2CONHCH(CH_2SH)CONHCH_2CO_2H$)	Sigma Aldrich
GST-prep column	GE Healthcare
Isopropyl β-thiogalactopyranoside	Fisher
Luria-Bertani broth	Difco
Phosphate buffered saline	(*20*)
Protoporphyrin IX ($C_{34}H_{34}N_4O_4$)	Sigma Aldrich
Protoporphyrin IX dimethyl ester ($C_{36}H_{38}N_4O_4$)	Sigma Aldrich
Pyridine (C_5H_5N)	Caledon
Sephadex G-25 Fine	Amersham
Sodium azide (NaN_3)	Fisher
Sodium chloride ($NaCl$)	Fisher
Sodium fluoride (NaF)	Fisher
Sodium hydrosulfite ($Na_2S_2O_4$)	Fisher

2.2.1 Cloning, overexpression, and purification of recombinant Isd proteins

The majority of the I*sd* genes (excluding signal sequence and C-terminal sorting signals), were cloned into the GST fusion vector pGEX-2T-TEV to generate pGST-IsdA, pGST-IsdC and p-GST-IsdE. Overexpression of GST-tagged Isd proteins in *E. coli* ER2566 (protease-deficient) was achieved by growing plasmid-containing cultures in Luria–Bertani broth (Difco) at 37 °C to an optical density at 600 nm of approximately 0.8. Isopropyl-β-D-thiogalactopyranoside (IPTG) (0.4 mM) was added and cultures were grown for a further 20 h at room temperature. Ampicillin (100 μg/ml) was incorporated into all growth media. Bacterial cells were pelleted, resuspended in phosphate-buffered saline (PBS), and lysed in a French pressure cell. Insoluble material was removed by centrifugation at 100,000 *g* for 20 min. The GST-Isd fusion proteins were purified by passage of the cell lysate across a 20 mL GSTPrep column (Amersham Biosciences). GST-Isd proteins were eluted from the column with 10 mM reduced glutathione, 100 mM NaCl, and 50 mM Tris–Cl, pH 9.0. Fusions were cleaved overnight at 4 °C with AcTEV protease (Amersham Biosciences) according to manufacturer's instructions. Cleaved GST was removed by two passages across a GSTPrep column and collection of the flowthrough.

2.2.2 Mutant Isd protein synthesis

All DNA mutations and cloning into *E. coli* were performed by Christie Vermeiren (Dr. D. E. Heinrichs' lab), Department of Microbiology and Immunology, University of Western Ontario. Once viable cells containing the mutant plasmid were obtained, expression and purification of the mutant protein were performed as outlined in section 2.2.1.

2.2.3 ESI-MS protein sample preparation and measurement

ESI mass spectra were recorded on a Micromass LCT, time of flight mass spectrometer operating in the positive ion mode. Samples were infused at flow rates of 15-20 μL /min into the ESI-MS instrument.

Stock Isd protein solutions, in 1x phosphate buffered saline (PBS) buffer (pH 7), were concentrated using centrifuge concentration tubes (Millipore) to approximately 1-2

mM. G-25 size exclusion columns (14 cm long, 1.5 cm diameter) were used for buffer exchange to ammonium formate (pH 7.3). Approximately 0.25 mL of concentrated protein in PBS was added to the column and eluted with the ammonium formate buffer. Samples were collected in small fractions, placed on ice, and run within 30 min following preparation on a Micromass LCT ESI mass spectrometer. To denature the proteins, small aliquots of 3 M formic acid were added (to bring the pH to approximately 2.3) prior to injection into the mass spectrometer. Instrumental settings varied depending on the protein sample being analyzed. Refer to sections 3.2.3 for rIsdA, 4.2.2 for rIsdC, and 5.2.3 for rIsdE.

2.2.4 UV-visible absorption and MCD sample preparation and measurement

Absorption spectra were recorded on a Cary 500 UV-visible spectrophotometer (Varian Inc. Canada). MCD spectra were recorded using an SM2 5.5 T superconducting magnet (Oxford Instruments Ltd, Oxford, UK) in a J-820 CD spectropolarimeter (Jasco Inc., Japan) (Figure 2.4). UV-visible absorption and MCD spectral data were recorded on identical solutions immediately following chemical changes at room temperature.

The following procedure was used for the preparation of rIsdA, rIsdC, rIsdE, and all mutant protein absorption and MCD samples. The pyridine hemochrome test was used to determine the concentration of the heme, as described in Berry *et al.* (*21*). The protein concentrations were estimated using the molar extinction coefficients; 15,930 $M^{-1}cm^{-1}$ for rIsdA, 18,490 $M^{-1}cm^{-1}$ for IsdC, and 19,890 $M^{-1}cm^{-1}$ for IsdE. Protein samples were diluted with 1x PBS to obtain absorbances in the B region of less than 0.8 in a 1 cm cuvette. Crystalline aliquots of sodium fluoride, sodium azide, and sodium cyanide were then added at approximately 5x, 10x, and 25x protein concentration and then very large excess, as needed to obtain constant absorption and MCD spectra. The solutions were measured over a period of 1-2 h to ensure no further changes were observed. To form ferrous heme, protein solutions were treated with increasing amounts of crystalline sodium hydrosulfite ($Na_2S_2O_4$) as the reducing agent until no further changes in the absorption and MCD spectra were observed. A key characteristic feature of ferrous hemes is the absorbance band 432 nm. To study carbon monoxide binding, gaseous CO was bubbled slowly into the sealed protein solutions, through a serum cap

changes in the absorption spectrum were measured. UV-visible absorption spectra of protein solutions containing sodium hydrosulfite were run before and after MCD measurements to ensure oxidation did not occur.

2.2.5 MCD data workup

MCD spectra are measured in ellipticity (θ_d), in millidegrees. Equation 2.1 was used to convert θ_d (degrees) into ΔA.

$$\theta_d = (2.303 / 4) \quad \Delta A \quad 180 / \pi \qquad (2.1)$$

All MCD spectra were recorded in a 5.5 T magnetic field. To normalize the data for the magnetic field strength, ΔA was divided by 5.5 T to give ΔA_M.

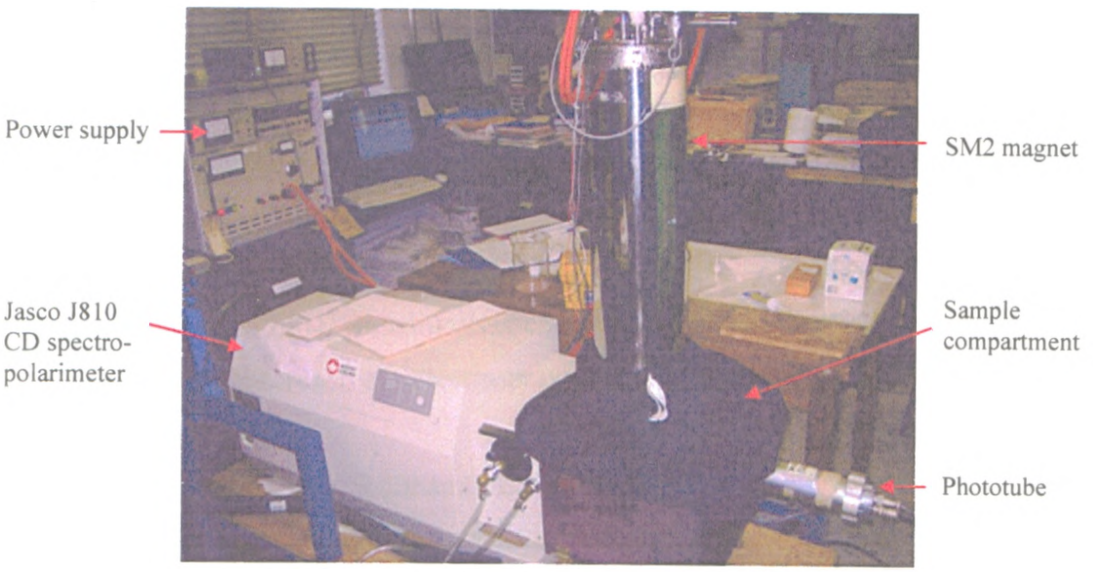

Figure 2.4. MCD spectropolarimeter instrumental setup.

2.3 References

1. Konnermann, L., and Douglas, D. J. (1997) Acid-induced unfolding of cytochrome c at different methanol concentrations: Electrospray ionization mass spectrometry specifically monitors changes in the tertiary structure, *Biochemistry 36*, 12296-12302.
2. Laskin, J., and Lifshitz, C. (2006) *Principles of mass spectrometry applied to biomolecules*, John Wiley & Sons, inc., Hoboken.
3. Kaltashov, I. A., and Eyles, S. J. (2005) *Mass spectrometry in biophysics*, John Wiley & Sons, New Jersey.
4. Yamashita, M., and Fenn, J. B. (1984) Electrospray ion source. Another variation on the free-jet theme, *J. Phys. Chem. 88*, 4451-4459.
5. Fenn, J. B., Mann, M., Meng, C. K., Wong, S. F., and Whitehouse, C. M. (1989) Electrospray ionisation for mass spectrometry of large biomolecules, *Science 246*, 64.
6. Yan, X., Watson, J., Ho, P. S., and Deinzer, M. L. (2004) Mass Spectrometric approaches using electrospray ionization charge states and hydrogen-deuterium exchange for determining protein structures and their conformational changes, *Mol. Cell. Proteomics 3*, 10-23.
7. Simmons, D. A., Wilson, D. J., Lajoie, G. A., Doherty-Kirby, A., and Konermann, L. (2004) Subunit disassembly and unfolding kinetics of hemoglobin studied by time-resolved electrospray mass spectrometry, *Biochemistry 43*, 14792-14801.
8. Browett, W. R., and Stillman, M. J. (1984) Temperature dependence in the absorption spectra of beef liver catalase, *Biophys. Chem. 19*, 311-320.
9. Sutherland, J. C. (1980) Magnetic circular dichroism of biological molecules, *Ann. Rev. Biophys. Bioeng. 9*, 293-326.
10. Browett, W. R., and Stillman, M. J. (1979) Magnetic circular dichroism studies of bovine liver catalase, *Biochim. Biophys. Acta. 577*, 291-306.
11. Dolphin, D. (1978) The Porphyrins, *Academic Press 3*.

12. Vickery, L., Nozawa, T., and Sauer, K. (1976) Magnetic circular dichroism studies of myoglobin complexes. Correlations with heme spin state and axial ligation, *J. Am. Chem. Soc. 98*, 343-350.

13. Springall, J., Stillman, M. J., and Thomson, A. J. (1976) Low temperature magnetic circular dichroism spectra of met- and myoglobin derivatives, *Biochim. Biophys. Acta. 453*, 494-501.

14. Mack, J., and Stillman, M. J. (2003) in *Handbook of porphyrins and related macrocycles* (Kadish, K. M., Smith, K. M., and Guilard, R., Eds.), p 43, Academic Press, New York.

15. Pluym, M. (2005) Characterizing the heme binding properties of Staphylococcus aureus iron-regulated surface determinant protein A., in *Chemistry* University of Western Ontario, London.

16. Eakanunkul, S., Lukat-Rodgers, G. S., Sumithran, S., Ghosh, A., Rodgers, K. R., Dawson, J. H., and Wilks, A. (2005) Characterization of the periplasmic heme-binding protein ShuT from the heme uptake system of *Shigella dysenteriae*, *Biochemistry 44*, 13179-13191.

17. Pond, A. E., Roach, M. P., Thomas, M. R., Boxer, S. G., and Dawson, J. H. (2000) The H92G myoglobin cavity mutant as a versatile template for modeling heme proteins: ferrous, ferric, and ferryl mixed-ligand complexes with imidazole in the cavity, *Inorg. Chem 39*, 6061-6066.

18. Shimizu, T., Nozawa, T., Hatano, M., Imai, Y., and Sato, R. (1975) Magnetic circular dichroism of *Pseudomonas putida* cytochrome P-450 in near infrared region, *Biochemistry 14*, 4172-4178.

19. Eglinton, D. G., Hill, B. C., Greenwood, C., and Thomson, A. J. (1984) Low temperature magnetic circular dichroism spectra and magnetization properties of extracted heme a3+ bis-imidazole. A model of cytochrome a in bovine cytochrome c oxidase, *J. Inorg. Biochem. 21*, 1-8.

20. Sambrook, J., Fritsch, E. F., and Maniatis, T. (1989) *Molecular cloning: a laboratory manual*, 2 ed., Cold Spring Harbour Laboratory Press, New York.

21. Berry, E. A., and Trumpower, B. L. (1987) Simultaneous determination of hemes a, b, and c from pyridine hemochrome spectra, *Anal. Biochem. 161*, 1-15.

Chapter 3: Iron regulated surface determinant protein A (IsdA)

3.1 Introduction

Based on its iron regulated synthesis, location within the cell wall of *S. aureus*, and ability to bind heme, IsdA has been proposed to function as an extra-cellular heme scavenging protein (*1, 2*). As expressed in *S. aureus,* IsdA is a 350 amino acid, cell wall anchored protein consisting of an N-terminal signal sequence, a hydrophobic C-terminal (containing an LPXTG sorting sequence), and a single NEAT (NEAr abc Transporter) domain (Figure 3.1) (*1*). Briefly, the signal sequence is involved in locating the protein to the cell wall, the IsdA NEAT domain is believed to function as a heme binding domain, and the C-terminal sorting signal is critical for anchoring the protein to the bacterial cell wall.

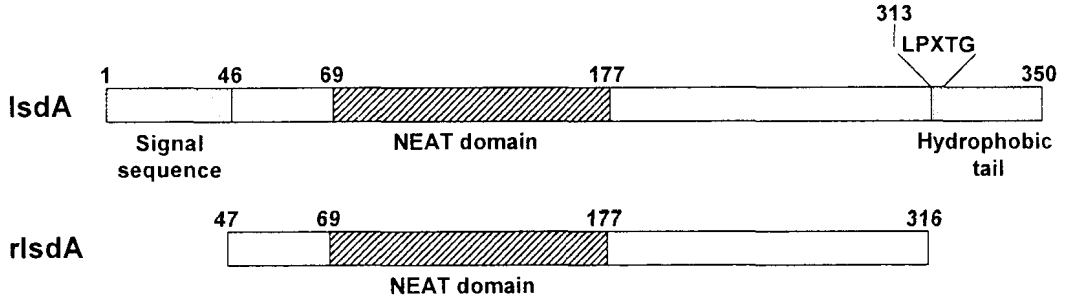

Figure 3.1. Schematic of the amino acid sequence of IsdA and rIsdA.

3.1.1 Bacterial cell wall structure and the IsdA anchoring mechanism

The cell wall of Gram-positive bacteria consists of a repeating disaccharide, N-acetylmuramyl-(β1-4)-N-acetylglucosamine (NAM-NAG) (Figure 3.2A). The lactyl group of NAM is linked to the N-terminal of a pentapeptide consisting of L-alanine, D-glutamine, L-lysine, D-alanine, and D-alanine. The great strength of bacterial cell walls comes from cross-linking the peptidoglycan units together with a pentaglycine cross-bridge (the cross-bridge shows some variation between bacterial species) (Figure 3.2B). In *S. aureus*, the terminal D-alanine residue is cleaved and a pentaglycine unit forms a cross-bridge between the amino group of the L-lysine side chain and the free carboxyl

A substantial part of this chapter has been published in *Biochemistry* [Vermeiren, C. L., Pluym, M., Mack, J., Heinrichs, D. E., and Stillman, M. J. (2006) Characterization of the heme binding properties of *Staphylococcus aureus* IsdA, *Biochemistry* **45**, 12867-12875]. This work was carried out in collaboration with Dr. D. E. Heinrichs' group, Department of Microbiology and Immunology, University of Western Ontario.

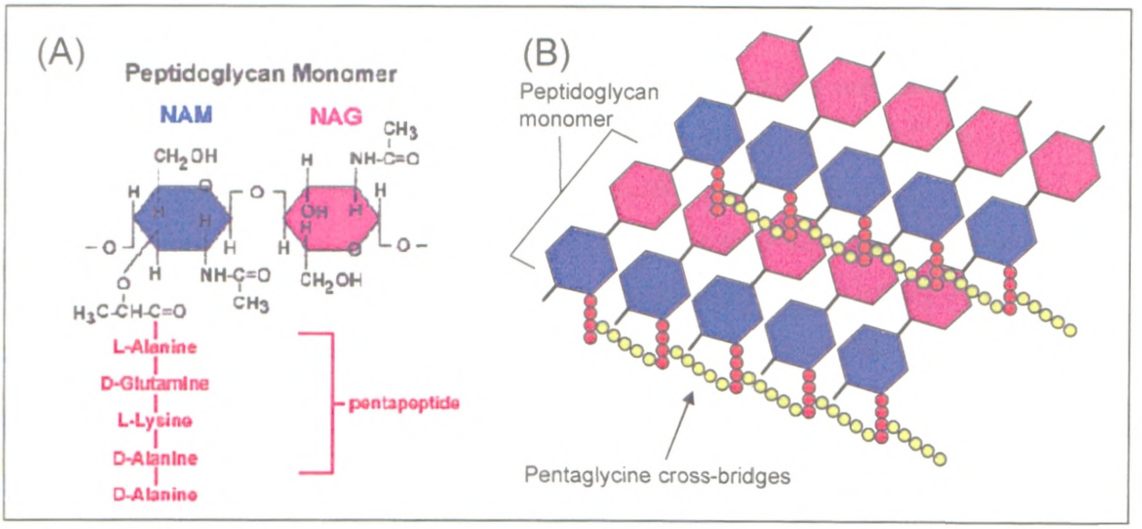

Figure 3.2. Structure of the cell wall of *S. aureus*. (A) The structure of the peptidoglycan units that make up the cell wall. (B) The cross linking of cell wall components via pentaglycine cross-bridges.

carboxyl group of the remaining D-alanine (Figure 3.2B) (*3*). The transpeptidase enzymes that catalyze the cross linking process are also the target of several β-lactam antibiotics, such as penicillin. Penicillin mimics the D-alanyl-D-alanine terminus of the pentapeptide side chain and acylates the active site of the enzyme, rendering it inactive (*4*).

Many Gram-positive bacterial surface proteins are also linked to the cell wall through a transpeptidation mechanism (*3, 5*). The C-terminal of a surface protein containing an LPXTG sequence is recognized by the enzyme sortase A (SrtA), which catalyzes the linkage to the cell wall. In the Isd system three proteins, IsdA, IsdB, and HarA/IsdH, are linked to the cell wall through the action of this enzyme (*2, 3, 6*). The C-terminal end of the protein is cleaved between the threonine and glycine residues. The freed threonine carboxyl group is then amide linked to the N-terminal end of a pentaglycine cross-link, anchoring the protein. Several surface proteins containing a similar sorting signal have been identified in a number of bacterial species, thus it is believed that SrtA catalyzed linkage is a universal mechanism in Gram-positive organisms (*7*). It is estimated that upwards of 900 surface proteins across 50 different species of Gram-positive bacteria serve as substrates for SrtA (*8*).

3.1.2 NEAr abc Transporter (NEAT) domains

The single IsdA NEAT domain is so named because of its presence in proteins expressed from genes in the vicinity of other genes predicted to encode Fe^{3+} transporters (*9*). IsdA and IsdC each contain one NEAT copy, IsdB possesses two copies, and HarA/ IsdH contains three copies (*10*). Although NEAT domains have now been identified in a growing number of Gram-positive surface proteins, the exact function of this domain has yet to be determined, but expressed in recombinant form, the IsdA NEAT domain has both heme and fibrinogen-binding ability (*1*), while the two most N-terminal HarA/IsdH NEAT domains are associated with hemoglobin-haptoglobin binding (*10*).

3.1.3 The role of IsdA in S. aureus

Not unlike other characterized Gram-positive bacterial cell-surface proteins, IsdA has been demonstrated to interact with more than one host component. Indeed, not only has it been demonstrated that IsdA provides physiologically relevant adherence to fibrinogen and fibronectin, but IsdA can also interact with several other host components such as transferrin and heme (*1, 11*). Although there is evidence supporting the role of IsdA as a broad-spectrum adhesin, this protein was initially suggested to play a role in iron acquisition given i) that the *Isd* transcripts are iron-regulated, ii) IsdEF, encoded from within the *Isd* locus, share similarity with ABC transporters that transport iron, and iii) the ability of IsdA to interact with both transferrin and heme. The exact role, however, of IsdA in iron acquisition is not clearly understood.

In the present chapter, ESI-MS, absorption spectroscopy and MCD spectroscopy show that recombinant IsdA (rIsdA) binds a single heme molecule. The native heme-rIsdA complex exists as a 5-coordinate, high spin ferric heme with restricted access to anionic ligands. Reduction to ferrous heme allows access to ligands, and significantly, this reaction is reversible so that subsequent reoxidation prevents access. Furthermore, mutational analysis shows that tyrosine 166 (Y166) of the IsdA NEAT domain is directly coordinated to the heme iron in the proximal position.

3.2 Experimental

To study IsdA, the signal and sorting sequences were removed to produce rIsdA, consisting of amino acids 49-316 (Figure 3.1). The resulting protein possessed high solubility in aqueous solution and showed no apparent aggregation for upwards of 2 weeks when stored at 4^0C.

3.2.1 rIsdA protein preparation

Refer to section 2.2.1.

3.2.2 Mutant rIsdA protein preparation

DNA mutations and cloning into *E. coli* were performed by Christie Vermeiren (Dr. D. E. Heinrichs' lab), Department of Microbiology and Immunology, University of Western Ontario. Mutant rIsdA protein expression and purification were performed as outlined in section 2.2.1.

3.2.3 Mass spectrometry sample preparation and measurement

Refer to section 2.2.3. The mass spectrometer settings used to study rIsdA and rIsdA mutants are given in Table 3.1. The remaining settings were tuned to give the strongest signal, and showed some variance between runs. To remove heme from rIsdA, the sample and extraction cone voltages were set to 100 V and 50 V, respectively.

Table 3.1. Micromass LCT-MS settings used for the analysis of rIsdA.

Capillary (V)	3500
Sample cone (V)	25-50
Extraction cone (V)	5-15
Desolvation temp. (^{0}C)	20
Source temp. (^{0}C)	80

3.2.4 UV-visible absorption and MCD spectroscopy sample preparation

Refer to section 2.2.3.

3.3 Results

3.3.1 Heme binding in rIsdA

When over-expressed and purified from *E. coli*, rIsdA was colored, indicating that it was bound to heme (Figure 3.3). While UV-visible spectroscopy can indicate fine detail of the heme binding domain, it was difficult to determine the heme:protein stoichiometry from those spectra. ESI-MS provided detailed stoichiometric and structural information from the mass/charge values, the number of charge states observed, and the subsequent changes in the distribution of these charge states as a function of solution conditions.

Figure 3.3. Sample vial containing rIsdA as purified from *E. coli*.

Figure 3.4A shows the measured charge states for the rIsdA at pH 7, with the deconvolution data shown in Figure 3.4B. The deconvolution shows all unique molecular species that, through protonation, gave rise to the large number of measured charge states. These data clearly identify the presence of two predominant molecular species. The major species had a maximum in the charge state distribution of +29, which corresponded to a mass of 30,671 Da (Figure 3.4B). This mass arose from one heme bound to one molecule of rIsdA. The second species had a maximum intensity near +30 and a mass of 30,055 Da, which correlated well with the predicted mass of 30.06 kDa for heme-free rIsdA. The increase in just +1 in the charge-state distribution for the heme-free rIsdA species indicated that only minor structural changes took place in the protein following loss of the heme, compared to changes that took place following denaturation (Figure 3.4C). There was no indication in the ESI-mass spectra of a rIsdA species with two bound hemes, which would have a mass of 31,287 Da, and there was also no

indication of any other protein species in the solution or of any significant concentration of free heme.

Denaturing rIsdA using formic acid changed the charge state distribution quite dramatically (Figure 3.4C). At least two series of charge states were observed, each with the molecular species of mass 30,065 Da as the parent molecule (Figure 3.4D). The predominant series had a charge state maximum at +35, while the lesser species had maxima between +24 and + 26. Because the parent molecule was the same for both series, it indicated the presence of two or more very different conformations coexisting in solution, one very much more open and, therefore, with more exposed basic residues available for protonation and the other conformation(s) considerably more closed. In both cases, the denaturing conditions resulted in loss of the bound heme. The two minor peaks in Figure 3.4B were 275 Da higher than the mass of the parent molecule and were present in all the mass spectra. These peaks were attributed to rIsdA proteins that were 275 Da heavier due to imperfect cleaving, an impurity not observable on gels. There was no reason to consider that the additional residues had any effect on the heme binding properties because the heavier peptide appeared in each mass spectrum.

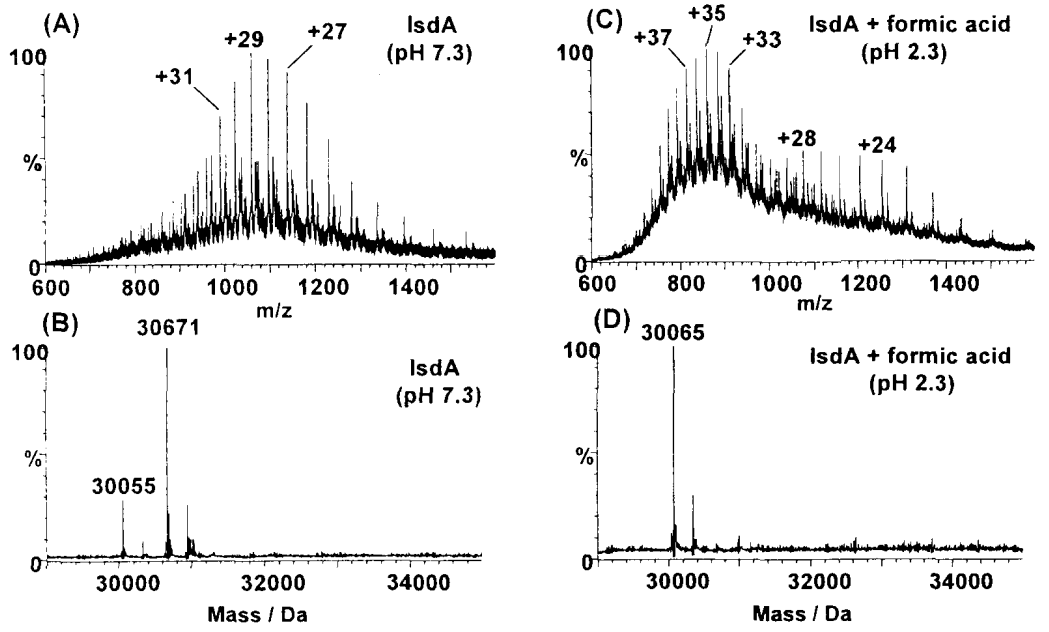

Figure 3.4. ESI mass spectra of rIsdA under native and denaturing conditions. (A) As it was purified from *E. coli* (pH 7). (B) The deconvoluted species were assigned as the heme-free protein (mass 30,055 Da) and the heme-containing protein (mass 30,671 Da). (C) Electrospray mass spectrum of IsdA following the addition of formic acid, which resulted in denaturing conditions. (D) The deconvolution showed that the single species is the heme-free protein with a mass of 30,065 Da.

3.3.2 Heme binding properties of rIsdA

The optical spectra of heme-binding proteins are dominated by the absorption bands of heme molecules between 300 and 700 nm. The UV-visible region spectrum of the heme in IsdA exhibited a major band near 408 nm (the B band), followed by a series of bands that extended from 450 to above 600 nm (the Q bands). Figure 3.5 shows the B band absorption spectra of the native rIsdA and the series of ligated species measured as part of this study. The native, ferric rIsdA had a B band maximum at 408 nm (line 1). No anionic ligands bound to this species. Reduction with sodium hydrosulfite resulted in the B band shifting to 432 nm (line 2). Addition of CO to reduced rIsdA resulted in a blue shift of the B band to 421 nm (line 3). The heme was reoxidized with potassium ferricyanide, resulting in a B band shift to 409 nm (line 4). The addition of excess cyanide to the reoxidized sample had no effect (line 5).

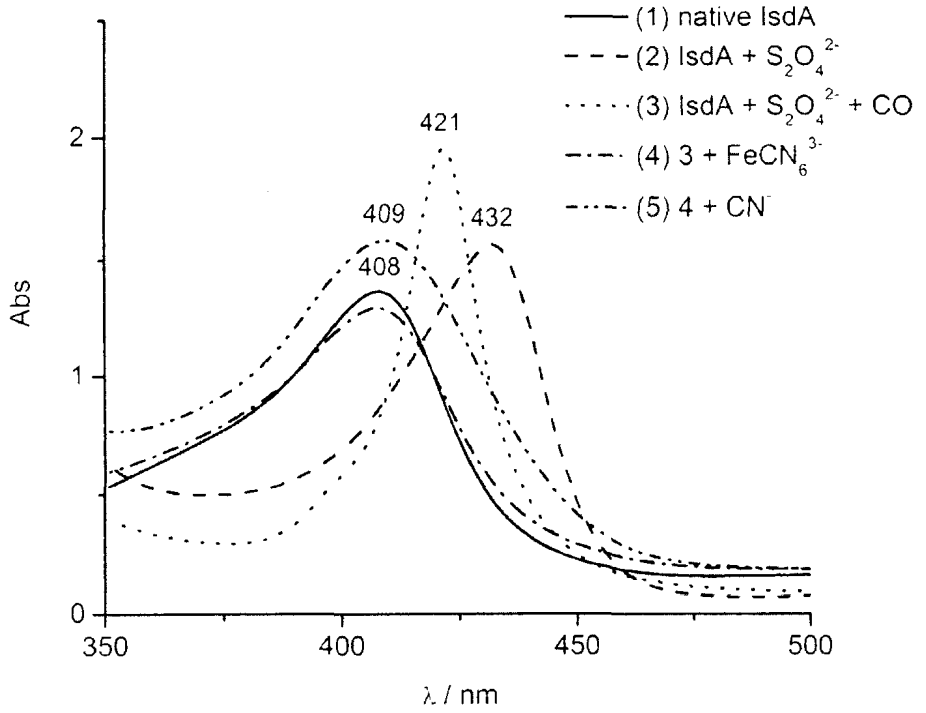

Figure 3.5. Absorption spectra recorded for solutions of rIsdA. (1) Native, ferric rIsdA, (2) following reduction with sodium hydrosulfite, (3) following addition of CO to the reduced rIsdA in (2) by bubbling through a serum cap into the sealed cuvette; (4) following addition of crystalline potassium ferricyanide to re-oxidize the rIsdA solution in (3); (5) following addition of cyanide to the re-oxidized solution from (4).

Figure 3.6A shows the absorption and MCD spectra of rIsdA. The band maxima in the absorption spectrum for the B band (at 407 nm) and the visible region bands (at 502, 540, and 625 nm) were characteristic of the high spin ferric heme "fingerprint pattern", which has typically been observed with heme proteins such as myoglobin with a phenolate axial ligand (*12*). Moreover, the well characterized absorption and MCD spectra for myoglobin (*13, 14*) provide an excellent model from which to draw conclusions concerning the identity of the 5th and 6th axial ligands of the heme iron in rIsdA since, for myoglobin, spectra have been published for a great many combinations of axial ligand and iron oxidation states (*12*). It is well established that all the band parameters change as a function of the protein environment of the heme. The spectral changes arise largely as a result of changes that take place at or near the iron, because charge transfer bands between the metal and the ring overlay the π to π^* bands of the porphyrin ring. These bands change in number, wavelength, and intensity depending on the oxidation state (ferrous, ferric, ferryl) and spin state (low, intermediate, high) of the iron, and the axial ligands of the iron control the spin.

In heme proteins, the proximal or 5th position axial ligand may be the nitrogen from histidine, the sulfur from cysteine, or the oxide from tyrosine. The distal or 6th position ligand may be i) other residues in the peptide chain, ii) water that allows full access for small ligands to the iron, iii) empty, or iv) empty but with residues in the vicinity of the heme pocket that block access to the iron. Alternatives (i) and (ii) would result in heme spectra characteristic of 6-coordination, whereas alternatives (iii) and (iv) would result in heme spectra characteristic of 5-coordinate iron. The MCD spectral data from native rIsdA (Figure 3.6A) showed that the heme contained a 5-coordinate, high spin ferric iron with an anionic oxygen ligand, likely from a proximal tyrosine and that the distal site was empty.

Axial coordination of the ferric heme in proteins with the 6th position accessible (for example, in myoglobin rather than in cytochrome c) is possible across the entire range of the spectrochemical series, starting with the very low Δ_{OCT} values of the halides and extending to the strong field ligand cyanide. Ligation by anionic ligands such as cyanide is thermodynamically preferred and takes place with strong binding constants. Strong field ligands such as cyanide systematically force a change from high or

intermediate to low spin if the existing ligand is a weaker field ligand. However, for rIsdA, it was found that there was a negligible effect on the absorption and MCD spectra following the addition of excess cyanide (Figure 3.6B). This was extremely unusual and contrasted the expectation based on the spectral properties of myoglobin (and other heme proteins), in which the MCD spectrum of the high spin ferric heme, which is characterized by the well resolved, derivative shaped band centered at ca. 540 nm, is replaced by a strong, low-spin marker band at 580 nm in ferric myoglobin (*13, 14*). The implication of the results presented here for the ferric rIsdA were that, in complete contrast with myoglobin, no 6^{th} position (distal) axial ligation took place in ferric rIsdA. As would be anticipated, therefore, the addition of even a large excess of weaker field ligands within the spectrochemical series, such as fluoride and azide, similarly resulted in no spectral changes (*15*). This implied that while unoccupied in the native protein the distal site was congested and blocked by other residues, which accounted for inability of free anionic ligands to bind to the high spin ferric heme. There is evidence in the literature that tyrosine binds to ferric heme proximally in both the ShuT periplasmic protein from *Shigella dysenteriae* (*16*) and bovine liver catalase (*17, 18*). In rIsdA, the oxidized ferric heme existed as the high spin iron (Figure 3.6A) with characteristic spectral properties of a 5-coordinate iron. This meant that the ferric heme in rIsdA was inaccessible to even very strong ligands so that the central part of the heme may be considered buried inside the protein structure, effectively blocking axial coordination of the Fe^{3+}.

The iron in heme proteins, even the six-coordinate heme in cytochrome c, can usually be reduced with reducing agents such as sodium hydrosulfite ($Na_2S_2O_4$) (*19*). This was also the case for rIsdA. Reduction of the heme in rIsdA, using sodium hydrosulfite, resulted in large red shifts in the B band wavelength and MCD spectral band shape (Figure 3.6C). The absorption band maxima of the B band (at 432 m) and of the Q bands (at 558 nm), observed after the addition of $Na_2S_2O_4$ were consistent with the presence of a 5−coordinate, high spin ferrous heme. A much more significant predictor of the oxidation state, spin state and coordination environment of the iron was the presence of an inverted pseudo-A term in the B region (+ve at 434; −ve at 418 nm) within the MCD spectrum and the collapse of all the visible region bands to the set observed

between 540 and 600 nm. This spectral pattern provided the definitive "fingerprint pattern" evidence for this assignment. Upon reduction, therefore, rIsdA clearly formed a high spin, 5-coordinate ferrous heme, with no coordination in the 6th position, just as observed in myoglobin (*12*). Bubbling CO into a sealed solution of the reduced rIsdA resulted in the immediate formation of low spin ferrous heme, which was characterized in the MCD spectrum by two intense positive A terms, centered at 421 and 569 nm (Figure 3.6D). Coordination by O_2 or CO resulted in the formation of low spin heme with an MCD spectrum dominated by two positive A terms (*13*). The relative intensities and band centers are different for the O_2 and CO bound hemes allowing ready identification of the axial ligand. This new pattern was characteristic of a ferrous heme with the 6th position coordinated by CO and the 5th position coordinated by histidine. While this reactivity was similar to that of myoglobin, it is quite unlike that of cytochrome c where the CO cannot break either of the two axially coordinated residues (the methionine or the histidine) (*19*). It appeared that the initial reduction took place at the edge of the heme that was exposed and not the iron center because the anionic hydrosulfite would not be able to reach the ferric center. Following this, electron transfer across the porphyrin resulted in the reduction of the iron to the 2+ state. This implied that while the iron was inaccessible to ligands, the heme ring was close to or exposed outside the surface of the protein allowing reduction from the reducing agent.

Addition of ferricyanide to the reduced rIsdA returned the spectral properties to those observed for the native protein (Figure 3.6A) with the 6th position again inaccessible to strong field ligands such as cyanide (Figure 3.5). This meant that the iron had been re-oxidized to the ferric high spin state and also that the heme iron exhibited electronic spectra characteristic of tyrosine proximal coordination. Once again the spectral data showed that even excess cyanide could not bind to the heme-rIsdA complex, providing evidence that access to the iron was again restricted. The significance of these results is that whereas reduction enabled access by CO, oxidation restricted this access. The structural model to describe such chemical properties involves a crevice or pocket that reversibly opens following reduction, and closes following oxidation of the iron.

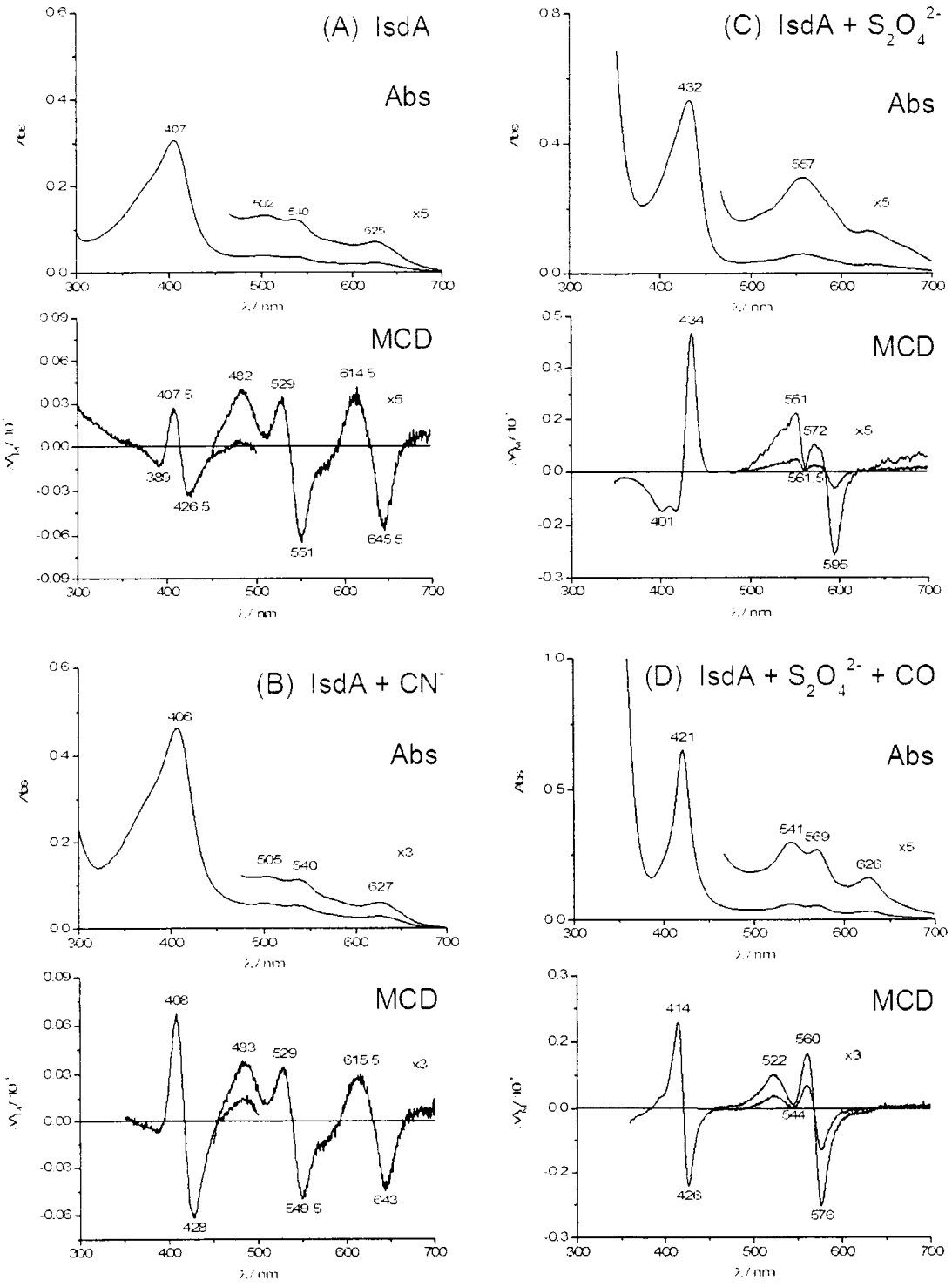

Figure 3.6. Absorption and MCD spectra of rIsdA. (A) As isolated from *E. coli*. (B) Following the addition of crystalline sodium cyanide in small aliquots up to extremely large excess. (C) With the addition of sodium hydrosulfite. Crystalline hydrosulfite was added in small aliquots until there were no further changes in the absorption and MCD spectra. (D) With the addition of sodium hydrosulfite and carbon monoxide.

3.3.3 rIsdA mutational analysis

The MCD spectrum of rIsdA was consistent with high-spin ferric heme coordinated by a phenolate oxygen in the 5th position (*16*). This implies that a tyrosine residue was the heme binding amino acid in rIsdA. The NEAT domains of IsdA, IsdC, and HarA/IsdH, show several conserved tyrosine residues, specifically Y87, Y102, Y166, and Y170 (*20, 21*). This suggests that these residues play an important role in heme binding.

Mutational analysis of each conserved residue, as well as all other tyrosine residues in the rIsdA NEAT domain, revealed that only Y166 was crucial for heme binding. Panels A and B of Figure 3.7 illustrate the lack of change in the absorption and MCD spectra for rIsdA Y170A, which suggested that Y170 did not play a large role in heme binding. Panel C of Figure 3.7 shows that in rIsdA Y170A, access for small anionic ligands was restricted when ferric heme was present, just as in the native protein. Furthermore, reduction to ferrous heme, as shown by the inverted A-term in the B region (Figure 3.7D), and axial ligation in the reduced state, as shown by the characteristic low-spin ferrous heme spectra (Figure 3.7E), were both possible. Similar results were found for all other NEAT domain tyrosine residues, with the exception of Y166. An interesting result arose upon mutation of both residues F112 and Y170, two rather bulky residues located within the rIsdA NEAT domain. Individually, these mutations produced no change in the MCD spectrum from that of native rIsdA (the MCD data for the rIsdA F112A were identical to that of rIsdA Y170A), however, in the double mutant, changes in the MCD spectrum were observed (Figure 3.7G). The increase in the B:Q band intensity ratio from that of rIsdA and rIsdA Y170A, suggested a shift to a more intermediate-spin state of the heme-iron (*13, 21*). Ligation of cyanide was also observed as indicated by the low-spin ferric heme marker band that appeared at 576 nm (Figure 3.7H). Evidently, removal of the bulky F112 and Y170 residues, aside from slightly altering the heme binding environment, provided a pathway for cyanide to bind in an axial heme site.

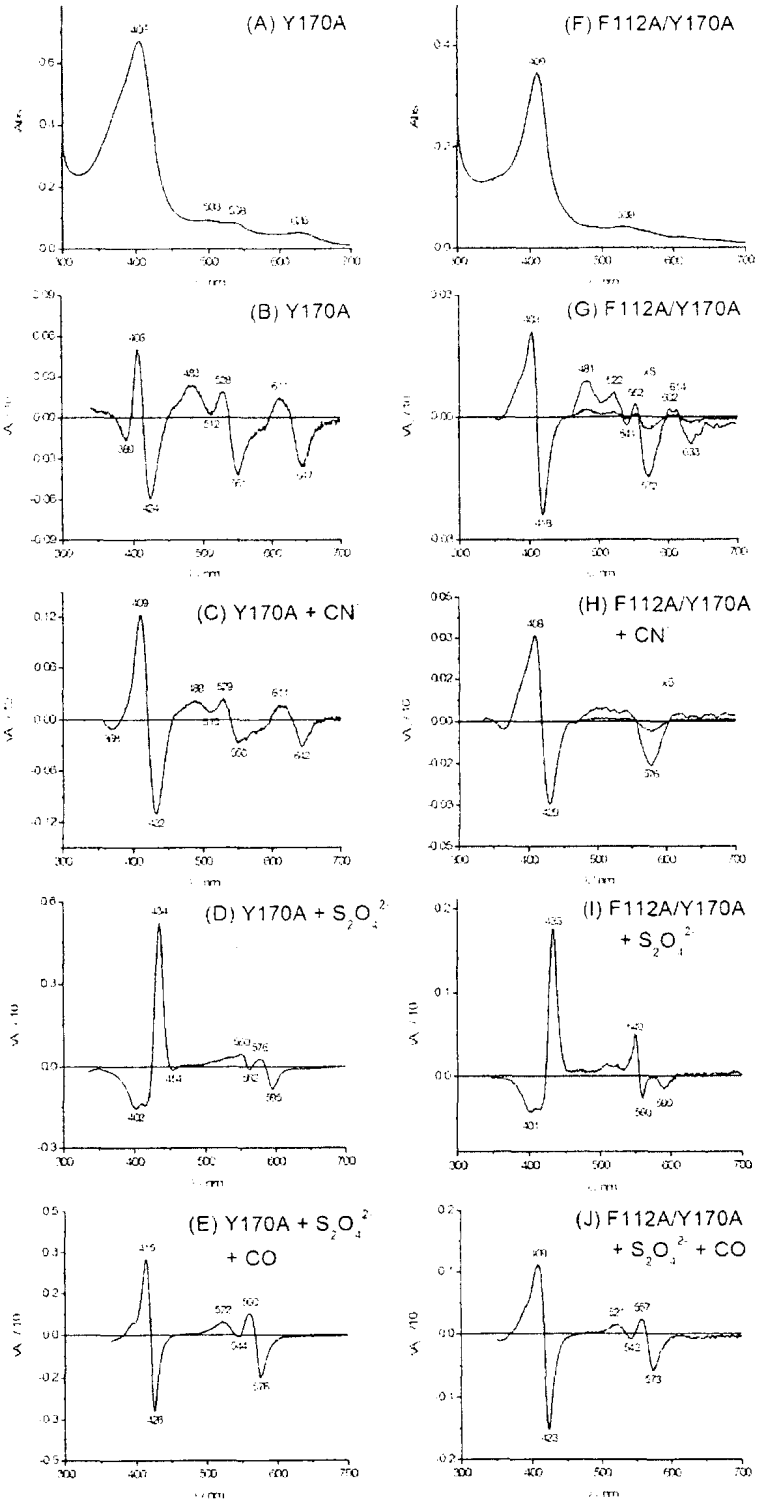

Figure 3.7. Absorption and MCD spectra of the rIsdA Y170A and F112A/Y170A mutants. (A, F, B, G) As purified from *E. coli*. (C, H) Following the addition of crystalline aliquots of sodium cyanide. (D, I) Following the addition of crystalline aliquots of sodium hydrosulfite. (E, J) Following the addition of crystalline sodium hydrosulfite and carbon monoxide.

The UV-visible spectrum of rIsdA Y166A showed reduced heme binding upon purification, compared to native rIsdA. The rise in the $\Delta\varepsilon_{280\ nm}$ / $\Delta\varepsilon_{407\ nm}$ (protein absorption / heme absorption) value from 0.83 for rIsdA to 1.85 for rIsdA Y166A illustrated this (Figure 3.8). These values were consistent over several protein preparations of both rIsdA and rIsdA Y166A. The mass spectrum of rIsdA Y166A (Panels A and B of Figure 3.9) offered further evidence of lowered heme binding affinity.

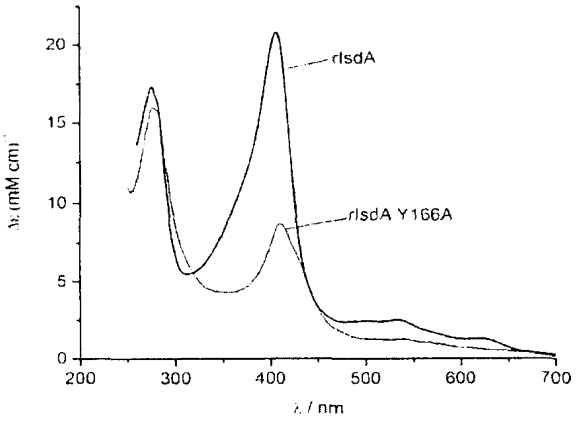

Figure 3.8. UV-visible absorption spectra of rIsdA and rIsdA Y166A.

Native rIsdA showed considerable heme binding upon mass analysis. Figure 3.9B illustrates that for rIsdA, the majority of protein was bound to heme. Under the same conditions, the mass spectrum of rIsdA Y166A (Figure 3.9E) clearly shows that heme binding was reduced. No significant sign of free heme was observed in the mass spectra of either native rIsdA or rIsdA Y166A. The charge states for rIsdA Y166A were centered about +27 (Figure 3.9C) and were identical to those of native rIsdA (Figure 3.9A), suggesting that the mutation did not alter the overall fold of the protein. Close examination of the peaks between 1000 and 1400 m/z revealed four charge state distributions, corresponding to four distinct protein molecules (Figure 3.9D). Molecular masses were calculated to be approximately 29,999 Da, 30,326 kDa, 30,616 kDa, and 30,936 kDa. The theoretical mass of IsdA rY166A, calculated from the amino acid sequence, was approximately 29.97 kDa and was in close agreement to the observed peak at 29,999 Da. The mass of heme is 616 Da, thus 30,616 Da represented single heme bound rIsdA Y166A. The peak at 30,326 Da was believed to represent rIsdA Y166A bound to an unidentified ligand approximately 320 Da in mass. 30,936 Da, thus, represented rIsdA Y166A bound to both heme and the unidentified ligand.

On a single occasion, considerable heme binding in the rIsdA Y166A mutant was observed. The mass spectrum of this sample (Figure 3.10B) shows that the majority of protein was heme bound, represented by the peak at 30,587 Da. Due to the increase in the unknown ligand concentration in this sample, a more accurate mass of 305 Da was assigned to it. It was also possible that the unidentified peak represented a 922 Da ligand, however, this was not believed to be the case due to the peak observed approximately 320 Da higher than the ligand-free protein peak in Figure 3.9D. Panels C and D of Figure 3.10 show that upon increasing the sample and extraction cone voltages to 100 V and 50 V, respectively, the ligands were removed from the protein, hence the dominance of the ligand-free rIsdA Y166A peak at 29,970 Da. This also confirmed that the peak observed at 30,892 Da did not represent a slightly heavier protein. If it did, a mass 305 Da higher than the ligand free rIsdA Y166A peak would still be have been observed following the increase in sample and extraction cone voltages. Although free heme was observed (616 m/z), no signals were observed for the unknown ligand at 305 or 922 m/z. Furthermore, no peaks were observed at fractions of 305 or 922 m/z, which would be observed if charge states higher than +1 existed for this ligand.

The UV-visible absorption and MCD spectra of IsdA Y166A resembled a mixture of species. The shoulder appearing to the red of the main B band (Figure 3.11A) illustrated this. The band pattern in the B region of the MCD spectrum resulted from the overlap of two A terms. This overlapping signal was apparent in all of the spectra presented in Figure 3.11. The B band in native rIsdA appeared at 407 nm. Mutation of Y166 resulted in a red shift to 412 nm, a change observed only for this mutation. Interestingly, whereas axial ligation of CN^- was shown to be restricted in native IsdA, the Y166A mutant protein permitted ligation to the bound heme. The 580 nm band (Figure 3.11B) was characteristic of a low spin ferric heme (*13, 14*), and was expected upon ligation of a strong field ligand, such as cyanide. Addition of $S_2O_4^{2-}$ gave the characteristic inverted pseudo A-term in the B region of the MCD spectrum, centered about 420 nm (Figure 3.11C). Carbon monoxide addition to reduced rIsdA Y166A produced a characteristic low-spin ferrous MCD spectrum with the addition of a second signal in the B region (Figure 3.11D).

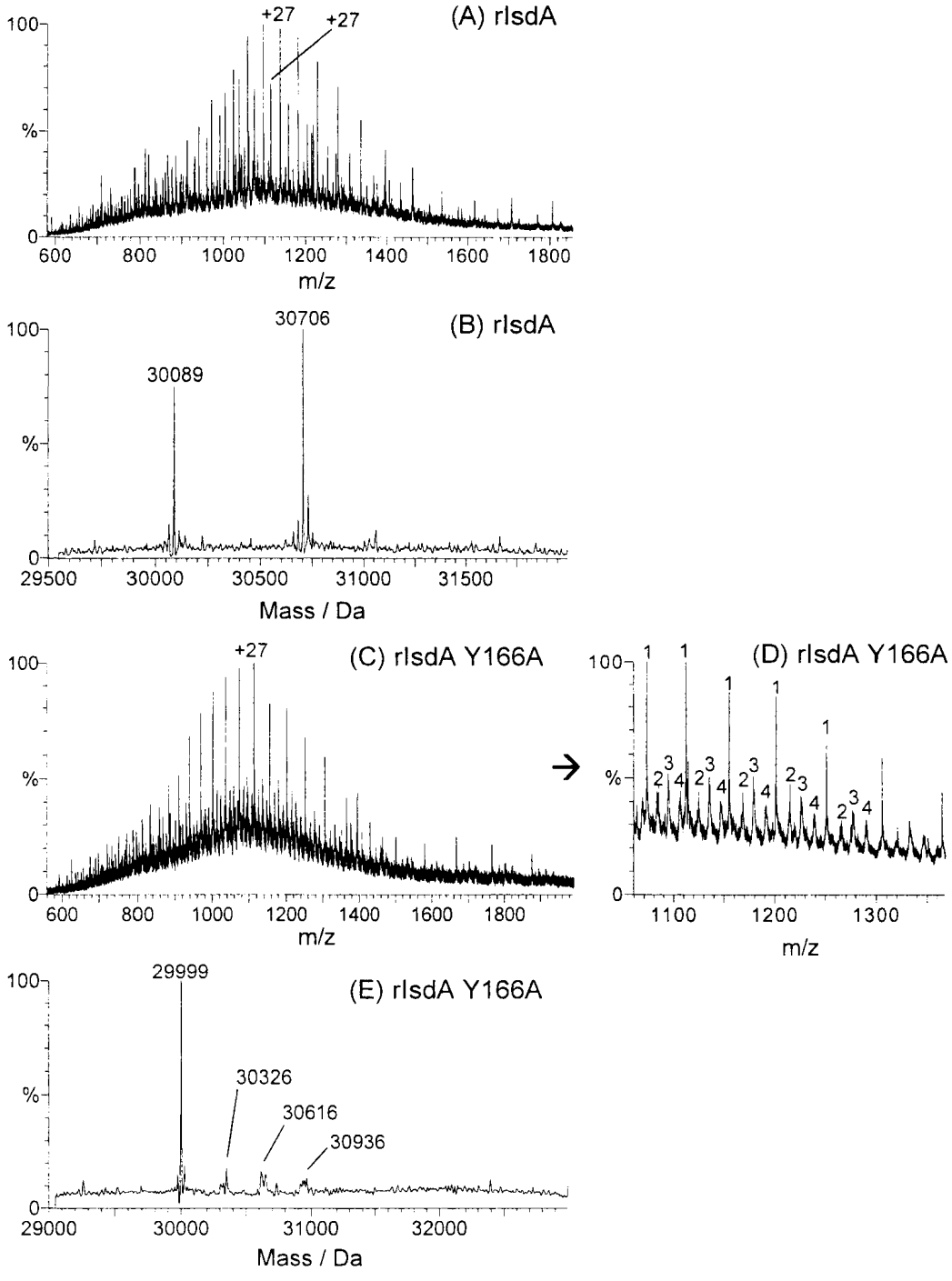

Figure 3.9. Charge state and deconvoluted mass spectra of rIsdA and rIsdA Y166A measured with matching instrumental parameters. (A, C) Charge state spectrum of the entire scan range. (D) Enlargement of the rIsdA Y166A charge state region. (B, E) Deconvoluted mass spectra of the proteins.

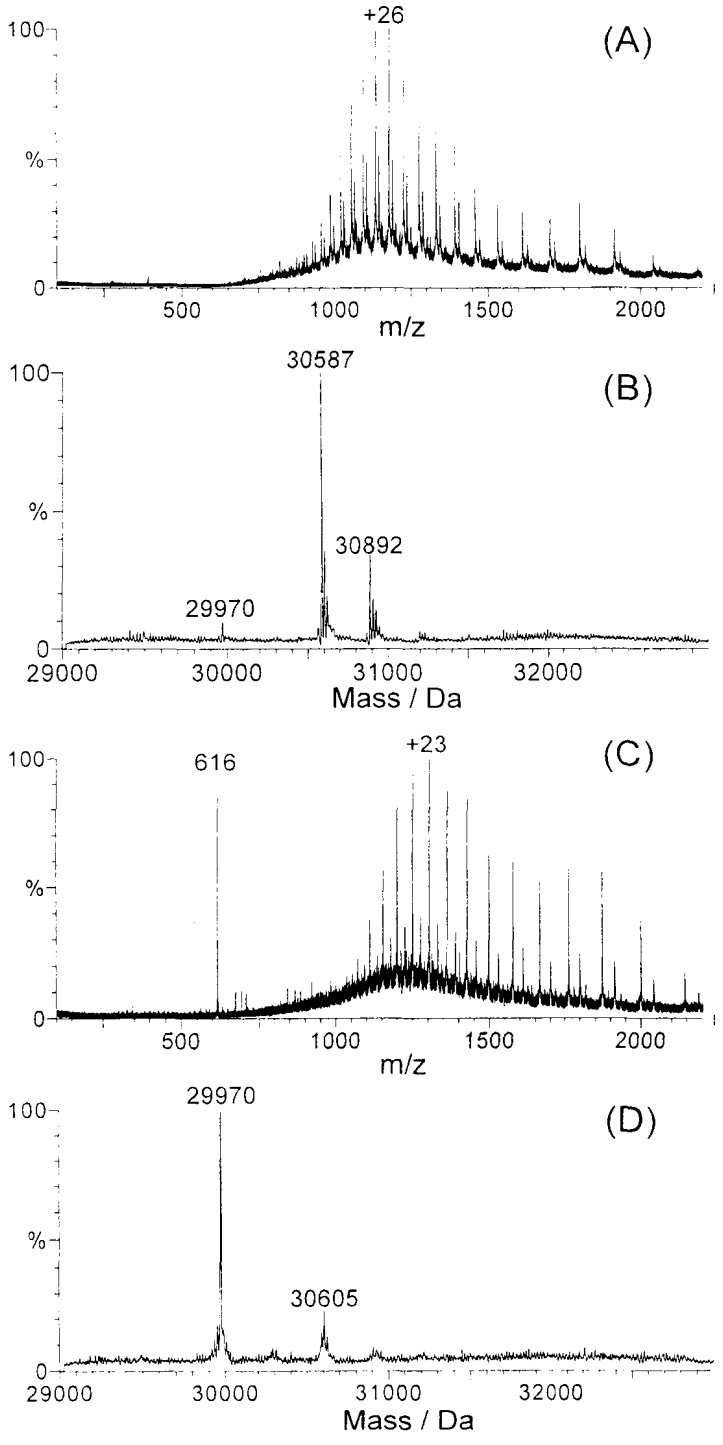

Figure 3.10. Charge state and deconvoluted mass spectra of rlsdA Y166A when purified bound to a large quantity of heme. (A) Charge state spectrum under mild conditions. (B) Deconvoluted mass spectrum under mild conditions. (C) Charge state spectrum under harsh conditions (sample cone at 100 V, extraction cone at 50 V). (D) Deconvoluted mass spectrum under harsh conditions.

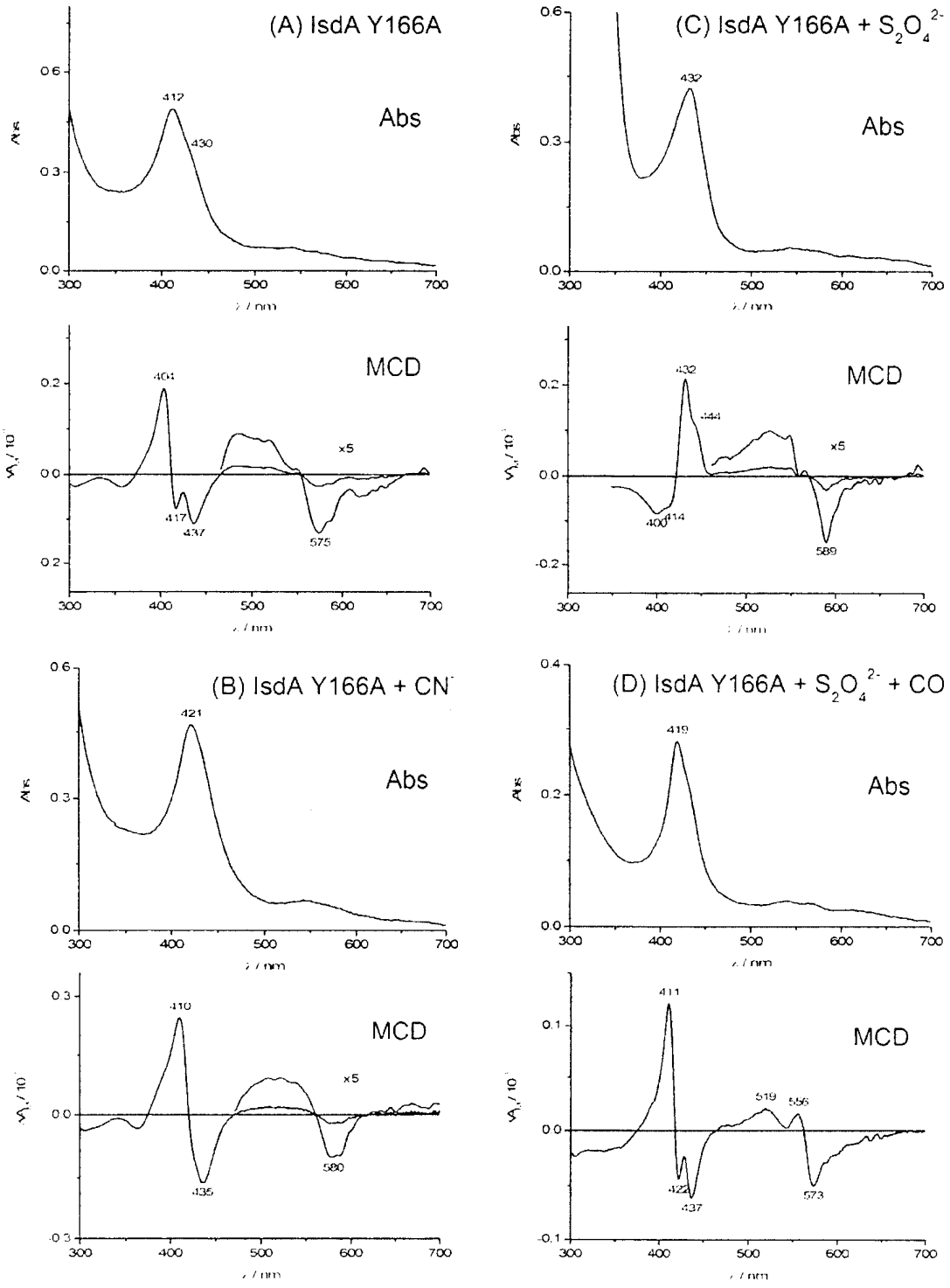

Figure 3.11. Absorption and MCD spectra of rIsdA Y166A. (A) As purified from E. coli. (B) Following the addition of crystalline aliquots of sodium cyanide. (C) Following the addition of crystalline aliquots of sodium hydrosulfite. (D) Following the addition of crystalline sodium hydrosulfite and carbon monoxide.

The spectra presented in Figure 3.11 represent rIsdA Y166A that was bound to approximately equal concentrations of heme and the unknown ligand, as shown by the corresponding mass spectrum (Figure 3.9E). Conversely, the rIsdA Y166A sample which contained a large quantity of heme, showed that the heme concentration was approximately 3x that of the unknown ligand. The absorption and MCD spectrum of this sample (Figure 3.12) were, therefore, dominated by heme and provided clearer insight into the spin and oxidation state of the heme in rIsdA Y166A. Figure 3.12 illustrates that this was the case. The overlapping signals in the B region were removed and a MCD spectrum resembling an intermediate-spin ferrous heme was obtained. The large B:Q band intensity ratio and visible region band pattern closely resembled that of intermediate-spin ferric heme myoglobin (*13, 15*), providing strong evidence for the

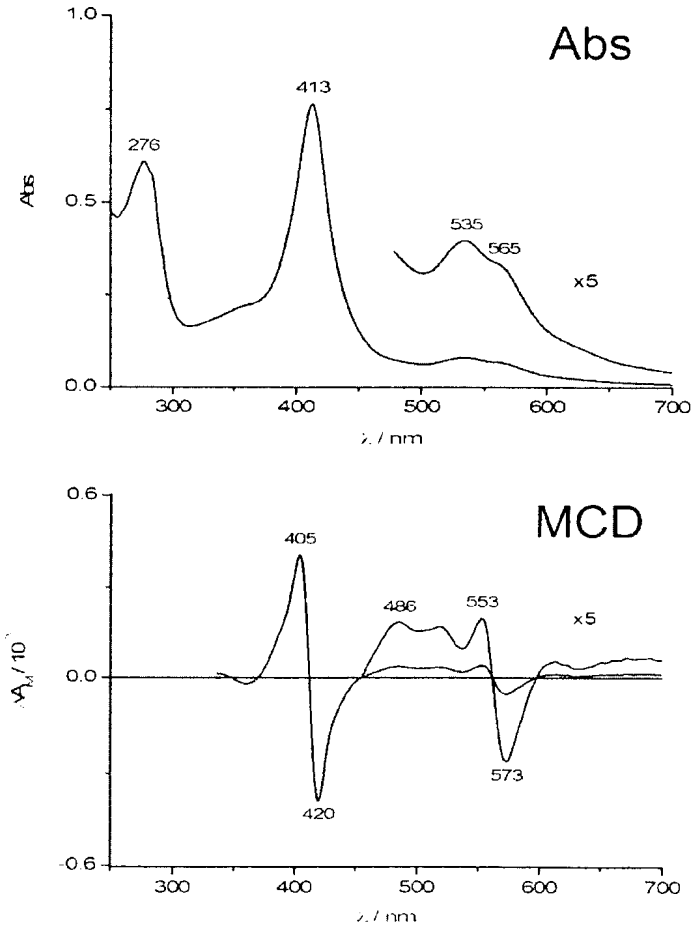

Figure 3.12. Absorption (top) and MCD (bottom) spectra of rIsdA Y166A when purified bound to a large quantity of heme.

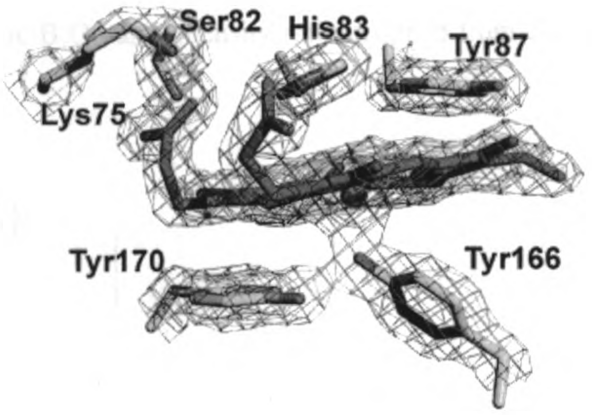

Figure 3.13. Structure of the IsdA NEAT domain heme binding pocket reported by Grigg *et al. (22)*.

presence of intermediate-spin ferric heme in rIsdA Y166A. The absence of a band at 625 nm, a high-spin ferric heme charge transfer band, offered further support for this conclusion.

The crystal structure of the IsdA NEAT domain (Figure 3.13), which has recently been published, confirmed that Y166 does in fact coordinate directly to the heme iron (*22*). Furthermore, H83, a conserved histidine residue, was shown to be located directly above the heme. To further investigate the role of H83 in IsdA, a rIsdA H83A mutant was constructed. The mass spectrum of rIsdA H83A (Figure 3.14B) showed a strong ligand free protein peak (29,982 Da), a strong single heme bound protein peak (30,595 Da), and weaker peak representing rIsdA H83A bound to an unidentified ligand of approximately 300 Da (30,280 Da). This result was very similar to that of native rIsdA.

The absorption and MCD spectra of rIsdA H83A showed that the spin and oxidation states of the heme were unaffected by the mutation (Figure 3.15A). The MCD data showed that an axially inaccessible (Figure 3.15B), high-spin ferric heme was still present. However, an unexpected result occurred following the addition of sodium hydrosulfite. Instead of generating the expected high-spin ferrous heme, the data remained consistent with high-spin ferric heme (Figure 3.15C). Even the addition of a large excess of sodium hydrosulfite did not reduce the ferric iron. Only following addition of carbon monoxide did the heme reduce to form low-spin ferrous heme. Figure 3.15D shows the two well defined A-terms, centered about 415 and 567 nm, characteristic of low spin ferrous heme. This spectrum, however, differed from that of

native rIsdA in that the B:Q band intensity ratio dropped from 2:1, as observed in native rIsdA, to 1:1.

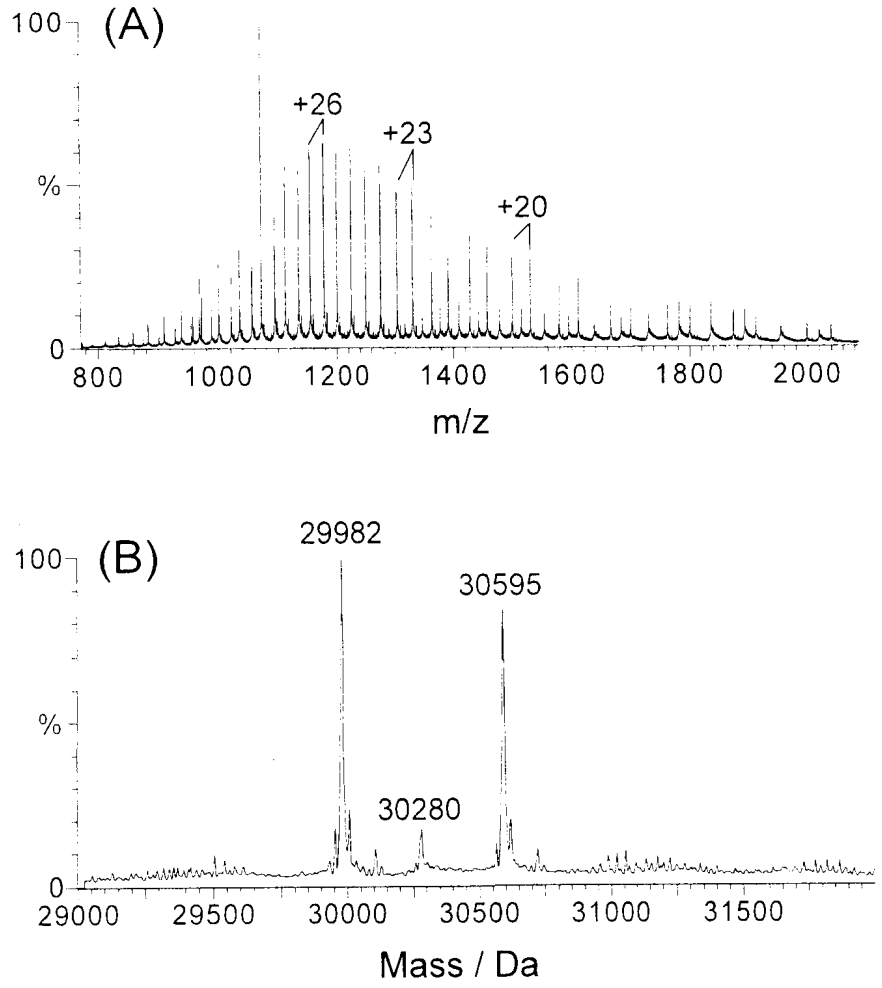

Figure 3.14. Charge state (A) and deconvoluted mass spectra (B) of rIsdA H83A. The large peak observed at 1072 m/z is due to contamination by the standard solution used to calibrate the instrument. Three pairs of charge states are indicated to aid in the assignment (at +20, +23, and +26.)

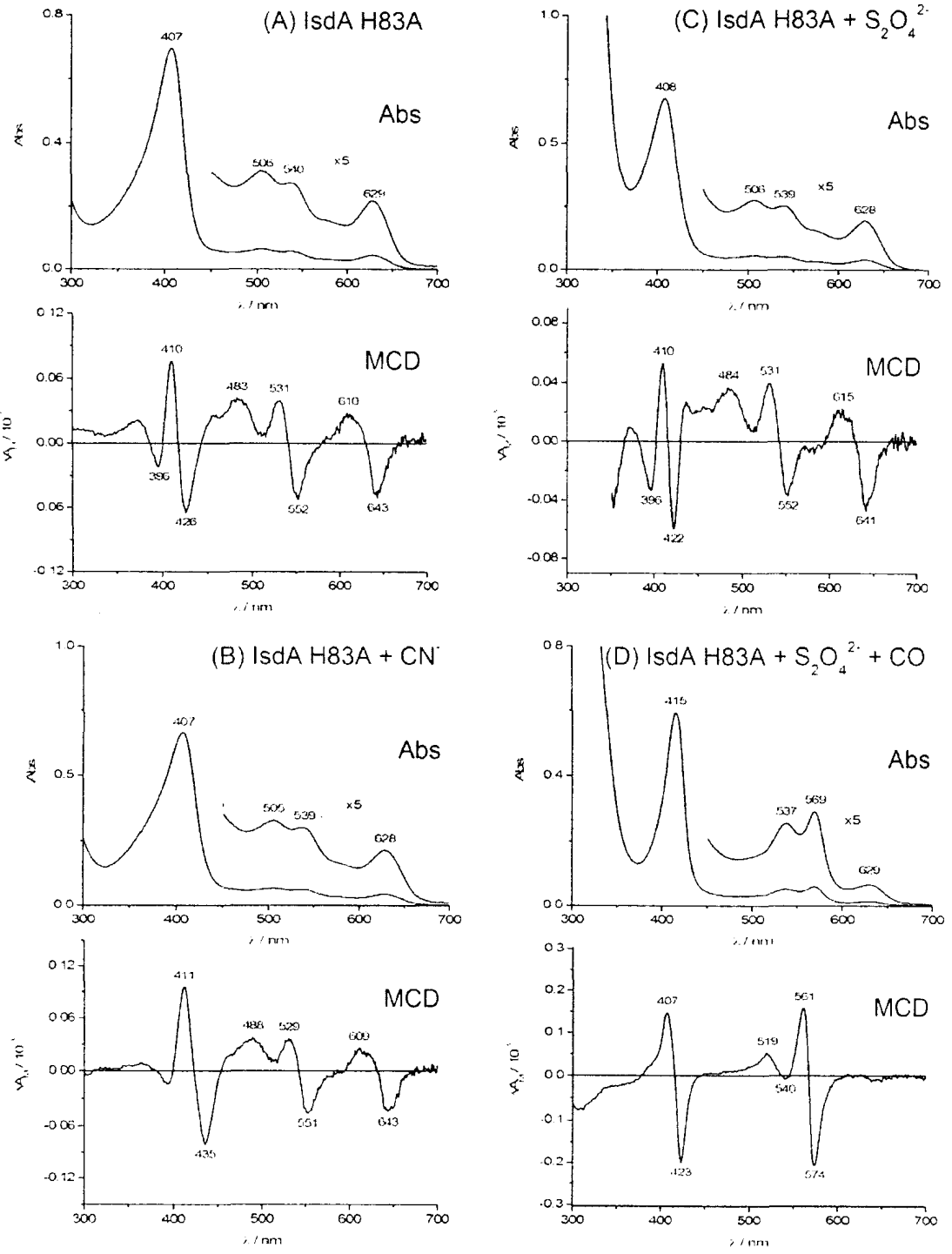

Figure 3.15. Absorption and MCD spectra of rIsdA H83A. (A) As purified from *E. coli*. (B) Following the addition of crystalline aliquots of sodium cyanide. (C) Following the addition of crystalline aliquots of sodium hydrosulfite. No change was observed even following the addition of a large excess of the reducing agent. (D) Following the addition of crystalline sodium hydrosulfite and carbon monoxide.

3.4 Discussion

The ESI-MS data in this study clearly demonstrate that rIsdA binds one heme group (Figure 3.4B). The charge state distributions for the protein with and without the heme are similar, which indicates that there is little rearrangement of the protein secondary or tertiary structures upon heme loss (Figure 3.4A). Denaturation of rIsdA takes place at low pH with an associated large shift in charge state maximum from +29 to +35 and the loss of heme (Figure 3.4C). It is considered that the more the charge state distribution shifts towards greater protonation, the more open, and more random the protein structure (*23, 24*). Following denaturation, two dominant envelopes of bands are observed in the mass spectra shown in Figure 3.4C, both arise from the same molecular mass (Figure 3.4D), neither set includes the heme. The charge states centered on +26 are the same as for the native rIsdA in which the heme is bound (except for the slight compensating reduction in mass) whereas the charge states centered on +35 appear only following acidification. The relative fraction of the more folded form of the denatured protein is approximately 30% with a charge state maximum near +26, whereas 70% adopts the more open structure with the charge states near +35. The +26 set of charge states may arise from the first stage in the unfolding process following loss of the heme. Altogether, the rIsdA ESI-MS data correlate well with analytical ultracentrifugation and gel filtration analyses that indicate that rIsdA exists as a monomer and adopts an extended conformation in solution (*6*).

Not surprisingly, given the relatively recent identification of IsdA, no information existed in the literature describing the environment of the heme bound to IsdA. Changes in the coordination environment of the heme iron, and potential 5^{th} and 6^{th} axial ligation positions above and below the plane of the porphyrinoid ring, result in MCD spectra with substantially modified band morphologies and sign sequences. Extensive studies of heme binding properties have identified a series of characteristic "fingerprint patterns" for different heme environments (*12*), which help to provide answers to a series of questions: i) How many ligands are attached to the iron in the native state and what is the nature of these coordinating ligands (nitrogen from His, sulfur from Cys, or oxygen from Tyr, for example)? ii) Can small axial ligands approach the iron? iii) Is the heme iron spin state high, intermediate or low, which relates to the binding strength of the axial ligand present

in the native state? (iv) What is the oxidation state of the central iron (Fe(II), Fe(III) and Fe(IV))?

In the experiments described here, rIsdA in solution was taken and to it added, in stepwise fashion, strong-sigma donor, anionic axial ligands known to coordinate the heme iron in its ferric state, which can result in changes in the spin state of the central metal. The absorption and MCD spectral data for myoglobin with a wide range of anionic axial ligands have been widely studied and serve as a model to compare with the rIsdA data presented here (*13, 15*). Therefore, rIsdA only partially follows the ligation properties observed with myoglobin. No ligation of cyanide takes place with the native ferric protein even in the presence of excess cyanide over periods of hours (Figure 3.6B). These experiments resolve the questions posed above and determine both the electronic structure and the environment of the bound heme.

The MCD spectral data of the rIsdA at pH 7 (Figure 3.6A) clearly indicate that the ferric iron is coordinated to a weak field ligand, most likely anionic, with tyrosine the key candidate (*16*). The MCD data closely resemble that of a number of heme proteins, including catalase in which tyrosine is known to be the proximal axial ligand. The lack of cyanide binding indicates that access to the 6^{th} position on the ferric iron is limited (in this case specifically to anionic ligands) since even in the presence of the excess of cyanide, the distal site could not be reached. Reduction to the ferrous heme, however, allowed access to CO, which suggests that the peptide relaxed in the region of the heme, possibly because the anionic tyrosine binds much more weakly to the ferrous iron. This reaction was reversible and subsequent oxidation back to the ferric again blocked access to cyanide. Reduction of the heme would have to be through an exposed edge of the heme porphyrin as the iron center is not accessible to the anionic hydrosulfite, although the mechanism for the reduction is not clear.

The conclusions on the environment of the heme in the native rIsdA are that the heme is isolated within the peptide with only an edge accessible, which resembles the situation in cytochrome c. The five-coordinate, high spin ferric iron is inaccessible to anionic axial ligands. Reduction to the ferrous state introduces access to the ferrous iron. The MCD spectral data provide strong evidence that reduction, in the absence of exogenous axial ligands, leads to the high-spin, 5-coordinate ferrous heme in which the

proximal ligand is now histidine (Figure 3.6C). Addition of CO leads to spectral data characteristic of low-spin, 6-coordinate ferrous heme, in which the proximal group is also histidine (Figure 3.6D). These MCD spectral data are almost identical to the well known data of myoglobin. However, reoxidation again closes access, providing evidence that the heme has not moved during this chemical process, which suggests that the heme environment is quite stable with respect to chemistry taking place at the heme. In this ferric state, the lack of anionic access, and the band maxima and MCD spectral pattern, again indicate that the proximal group is tyrosine. These results suggest that different residues coordinate the heme under these different redox states.

The NEAT domain in IsdA, which was also included in the rIsdA construct used in this study, contains several tyrosine residues that could function as a coordinating ligand of the heme molecule. Notably, Y87, Y102, Y166, and Y170 are conserved in the NEAT domains of IsdA and IsdC which bind heme (*20, 21*), and also the C-terminal NEAT domains of HarA/IsdH and IsdB from *S. aureus*. Notably, Pilpa *et al.* (*20*) have shown that the most N-terminal NEAT domain of IsdH/HarA does not bind heme and lacks these conserved tyrosines, lending support to the idea that at least one of these conserved tyrosines plays an integral role in heme binding. It is interesting to note that of several histidine residues present within IsdA only one, His83, is partially conserved among IsdA, IsdB, IsdC, and HarA/IsdH NEAT domains, and may be the residue that provides axial ligation for the heme iron when in the high-spin reduced state, provided that the heme is similarly bound by these other NEAT domains.

The mass spectra of rIsdA Y166A shows that replacement of the tyrosine phenolate group with a methyl group, heme binding is greatly reduced compared to that of native rIsdA (Figure 3.9). The appearance of additional peaks, approximately 305 Da higher in mass, suggests that upon removal of Y166, the reduction in heme binding affinity allows for the coordination of other ligands into the rIsdA binding pocket. Alternatively, the presence of a second ligand could suggest that the ligand binding restrictions are somewhat reduced and, therefore, rIsdA Y166A picks up a second ligand during expression in *E. coli*. Described in later chapters of this thesis, a peak of similar mass also appears for both rIsdC and rIsdE, suggesting it is not mere chance that this ligand is present.

The absorption spectrum of native rIsdA shows that the B band is observed at 407 nm (Figure 3.8). In rIsdA Y166A that band is blue shifted to 412 nm, with a second band appearing as a shoulder at approximately 430 nm (Figure 3.11A). This dual band is more evident in the MCD spectrum, which clearly shows the overlap between the two derivative shaped bands giving rise to two negative peaks at 417 and 437 nm. These overlapping of bands may suggest that two different heme coordinations exist in rIsdA Y166A. Many iron containing hydroxamate siderophores have strong absorptions in the 400-440 nm range (*25*), which arise from charge transfer between the hydroxyl groups of the siderophore and central ferric-iron atom. However, their extinction coefficients (approximately 10^3) are orders of magnitude smaller than those of heme (approximately 10^5) and would not exert such a major influence on the absorption and MCD spectra (*26, 27*). Removal of Y166 may result in two different orientations of bound heme molecules, and this gives rise to the overlapping signals. Following the addition of ligands (CN^- and CO) and a reducing agent ($Na_2S_2O_4$) the shift in the overlapping band pattern in the B region of the spectra appeared to parallel each other, offering support for this conclusion. Why then do these odd band patterns disappear when the quantity of heme bound to the protein is increased? The bands appearing in Figure 3.12 can also be identified in Figure 3.11A, with the only major difference being the presence of a negative 437 nm peak in Figure 3.11A. This would suggest that the unknown ligand is causing the 437 nm band, possibly through an interaction with bound heme, and that only when its concentration is comparable to that of the heme, are the resulting spectral bands observed. Evidently, future work is required to resolve this issue. Identification of the unknown ligand, and subsequent MCD analysis would most likely provide the answer.

In summary rIsdA binds a high-spin ferric heme through residue Y166 of the NEAT domain. These results provide strong evidence for the involvement of the NEAT domain in heme binding. Similar results may be expected upon analysis of rIsdC and HarA/IsdH, the other NEAT domain containing proteins of the Isd system. rIsdA has also been shown to bind a ligand other than heme-*b*. Although its identity remains unknown, its reappearance in the mass spectra of both rIsdC and rIsdE suggests it plays an actual role in the functioning of *S. aureus*. This, however, is yet to be confirmed.

3.5 References

1. Clarke, S. R., Wiltshire, M. D., and Foster, S. J. (2004) IsdA of *Staphylococcus aureus* is a broad spectrum iron-regulated adhesin, *Mol. Microbiol. 51*, 1509-1519.
2. Mazmanian, S. K., Skaar, E. P., Gaspar, A. H., Humayun, M., Gornicki., P., Jelenska, J., Joachmiak, A., Missiakas, D. M., and Schneewind, O. (2003) Passage of heme-iron across the envelope of *Staphylococcus aureus*, *Science 299*, 906-909.
3. Navarre, W. W., Ton-That, H., Faull, K. F., and Schneewind, O. (1998) Anchor structure of Staphylococcal surface proteins, *J. Biol. Chem. 273*, 29135-29142.
4. Yocum, R. R., Waxman, D. J., Rasmussen, J. R., and Strominger, J. L. (1979) Mechanism of penicillin action: Penicillin and substrate bind covalently to the same active site serine in two bacterail D-alanine carboxypeptidases., *Proc. Nat. Acad. Sci. U.S.A. 76.*
5. Mazmanian, S. K., Ton-That, H., Su, K., and Schneewind, O. (2002) An iron-regulated sortase anchors a class of surface protein during *Staphylococcus aureus* pathogenesis, *Proc. Nat. Acad. Sci. U.S.A. 99*, 2293-2298.
6. Vermeiren, C. L., Pluym, M., Mack, J., Heinrichs, D. E., and Stillman, M. J. (2006) Characterization of the heme binding properties of *Staphylococcus aureus* IsdA, *Biochemistry 45*, 12867-12875.
7. Maresso, A. W., and Schneewind, O. (2006) Iron acquisition and transport in *Staphylococcus aureus*, *Biometals 19*, 193-203.
8. Boekhorst, J., Been, M. W. d.. Kleerebezem, M., and Siezen, R. (2005) Genome-wide detection and analysis of cell wall-bound proteins with LPxTG-like sorting motifs, *J. Bacteriol. 187*, 4928-4934.
9. Andrade, M. A., Ciccarelli, F. D., Perez-Iratxeta, C., and Bork, P. (2002) NEAT: a domain duplicated in genes near the components of a putative Fe^{3+} siderophore transporter from Gram-positive pathogenic bacteria, *Genome Biology 3*, 0047.0041-0047.0045.

10. Dryla, A., Glebmann, D., Gabain, A. v., and Nagy, E. (2003) Identification of a novel iron regulated staphylococcal surface protein with haptoglobin-haemoglobin binding activity, *Mol. Microbiol. 49*, 37-53.

11. Taylor, J. M., and Heinrichs, D. E. (2002) Transferrin binding in *Staphylococcus aureus*: Involvement of a cell wall anchored protein, *Mol. Microbiol. 43*, 1603-1614.

12. Cheek, J., and Dawson, J. H. (2000) in *The handbook of porphyrins and related macrocycles* (Kadish, K. M., Smith, K. M., and Guilard, R., Eds.), pp 339-369, Academic press, New York.

13. Vickery, L., Nozawa, T., and Sauer, K. (1976) Magnetic circular dichroism studies of myoglobin complexes. Correlations with heme spin state and axial ligation, *J. Am. Chem. Soc. 98*, 343-350.

14. Springall, J., Stillman, M. J., and Thomson, A. J. (1976) Low temperature magnetic circular dichroism spectra of met- and myoglobin derivatives, *Biochim. Biophys. Acta. 453*, 494-501.

15. Pluym, M. (2005) Characterizing the heme binding properties of Staphylococcus aureus iron-regulated surface determinant protein A., in *Chemistry* University of Western Ontario, London.

16. Eakanunkul, S., Lukat-Rodgers, G. S., Sumithran, S., Ghosh, A., Rodgers, K. R., Dawson, J. H., and Wilks, A. (2005) Characterization of the periplasmic heme-binding protein ShuT from the heme uptake system of *Shigella dysenteriae*, *Biochemistry 44*, 13179-13191.

17. Browett, W. R., and Stillman, M. J. (1984) Temperature dependence in the absorption spectra of beef liver catalase, *Biophys. Chem. 19*, 311-320.

18. Browett, W. R., and Stillman, M. J. (1979) Magnetic circular dichroism studies of bovine liver catalase, *Biochim. Biophys. Acta. 577*, 291-306.

19. Schejter, A., Ryan, M. D., Blizzard, E. R., Zhang, C., Margoliash, E., and Feinberg, B. A. (2006) The redox couple of the cytochrome c cyanide complex: The contribution of heme iron ligation to the structural stability, chemical, reactivity, and physiological behavior of horse cytochrome c, *Protein Sci. 15*, 234-241.

20. Pilpa, R. M., Fadeev, E. A., Villareal, V. A., Wong, M. L., Phillips, M., and Clubb, R. T. (2006) Solution structure of the NEAT domain (NEAr Transporter) domain from IsdH/HarA: The human hemoglobin receptor in *Staphylococcus aureus*, *J. Mol. Biol. 360*, 435-447.

21. Mack, J., Vermeiren, C., Heinrichs, D. E., and Stillman, M. J. (2004) In vivo heme scavenging by *Staphylococcus aureus* IsdC and IsdE proteins, *Biochem. Biophys. Res. Comm. 320*, 781-788.

22. Grigg, J. C., Vermeiren, C. L., Heinrichs, D. E., and Murphy, M. E. P. (2006) Haem recognition by a *Staphylococcus aureus* NEAT domain, *Mol. Microbiol.*

23. Cunsolo, V., Foti, S., Rosa, C. L., Saletti, R., Canters, G. W., and Verbeet, M. P. (2003) Monitoring of unfolding of metallo-proteins by electrospray ionization mass spectrometry, *J. Mass Spec. 38*, 502-509.

24. Konnermann, L., and Douglas, D. J. (1997) Acid-induced unfolding of cytochrome c at different methanol concentrations: Electrospray ionization mass spectrometry specifically monitors changes in the tertiary structure, *Biochemistry 36*, 12296-12302.

25. Brickman, T. J., Hansel, J. G., Miller, M. J., and Armstrong, S. K. (1996) Purification, spectroscopic analysis and biological activity of the macrocyclic dihydroxamate siderophore alcaligin of *Bordetella pertussis* and *Bordetella bronchiseptica*, *BioMetals 9*, 191-203.

26. Karpishin, T. B., Gebhard, M. S., Solomon, E. I., and Raymond, K. N. (1991) Spectroscopic studies of the electronic structure of iron (III) tris (catecholates), *J. Am. Chem. Soc. 113*, 2977-2984.

27. Dolphin, D. (1978) The Porphyrins, *Academic Press 3*.

Chapter 4: Iron regulated surface determinant protein C (IsdC)

4.1 Introduction

IsdC is a relatively small (15 kDa) heme binding protein buried within the cell wall of *S. aureus (1)*. As synthesized in the bacterial cytoplasm it consists of an N-terminal signal sequence, a single NEAT domain, and a C-terminal hydrophobic domain containing an NPQTN sorting signal (Figure 4.1) (*2-4*). The enzyme sortase B (SrtB) recognizes the NPQTN sequence and catalyzes the linkage of IsdC to the cell wall, in a fashion very similar to SrtA and IsdA (section 3.1) (*3, 5, 6*). A recent study showed that *Bacillus anthracis* IsdC, which contains a similar NPKTG sorting signal, is cleaved by SrtB between the threonine and glycine residues (*3*). Linkage occurs through the threonine carboxyl group of IsdC and the N-terminal amino group of a pentaglycine cross-bridge in the cell wall. This implies that *S. aureus* IsdC is cleaved between the threonine and asparagines residues found in the sorting signal. Unlike SrtA, which has numerous protein substrates, SrtB has very few. In fact, bioinformatics studies have failed to show other surface proteins in *S. aureus* which contain an NPQTN sorting signal, other than IsdC (*5*).

Proteinase K digestion studies have demonstrated that, unlike the surface proteins HarA/IsdH, IsdA and IsdB, IsdC is completely sealed within the cell wall envelope (*1*). Due to its location, IsdC has been proposed to function as a heme transfer protein, shuttling heme from the surface proteins IsdA, IsdB, and HarA/IsdH to the membrane proteins IsdD, IsdE, and IsdF (*1, 7, 8*). So far, very few studies on the heme binding properties of IsdC and its function in the Isd heme transport mechanism have been reported. The ability of IsdC to bind heme and it's preference to bind PPIX comprises all that has been reported for IsdC (*1, 4*). This study is aimed at further characterizing the PPIX and heme binding properties of IsdC.

```
1     MKNILKVFNT TILALIIIIA TFSNSANAAD SGTLNYEVYK YNTNDTSIAN
51    DYFNKPAKYI KKNGKLYVQI TVNHSHWITG MSIEGHKENI ISKNTAKDER
101   TSEFEVSKLN GKIDGKIDVY IDEKVNGKPF KYDHHYNITY KFNGPTDVAG
151   ANAPGKDDKN SASGSDKGSD GTTTGQSESN SSNKDKVENP QTNAGTPAYI
201   YTIPVASLAL LIAITLFVRK KSKGNVE
```

Figure 4.1. Amino acid sequence of IsdC of *S. aureus*. Underlined is the amino acid sequence of rIsdC. In blue is the IsdC NEAT domain. In red is the NPQTN sorting sequence through which linkage to the cell wall occurs.

A substantial part of this chapter is to be published in *The Journal of Porphyrins and Phthalocyanines* [Pluym, M., Vermeiren, C. L., Mack, J., Heinrichs, D. E., and Stillman, M. J. (2007) Protoporphyrin IX and heme binding properties of *S. aureus* IsdC.] This work was carried out in collaboration with Dr. D. E. Heinrichs' group, Department of Microbiology and Immunology, University of Western Ontario.

4.2 Experimental procedures

4.2.1 rIsdC protein preparation

Refer to section 2.2.1.

4.2.2 Mass spectrometry sample preparation and measurement

Refer to section 2.2.3. The mass spectrometer settings listing in Table 4.1 proved to optimize the signal when analyzing rIsdC. The remaining settings showed some inconsistency and were tuned individually during each run.

Table 4.1. Micromass LCT-MS settings used for measuring samples of rIsdC.

Capillary (V)	3500
Sample cone (V)	25-50
Extraction cone (V)	5-15
Desolvation temp. (^{0}C)	20
Source temp. (^{0}C)	80

4.2.3 UV-visible absorption and MCD spectroscopy sample preparation

Refer to section 2.2.3

4.2.4 Photobleaching PPIX

Stock PPIX-dimethyl ester (Sigma-Aldrich) was dissolved in 2-butanone and diluted to give an absorption below 1.5. A quartz-iodine lamp (90 V; 250 W) was then shone on the sample cuvette for 5, 10, 15 and 30 min intervals. Absorption spectra were recorded immediately following irradiation.

4.3 Results

4.3.1 rIsdC binds PPIX and heme

Purified rIsdC retained an intense red colour, indicative of its ability to scavenge protoporphyrin and heme from within *E. coli (4).* Figure 4.2 shows the similar appearance of PPIX dimethyl ester (PPIX-DME) to rIsdC, supporting the conclusion that rIsdC primarily bound PPIX (*4*). ESI-MS data can readily identify the presence of both protein-bound and unbound porphyrin in any given sample through the masses of each

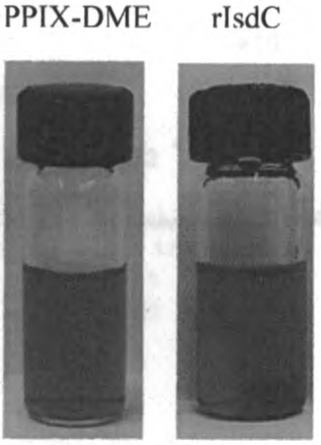

Figure 4.2. Sample vials containing (A) PPIX dimethyl ester in 2-butanone and (B) rIsdC as purified from *E. coli.*

species if the conditions are soft enough to allow the porphyrin bound to the protein to remain undissociated (*9*). In the presence of multiple compounds, as in the case of rIsdC, information regarding the relative amounts of each component can also be obtained. The charge state and deconvoluted mass spectra of rIsdC were measured under soft ionization conditions and are shown in Figure 4.3. The intense peak at 564 m/z (charge +1) was from PPIX (Figure 4.3A). In the 1,000 – 2,500 m/z region several charge state distributions representing rIsdC were observed (Figure 4.3B). The peak at 19,759 Da (Figure 4.3C) corresponded to PPIX-free and heme-free rIsdC. The peak at 20,375 Da was due to heme-bound IsdC. The lack of a peak at 20,323 Da (Figure 4.3C) and the strong PPIX peak (Figure 4.3A) showed that PPIX did not remain bound to rIsdC during ESI-MS analysis even though the experimental conditions allowed for the iron-containing heme to remain bound. That PPIX was observed for solutions rigorously purified on gel columns indicated very weak association between the protein and the iron-free PPIX.

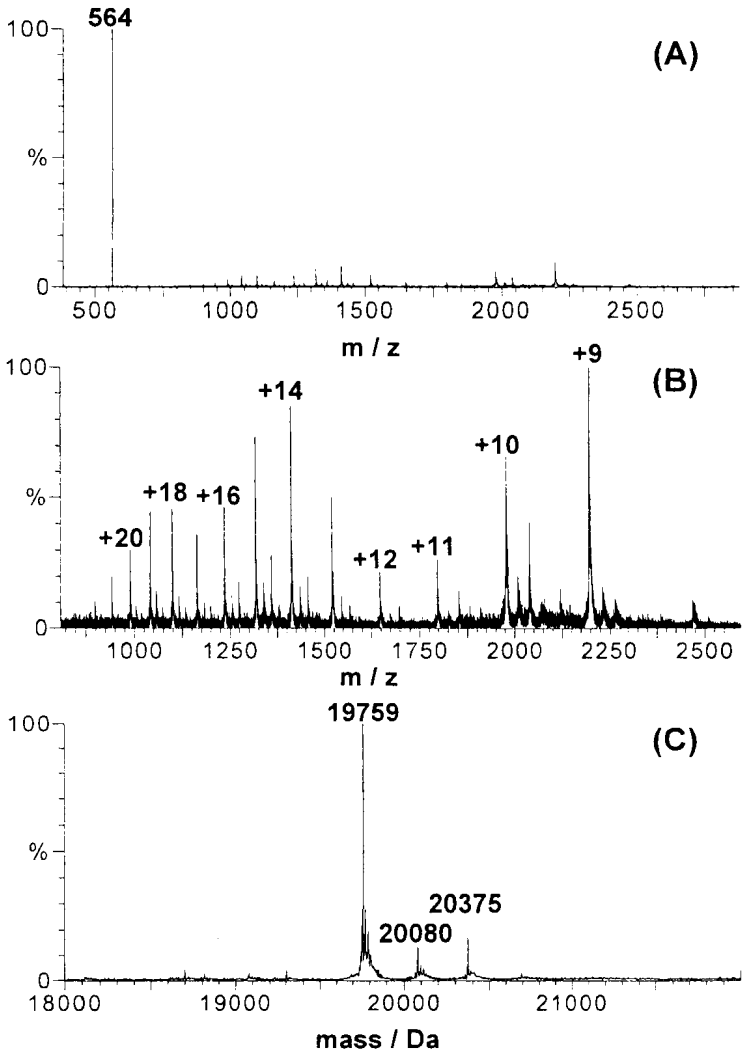

Figure 4.3. Charge state and deconvoluted mass spectra of rIsdC. (A) The entire scan range. (B) Expansion of the 1000-2500 m/z region showing the rIsdC charge states. (C) The deconvoluted mass spectrum of rIsdC.

There was no sign of multiple porphyrin (heme or PPIX) binding. The identity of the peak at 20,080 Da remains unknown, however, the mass increase of 321 Da is fairly close to that observed for rIsdA Y166A (305 Da). Furthermore, a similar peak also appears in the mass spectrum of IsdE (Chapter 5).

4.3.2 rIsdC heme binding properties

Lysates of rIsdC were previously reported to bind primarily PPIX with traces of low spin ferric and ferrous hemes (*4*). The absorption and MCD spectra of PPIX are shown in Figure 4.4. Figure 4.5A clearly shows the PPIX influence on the spectral data of rIsdC, in that four distinct bands arising from PPIX were observed in the visible region of the spectrum. The additional peak appearing in the UV-visible absorption spectrum at 669 nm is characteristic of PPIX degradation (*10*). A band at 668 nm appeared following irradiation of a PPIX dimethyl ester solution, with visible light for 15 minutes (Figure 4.6). This coincided with a reduction in the intensity of the PPIX absorption bands at 504, 538, 576 and 631 nm. Irradiation for 30 minutes resulted in complete decomposition of the PPIX.

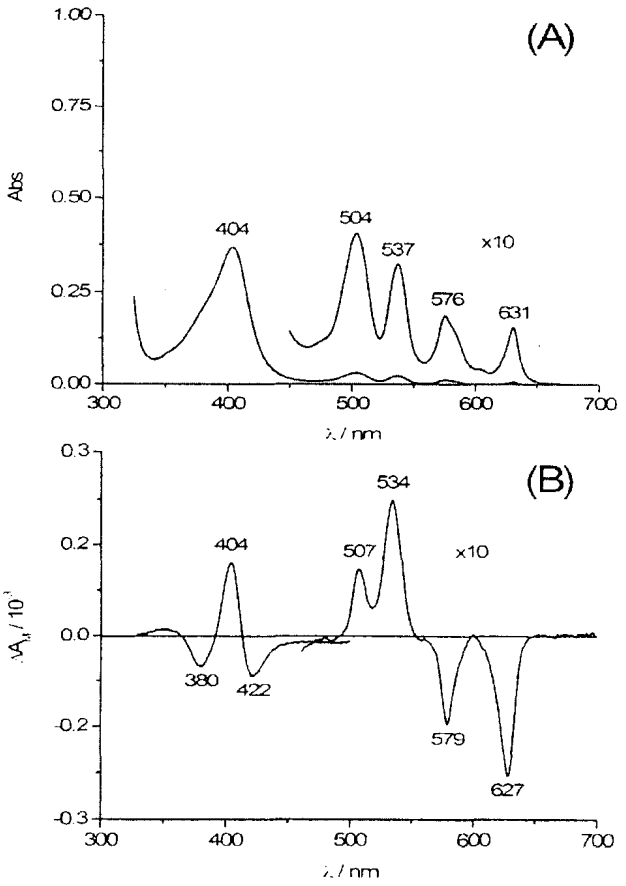

Figure 4.4. (A) Absorption and (B) MCD spectra of PPIX dimethyl ester in 2-butanone.

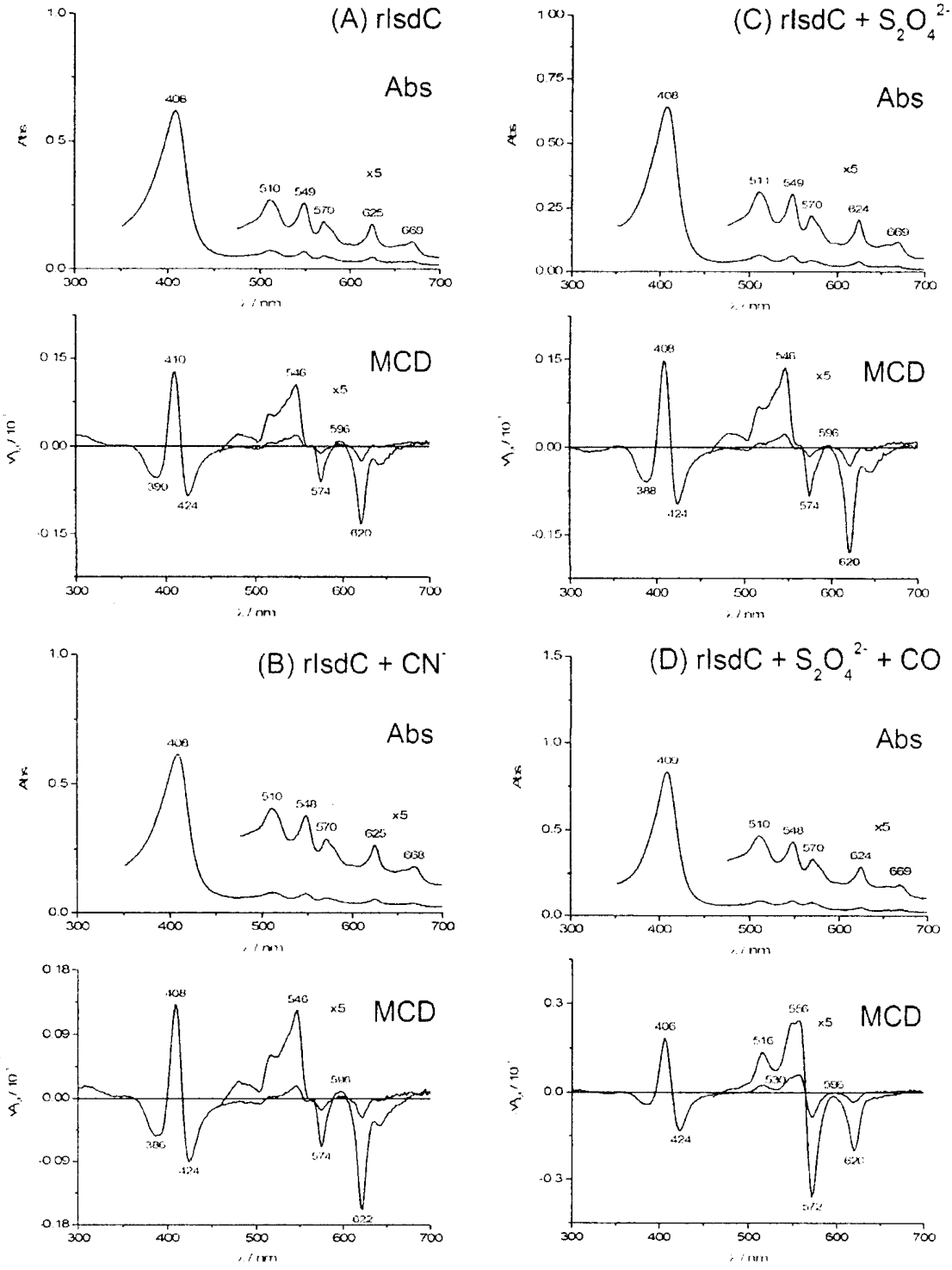

Figure 4.5. Absorption and MCD spectra of rIsdC. (A) As it is purified from *E. coli,* (B) with the addition of sodium cyanide, (C) with the addition of sodium hydrosulfite, (D) with the addition of sodium hydrosulfite and carbon monoxide.

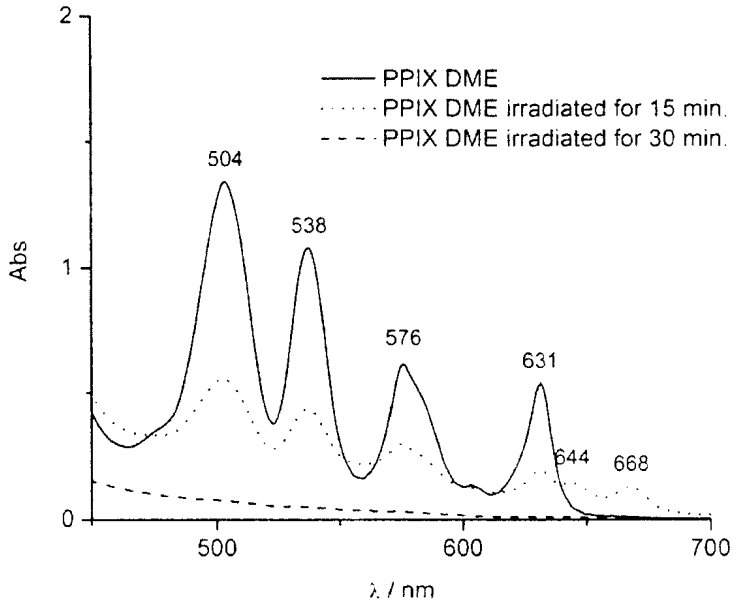

Figure 4.6. Absorption spectra of PPIX in 2-butanone immediately following preparation and following irradiation with a quartz iodine lamp for 15 and 30 minutes.

The MCD spectrum of the isolated rIsdC is complex due to superposition of spectral bands from both the iron-free PPIX and from heme, which contribute overlapping bands throughout the visible region. Nevertheless, the four characteristic bands arising from PPIX, at 510, 549, 570 and 625 nm (Figure 4.5A) were clearly observed in the absorption and MCD spectra. The slight shifts in wavelength of the MCD signals compared with those of PPIX were most likely a result of the interaction between the protein and bound PPIX (*11*). The addition of ligands such as cyanide (Figure 4.5B), azide, and fluoride (both identical to Figure 4.5B) to the solution resulted in very little change in the either the absorption or MCD spectrum. Addition of $Na_2S_2O_4$ also resulted in little change (Figure 4.5C). However, addition of CO to a sealed solution of rIsdC containing $Na_2S_2O_4$ resulted in the appearance of a band at 556 nm in the MCD spectrum (Figure 4.5D). Intensification and a slight shift of the peak at 574 nm were also observed. The CO complex of ferrous heme exhibits very narrow bands, which allows identification in the presence of other spectral features more easily than for weak field ligands (*11, 12*).

4.4 Discussion

Previous reports based on analysis of the MCD spectra of *E. coli* lysates containing over-expressed rIsdC indicated that the primary species bound by rIsdC was PPIX, although minimal traces of heme were also observed (*4*). In the current study presents much more detailed spectroscopic data from purified rIsdC protein and provides further critical detail from new ESI-MS measurements regarding the PPIX and heme binding properties of rIsdC. The mass spectrum of purified rIsdC (Figure 4.3A) shows that the primary species scavenged from within the *E. coli* cell is, as previously proposed, PPIX. Given that chromatographic purification would have removed both unbound heme and unbound PPIX, the fact that unbound PPIX is observed in the mass spectrum suggests that PPIX was bound to rIsdC in solution following purification and that this binding is much weaker than that of the heme, possibly relying on $\pi-\pi$ interactions and/or propionic side chain interactions. The dominant PPIX- and heme-free rIsdC peak (Figure 4.3C) reasonably results from the dissociation of PPIX from the protein during ESI-MS analysis. The lack of a peak at 20,323 Da (the mass of rIsdC + PPIX) suggests that without coordination to the iron, PPIX is only weakly bound to the protein and that the ESI-MS conditions are too harsh to maintain binding. The presence of rIsdC with bound heme (20,375 Da) also signifies the increased binding strength when rIsdC is able to coordinate to the heme iron.

The absorption and MCD spectra of rIsdC show a major contribution from bound PPIX with lesser contribution from heme (Figure 4.5A) (*4, 12*). This is in sharp contrast to the MCD spectra of IsdA and IsdE proteins where the primary species bound is heme. The MCD spectrum of the iron-free PPIX is distinctive because due to the reduction in symmetry from D_{4h} to D_{2h} upon removal of the iron atom, the Q band transition splits (*13, 14*). Each of the split transitions has its own vibronic overtone and, therefore, four bands are observed. The data show that the bound heme in rIsdC is reducible and capable of ligation in the reduced state. Addition of $S_2O_4^{2-}$ as a reducing agent, and CO as a strong field ligand to rIsdC under reducing conditions does produce a distinct change in the visible region of the MCD spectra (Figure 4.5D). A new peak at 556 nm and intensification of the peak at 572 nm, in relation to the 620 nm band, are observed. This

is the result of the overlap of an A term from a low spin ferrous heme with a B term from the PPIX.

The question of the oxidation and spin state of this bound heme remains to be addressed. High spin ferrous heme gives a very distinct positive MCD signal at approximately 434 nm. There is no evidence of this signal in the MCD spectrum of rIsdC (Figure 4.5A). Low spin ferric heme has a very intense MCD signal in the B region. Due to the identical band morphology observed for PPIX and rIsdC it is unlikely that rIsdC binds a low spin ferric heme, since its presence would distort the B band of rIsdC away from that of PPIX. The reduced intensity of the B region in both high- and intermediate-spin ferric heme would have a smaller influence on the B region MCD bands. In light of the fact that both rIsdA and rIsdC contain a single NEAT domain and that rIsdA binds a high-spin ferric heme, it is reasonable to assume rIsdC also coordinates a high-spin ferric heme. The lack of change following cyanide addition (Figure 4.5B) is not surprising because a similar result was also observed in rIsdA.

In summary, mass spectrometry and MCD spectroscopic analysis showed that the rIsdC binds predominantly PPIX and to a lesser extent heme, unlike the case of rIsdA. The bound heme in rIsdC exhibits spectral properties characteristic of a high-spin ferric heme.

4.5 References

1. Mazmanian, S. K., Skaar, E. P., Gaspar, A. H., Humayun, M., Gornicki., P., Jelenska, J., Joachmiak, A., Missiakas, D. M., and Schneewind, O. (2003) Passage of heme-iron across the envelope of *Staphylococcus aureus*, *Science 299*, 906-909.
2. Vermeiren, C. L., Pluym, M., Mack, J., Heinrichs, D. E., and Stillman, M. J. (2006) Characterization of the heme binding properties of *Staphylococcus aureus* IsdA, *Biochemistry 45*, 12867-12875.
3. Maresso, A. W., Chapa, T. J., and Schneewind, O. (2006) Surface protein IsdC and Sortase B are required for heme-iron scavenging of *Bacillus anthracis*, *J. Bacteriol. 188*, 8145-8152.
4. Mack, J., Vermeiren, C., Heinrichs, D. E., and Stillman, M. J. (2004) In vivo heme scavenging by *Staphylococcus aureus* IsdC and IsdE proteins, *Biochem. Biophys. Res. Comm. 320*, 781-788.
5. Mazmanian, S. K., Ton-That, H., Su, K., and Schneewind, O. (2002) An iron-regulated sortase anchors a class of surface protein during *Staphylococcus aureus* pathogenesis, *Proc. Nat. Acad. Sci. U.S.A. 99*, 2293-2298.
6. Navarre, W. W., Ton-That, H., Faull, K. F., and Schneewind, O. (1998) Anchor structure of Staphylococcal surface proteins, *J. Biol. Chem. 273*, 29135-29142.
7. Maresso, A. W., and Schneewind, O. (2006) Iron acquisition and transport in *Staphylococcus aureus*, *Biometals 19*, 193-203.
8. Skaar, E. P., and Schneewind, O. (2004) Iron-regulated surface determinant (Isd) of *Staphylococcus aureus*: stealing iron from heme, *Microb. Infect. 6*, 390-397.
9. Laskin, J., and Lifshitz, C. (2006) *Principles of mass spectrometry applied to biomolecules*, John Wiley & Sons, inc., Hoboken.
10. Ericson, M. B., Grapengiesser, S., Gudmundson, F., Wennberg, A.-M., Larko, O., Moan, J., and Rosen, A. (2003) A spectroscopic study of the photobleaching of protoporphyrin IX in solution, *Lasers Med. Sci. 18*, 56-62.
11. Vickery, L., Nozawa, T., and Sauer, K. (1976) Magnetic circular dichroism studies of myoglobin complexes. Correlations with heme spin state and axial ligation, *J. Am. Chem. Soc. 98*, 343-350.

12. Cheek, J., and Dawson, J. H. (2000) in *The handbook of porphyrins and related macrocycles* (Kadish, K. M., Smith, K. M., and Guilard, R., Eds.), pp 339-369, Academic press, New York.

13. Mack, J., and Stillman, M. J. (2003) in *Handbook of porphyrins and related macrocycles* (Kadish, K. M., Smith, K. M., and Guilard, R., Eds.), p 43, Academic Press, New York.

14. Dolphin, D. (1978) The Porphyrins, *Academic Press 3*.

Chapter 5: Iron regulated surface determinant protein E (IsdE)

5.1 Introduction

Following binding at the bacterial cell surface by IsdA, IsdB and/or HarA/IsdH, scavenged heme is shuttled to the cell membrane, presumably through the action of IsdC. The membrane transport system (IsdDEF) then acts to shuttle the bound heme into the cytoplasm (*1*), where IsdG cleaves the PPIX ring releasing the central iron atom. Due to its location on the exterior side of the bacterial plasma membrane (*1, 2*), it is possible that IsdE plays a role in transferring heme from the cell wall anchored Isd proteins to IsdF, a permease (*3*), however, direct evidence for this has yet to be revealed.

Studies have shown that, along with all other Isd proteins, IsdE binds heme (*1*). MCD data on *E. coli* cell lysates containing over-expressed recombinant IsdE (rIsdE) showed that the protein bound low spin ferric and low spin ferrous hemes (*2*), however, the heme binding stoichiometry was unknown. Sequence analysis shows that the IsdE heme binding domain is distinct from the NEAT domains found in IsdA, IsdC and HarA /IsdH (*1, 4*). This brief account represents the sum of what is known of IsdE in the literature.

Examination of the IsdE amino acid sequence reveals considerable sequence homology to the bacterial iron transport protein FhuD, a component of a siderophore transport system found in Gram-negative bacteria. FhuD is capable of binding several hydroxamate siderophores, including as aerobactin, and ferrichrome (Figure 5.1) (*5*). Figure 5.2 shows a model of IsdE, based on the crystal structure of FhuD. FhuD consists of two lobes surrounding a hydrophobic siderophore binding pocket, composed

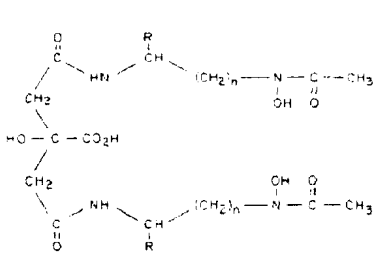

Aerobactin

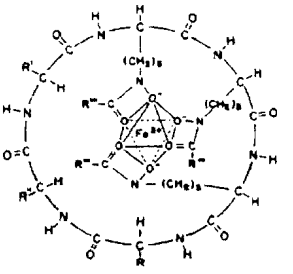

Ferrichrome

Figure 5.1. Stuctures of the hydroxamate siderophores aerobactin (R = COOH) and ferrichrome.

This work was carried out in collaboration with Dr. D. E. Heinrichs' group, Department of Microbiology and Immunology, University of Western Ontario.

primarily of aromatic residues (*3*). This siderophore binding pocket corresponds to a potential heme binding pocket in rIsdE and is outlined by the highlighted amino acid residues in Figure 5.2. These residues represent potential heme-iron coordination sites located within the pocket and as such are candidates for mutational analysis. Although there is no direct evidence for the complete accuracy of this model, it becomes a valuable tool for experimental design.

Currently, the specifics regarding IsdE heme binding remain unexplored. The heme binding stoichiometry, key amino acids involved in binding, and exact function of IsdE are currently unknown. This chapter will help shed light on the heme binding properties of IsdE and on its role in the Isd heme scavenging system.

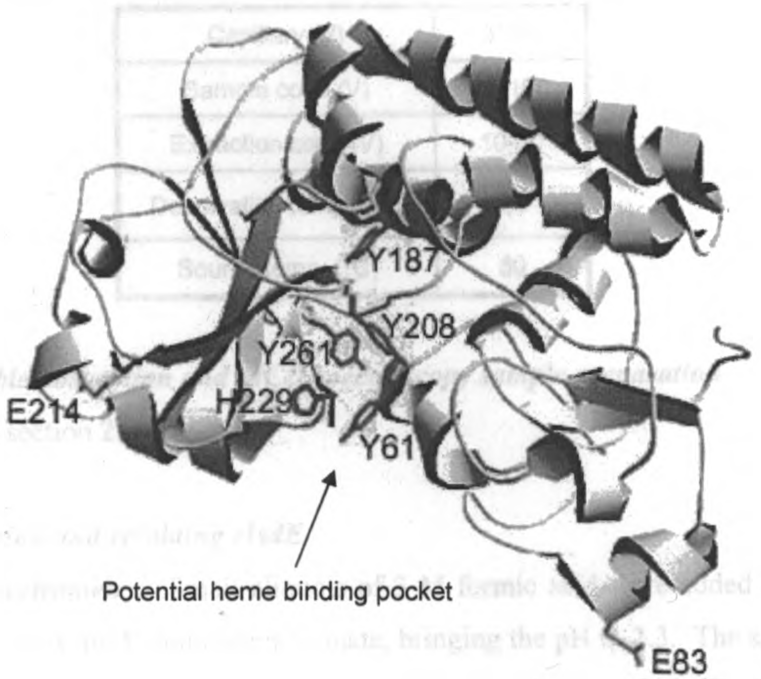

Figure 5.2. Theoretical structure of IsdE modeled on the structure of FhuD, a bacterial iron transport protein. The bilobal structure surrounds a potential heme binding pocket, highlighted by several possible heme binding residues (unpublished data from Dr. D. E. Heinrichs, Deparment of Microbiology and Immunology, University of Western Ontario.)

5.2 Experimental

5.2.1 rIsdE protein preparation

Refer to section 2.2.1.

5.2.2 Mutant rIsdE protein preparation

DNA mutations and cloning into *E. coli* were performed by Christie Vermeiren (Dr. D. E. Heinrichs' lab), Department of Microbiology and Immunology, University of Western Ontario. Mutant IsdE protein expression and purification were performed as outlined in section 2.2.1.

5.2.3 Mass spectrometry sample preparation and measurement

Table 5.1 shows the mass spectrometer settings used for rIsdE. The remaining settings showed some variance between runs and were tuned during analysis.

Table 5.1. Micromass LCT-MS settings used for the analysis of rIsdE.

Capillary (V)	3300
Sample cone (V)	75-100
Extraction cone (V)	10-30
Desolvation temp. (^{0}C)	20
Source temp. (^{0}C)	80

5.2.4 UV-visible absorption and MCD spectroscopy sample preparation

Refer to section 2.2.4.

5.2.5 Denaturing and refolding rIsdE

Mass spectrometry. Small aliquots of 3 M formic acid were added to a 1 mL sample of rIsdE in 20 mM ammonium formate, bringing the pH to 2.3. The sample was then injected into the mass spectrometer to obtain the denatured rIsdE charge state spectrum. A 500 μL sample of the acidified rIsdE solution was then placed on a G-25 size exclusion column, equilibrated with 20 mM ammonium formate (pH 7.2). The colourless eluent was collected in fractions. Each fraction was then injected into the mass spectrometer, monitoring for peaks near 2000 m/z.

UV-visible absorption spectroscopy. To a sample of rIsdE in 1x PBS, small aliquots of 3 M formic acid were added to reach a pH of 2.5. The absorption spectrum

was run immediately from 300-700 nm. Aliquots of 3 M ammonium hydroxide were then added to raise the pH to 7.5.

5.3 Results

5.3.1 rIsdE ligand stoichiometry

Following purification from *E. coli*, rIsdE gave a reddish-brown solution, a feature common among heme-containing proteins. The charge state spectrum of rIsdE (Figure 5.3A), showed a group of charge states centered on +12. Deconvolution of those states gave four distinct masses (Figure 5.3B). The theoretical mass of rIsdE is 31.11 kDa, thus, the peak at 31,112 Da represented heme-free rIsdE. 616 Da (mass of heme) higher was a very intense peak at 31,728 Da which represented single heme bound rIsdE. The small peaks appearing at 32,051 and 32,423 Da represented rIsdE bound to two unidentified ligands of approximately 323 and 634 Da, respectively. Close examination also revealed a peak approximately 320 Da higher than the heme-

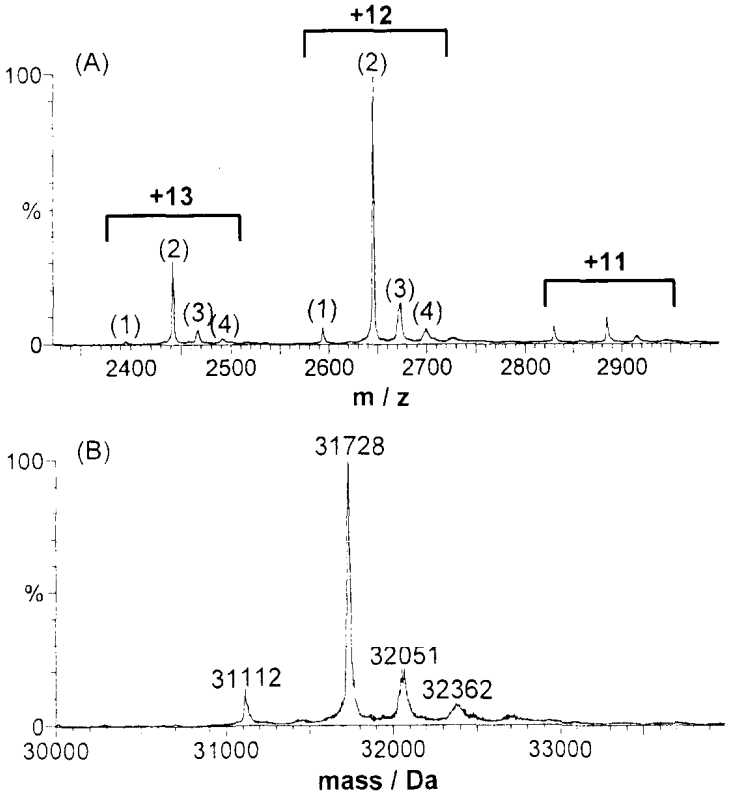

Figure 5.3. Charge state (A) and mass (B) spectra of rIsdE.

free rIsdE peak, however, this peak was very weak. The four labeled peaks in Figure 5.3B were consistently observed for multiple spectral analysis of rIsdE.

To further investigate the origin of the 320 Da increase in mass, the ligands were dissociated from rIsdE by lowering the pH. The charge state spectrum of rIsdE (neutral pH) is presented in Figure 5.4A. Following addition of formic acid, lowering the pH to 2.3, a shift in the charge state distribution was observed (Figure 5.4B). Initially dominated by the +11, +12, and +13 charge states, acidifying the solution resulted in

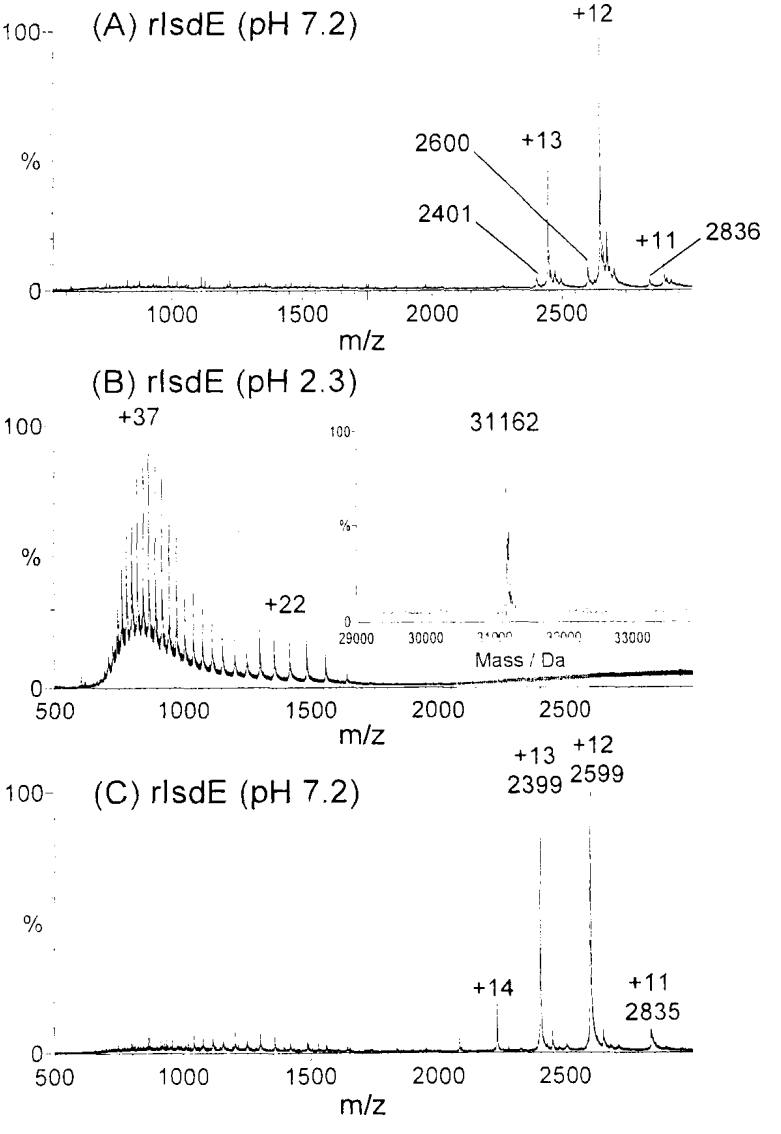

Figure 5.4. Charge state spectra of rIsdE monitoring protein folding. (A) Charge state distribution of rIsdE as purified from *E. coli* (A), following the addition of formic acid to pH 2.3 (B), and following re-neutralization to pH 7.2.

two distributions centered on +37 and separately on +22, suggesting that these forms of rIsdE were in an unfolded state (*6, 7*). Isolation of these higher charge states revealed that rIsdE is ligand free (both heme- and unidentified ligand-free) at pH 2.3, a result to be expected for an unfolded protein. The deconvoluted mass spectrum showed a single peak at 31.16 kDa (Figure 5.4B inset), very close to the theoretical mass of 31.11 kDa. This result showed that the peaks observed in the original rIsdE mass spectrum all arose from ligands bound to the same protein molecule. Cleavage products that can produce proteins of slightly different masses were, therefore, not present. Following elution from a G-25 size exclusion column, using ammonium formate buffer at pH 7.2, the charge state spectrum shown in Figure 5.4C was obtained. The reappearance of the +11-+14 charge states indicated that upon neutralization, rIsdE returned to its native conformation. The major species present in the re-neutralized sample was heme-free rIsdE (Figure 5.4C), as indicated by the intensification of the heme free rIsdE charge states at 2399, 2599, and 2835 m/z. Trace amounts of ligand-bound rIsdE were still observed, however, not nearly the amount observed for rIsdE following purification (Figure 5.4A). The small amount of ligand bound rIsdE can be attributed to the fact that rIsdE refolded near the top of the column, a location where the small ligands and large protein had only partially resolved. Once refolded, the presence of a small concentration of ligand in the direct environment of rIsdE, therefore, led to a small degree of binding.

This unfolding and refolding nature of rIsdE was supported by the UV-visible absorption data presented in Figure 5.5. Under native conditions (~pH 7.3), the B band of rIsdE was observed at 412 nm. Addition of formic acid to pH 2.5 showed a blue shift in the B band to 393 nm, a characteristic of unbound heme. Upon neutralization of the acidic solution to pH 7.5, the B band returned close to its original position at 410 nm. These results indicated that upon acidification, the bound heme was released into solution. Upon neutralization, the protein refolded and re-bound the heme present in solution, giving the 410 nm absorption band. The 2 nm shift may have been due to the presence of a slightly different mixture of ferric and ferrous hemes in the rIsdE solution following refolding.

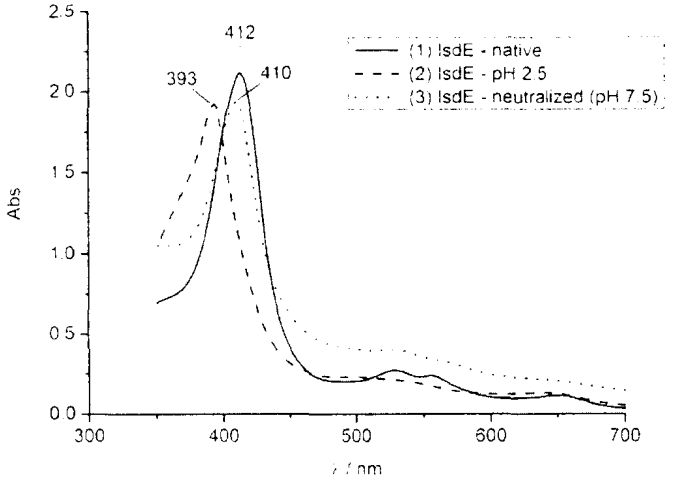

Figure 5.5. UV-visible absorption spectra of rIsdE monitoring heme binding.

5.3.2 Heme binding properties of rIsdE

The MCD spectrum of rIsdE cell lysate has been reported to contain a mixture of ferric and ferrous hemes (*2*). The MCD spectrum of purified rIsdE supported this conclusion. The combination of multiple heme species gave rise to the complex absorption and MCD spectra presented in Figure 5.6A. The overall pattern of the bands closely resembled that of a low spin ferrous heme (*8*). Absorption spectra of low-spin ferrous heme typically contain two well defined bands in the visible region, corresponding to the Q_{00} and Q_{vib} transitions. In rIsdE, these were observed at 558 and 530 nm, respectively. A third band was also observed far to the red at 650 nm. This band is thought to arise from i) the photooxidation of PPIX (*9, 10*), ii) a charge transfer band coming from a high-spin ferric heme (*11*), or iii) an electronic transition in the unidentified ligand. This band also appeared unchanged following the addition of sodium cyanide, sodium hydrosulfite, and carbon monoxide (Figure 5.6).

A major difference was observed between the MCD spectra that have been reported for low-spin ferrous hemes and that of rIsdE. The large intensity ratio between the B and Q bands for rIsdE (approximately 5:1) was much larger than those previously reported (usually closer to 2:1 or less) (*8*). Those reports, however, were based on protein solutions containing a single heme species. rIsdE contained both ferric and ferrous hemes, thus, the abnormally large B:Q intensity ratio may have resulted from the overlap of a ferric heme A term with the low-spin ferrous heme A term.

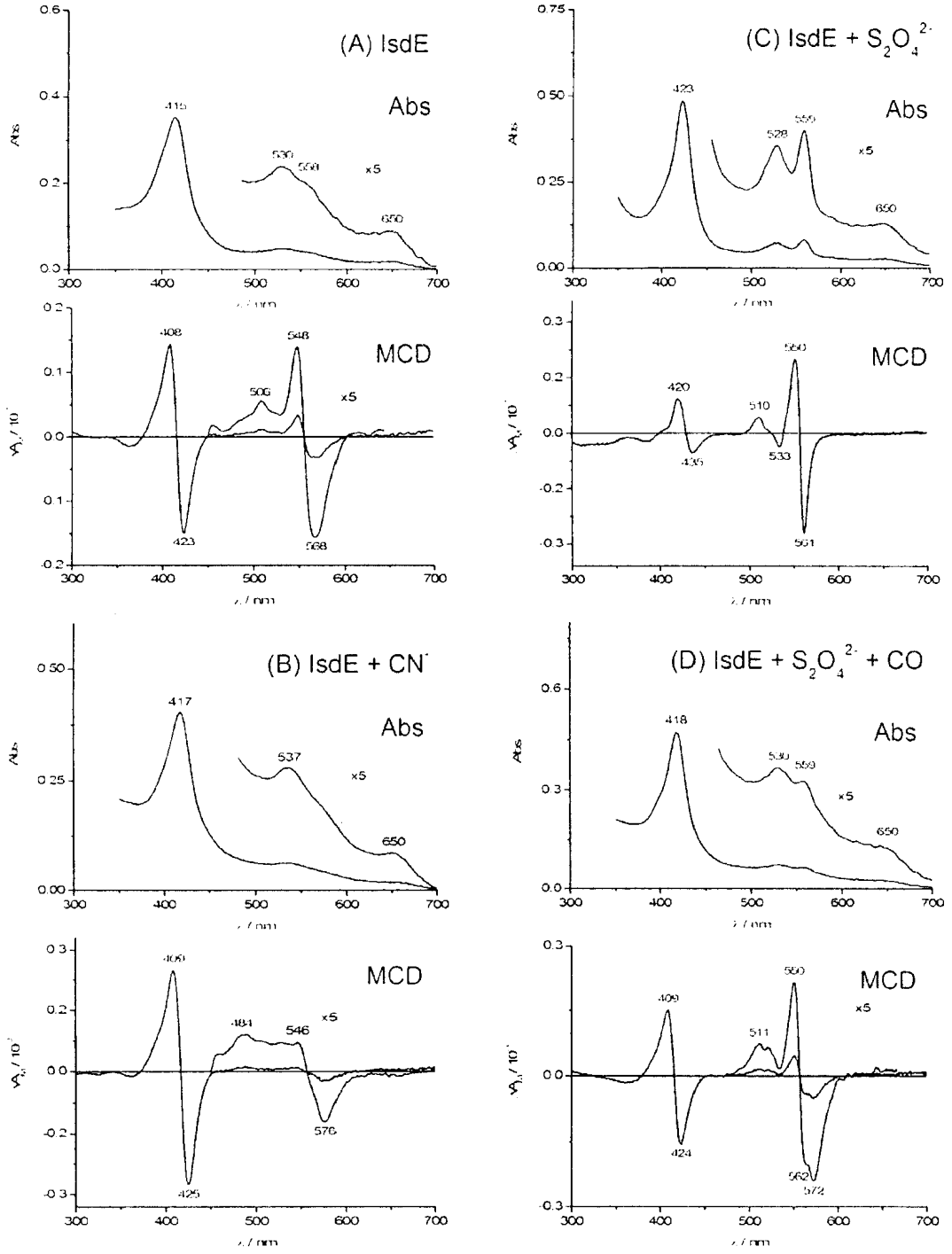

Figure 5.6. Absorption and MCD spectra of rIsdE. (A) As it is purified from *E. coli.* (B) Following the addition of sodium cyanide. (C) Following the addition of sodium hydrosulfite. (D) Following the addition of sodium hydrosulfite and carbon monoxide.

Coordination of a strong field ligand, such as cyanide, to heme results in the formation of a low-spin iron center (*8, 12*). Examination of a myoglobin heme MCD model shows that upon binding of cyanide, two main features are observed. A negative band near 580 nm appears in addition to an increase in the B:Q band intensity ratio (*8*). These features were both observed for rIsdE in the appearance of a negative band at 576 nm, and an increase in the B:Q band intensity ratio from 5:1 to approximately 10:1 (Figure 5.6B). The addition of a reducing agent to rIsdE produced a significant drop in the B band intensity, reversing the B:Q band intensity ratio from 5:1 to 1:3 (Figure 5.6C). High-spin ferrous heme gives an inverted pseudo-A term in the B region, thus, the overlap of an inverted pseudo-A term with the A term from a low-spin ferrous heme would partially cancel out the intensity in this region. It appears that upon addition of a reducing agent, the ferric heme was reduced to high-spin ferrous heme, while the low-spin ferrous heme remained unaffected. The addition of carbon monoxide to the reduced solution then brought back the B band intensity (Figure 5.6D), suggesting that both bound hemes became low-spin ferrous. The addition of carbon monoxide to rIsdE without the addition of a reducing agent resulted in no change of the MCD spectrum. The double band appearing at 562 nm and 573 nm suggests that either two slightly different low-spin ferrous hemes were present in the protein or that there was incomplete ligation of carbon monoxide. Collectively, Figures 5.3 and 5.6 show that ferric heme (unknown spin state) and low-spin ferrous heme coordinated to rIsdE. Access to the ferrous heme distal site was restricted, however, access to ferric heme was possible for small anionic ligands such as cyanide.

Periodically, a green solution of rIsdE was isolated from *E. coli* in place of the usual reddish-brown solution (Figure 5.7). The mass spectra of the two different solutions show that the color change was related to the loss of the strong single heme bound peak (Figure 5.8). This was illustrated by the dominance of the charge states at 2400, 2600, and 2838 m/z, which represent ligand-free rIsdE. Low spin ferrous heme produces a deep red solution, which can be seen in myoglobin with carbon monoxide axially coordinated to the heme (*13*). The green color observed was similar to that of

high-spin ferric myoglobin (*13*), indicating that rIsdE contained high-spin ferric heme. The PPIX photooxidation product biliverdin, however, also exhibits a greenish color (*14*).

Figure 5.7. Sample vials containing reddish-brown (left) and green (right) solutions of rIsdE.

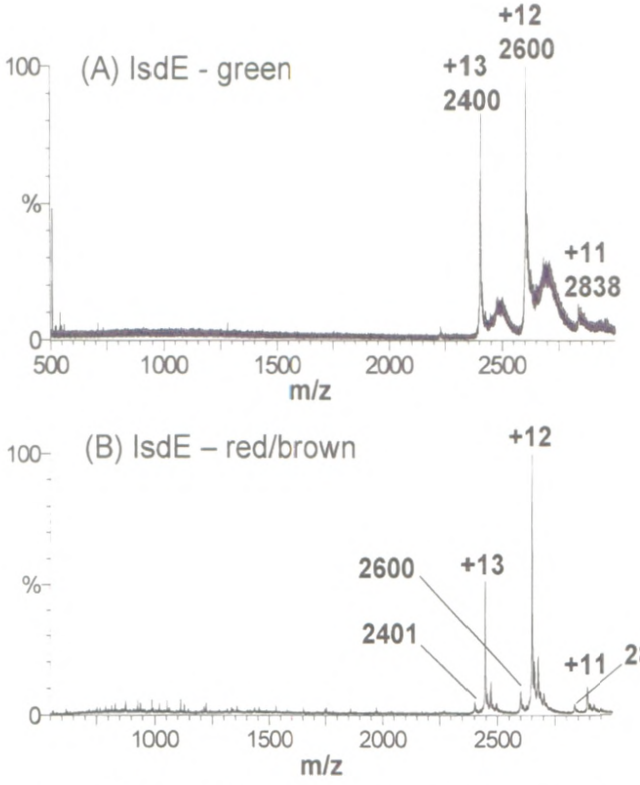

Figure 5.8. Charge state spectra of (A) green and (B) reddish-brown (B) samples of rIsdE.

5.3.3 rIsdE mutational analysis

The computer generated model of IsdE presented in Figure 5.2 highlights several potential heme binding amino acid residues. Tyrosine 61 (Y61), tyrosine 187 (Y187), tyrosine 261 (Y261), and histidine 229 (H229) surround the central pocket of the bilobar IsdE structure and, therefore, appeared to be the best candidates for amino acids involved in direct heme-iron coordination. Individual point mutations were introduced, replacing the native residue with alanine, so that their functions could be examined. For all of the tyrosine residues listed above, mutation did not significantly alter the results compared to those of native rIsdE. For example, the charge state spectrum for rIdE Y261A showed that the +12, +13 charge states still dominated (panels A and B of Figure 5.9), indicating that the overall fold of the protein was not

affected by the mutation. The ligand binding pattern was also very similar to that of native rIsdE (Figure 5.9C). Overall, the MCD band pattern resembled that of a low-spin ferrous heme (Figure 5.10A), as in native rIsdE. Ligation of cyanide was observed as shown by the appearance of the negative MCD band at 577 nm (Figure 5.10B) and, furthermore, the addition of a reducing agent caused a marked reduction in the B band intensity (Figure 5.10C). Carbon monoxide addition then brought back the B band intensity and produced a splitting of the peaks in the Q band (Figure 5.10D). Similar results were observed for the rIsdE Y61A and Y187A mutants. Collectively, the data suggests that Y61A, Y187, and Y261 do not participate directly in heme binding.

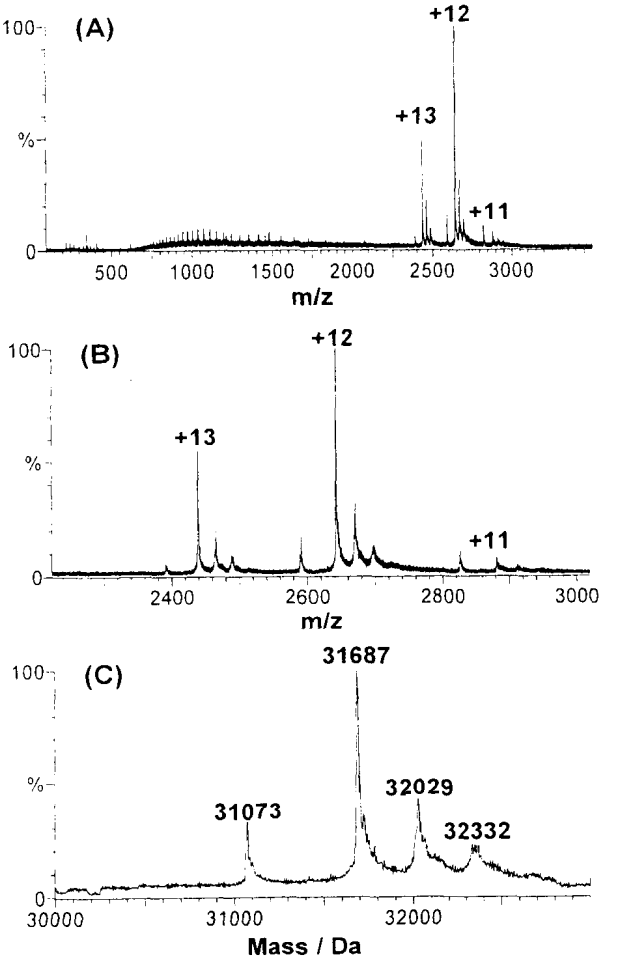

Figure 5.9. Charge state (A, B) and deconvoluted mass specum (C) of rIsdE Y261A.

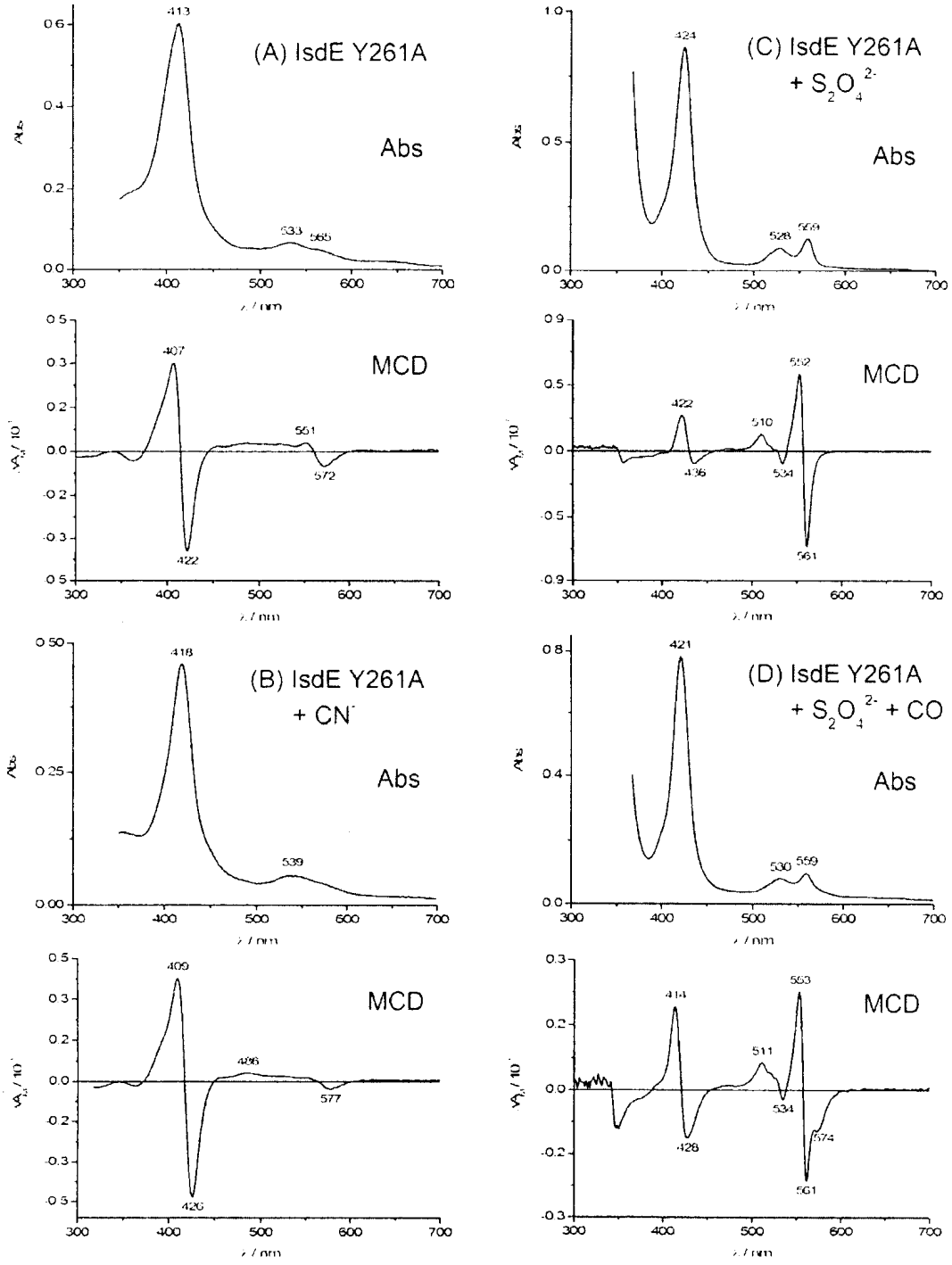

Figure 5.10. Absorption and MCD spectra of rIsdE Y261A. (A) As it is purified from *E. coli*. (B) Following the addition of sodium cyanide. (C) Following the addition of sodium hydrosulfite. (D) Following the addition of sodium hydrosulfite and carbon monoxide.

Mutation of H229 did result in significant changes in both the mass and MCD spectra of the mutant protein. The mass spectrum of rIsdE H229A clearly shows that only heme free (30,995 Da) and single heme-bound protein (31,617 Da) were present (Figure 5.11). The most significant difference to that of the native protein was that no indication of the unidentified peaks observed was observed. Again the +12 and +13 charge states dominated the spectrum, suggesting that the changes observed were due to the lack of an imidazole side group at amino acid 229 and not an alteration in the fold of the protein.

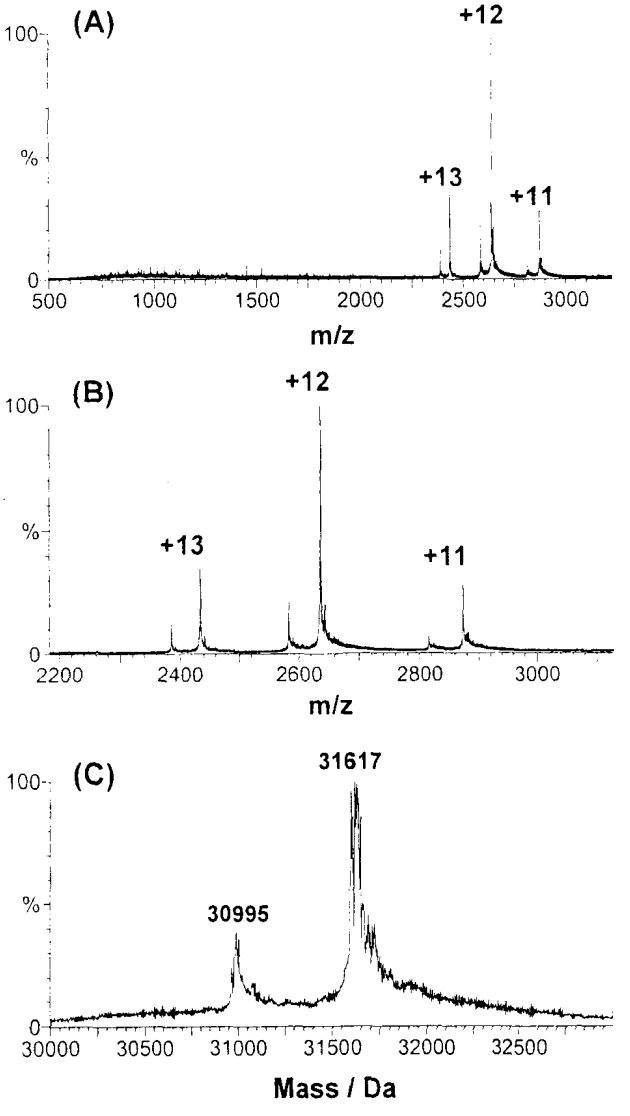

Figure 5.11. Charge state (A and B) and deconvoluted mass spectra (C) of rIsdE H229A.

The MCD spectrum of IsdE H229A closely resembled that of a low-spin ferrous heme (Figure 5.12A). The two A terms, with crossover points at 421 and 576 nm, along with the positive B term at 519 nm fit the band pattern of a low-spin ferrous heme very closely (*8*). Previously it was observed in the MCD spectrum of native rIsdE that cyanide did bind. Following the addition of cyanide in rIsdE H229A, no change was observed (Figure 5.12 B). This suggested that the missing ferric heme in rIsdE H229A bound cyanide and not the low-spin ferrous heme that remained. The addition of a reducing agent did produce minor changes, however, these were most likely due to some ferric heme contamination (Figure 5.12C). Overall, the band patterns remained in close agreement to that of a low-spin ferrous heme. Following the addition of CO, no change was observed (Figure 5.12D). It is interesting to note that all rIsdE mutants containing the H229A mutation did not give an absorption band at 650 nm. The fact that this band's disappearance coincided with the elimination of the unidentified peak and ferric heme components (as shown in Figure 5.11) suggests that one of these ligands was the source of the 650 nm absorption band. Overall, the data for rIsdE H229A suggest that an unidentified amino acid(s) binds a low-spin ferrous heme, with restricted axial positions, and that H229 is directly involved in binding ferric heme and the unidentified ligand observed in native rIsdE.

The model of rIsdE presented in Figure 5.2 shows that Y61 and H229 may form a slot that a heme molecule could slide into. A rIsdE Y61A/H229A mutant construct was produced to determine if Y61, in fact, played a more important role than was previously thought. The mass spectrum and MCD spectra of rIsdE Y61A/H229A closely resemble those of rIsdE H229A. Only heme-free and single heme-bound rIsdE were observed in the mass spectrum of rIsdE Y61A/H229A (Figure 5.13), and its corresponding MCD spectrum was virtually identical to that of rIsdE H229A (Figure 5.14A). The only difference occurred following the addition of sodium hydrosulfite (Figure 5.14C). In the rIsdE H229A, the 566 nm peak appeared to split into peaks at 552 and 568 nm following addition of the reducing agent. In rIsdE Y61A/H229A, this was not observed.

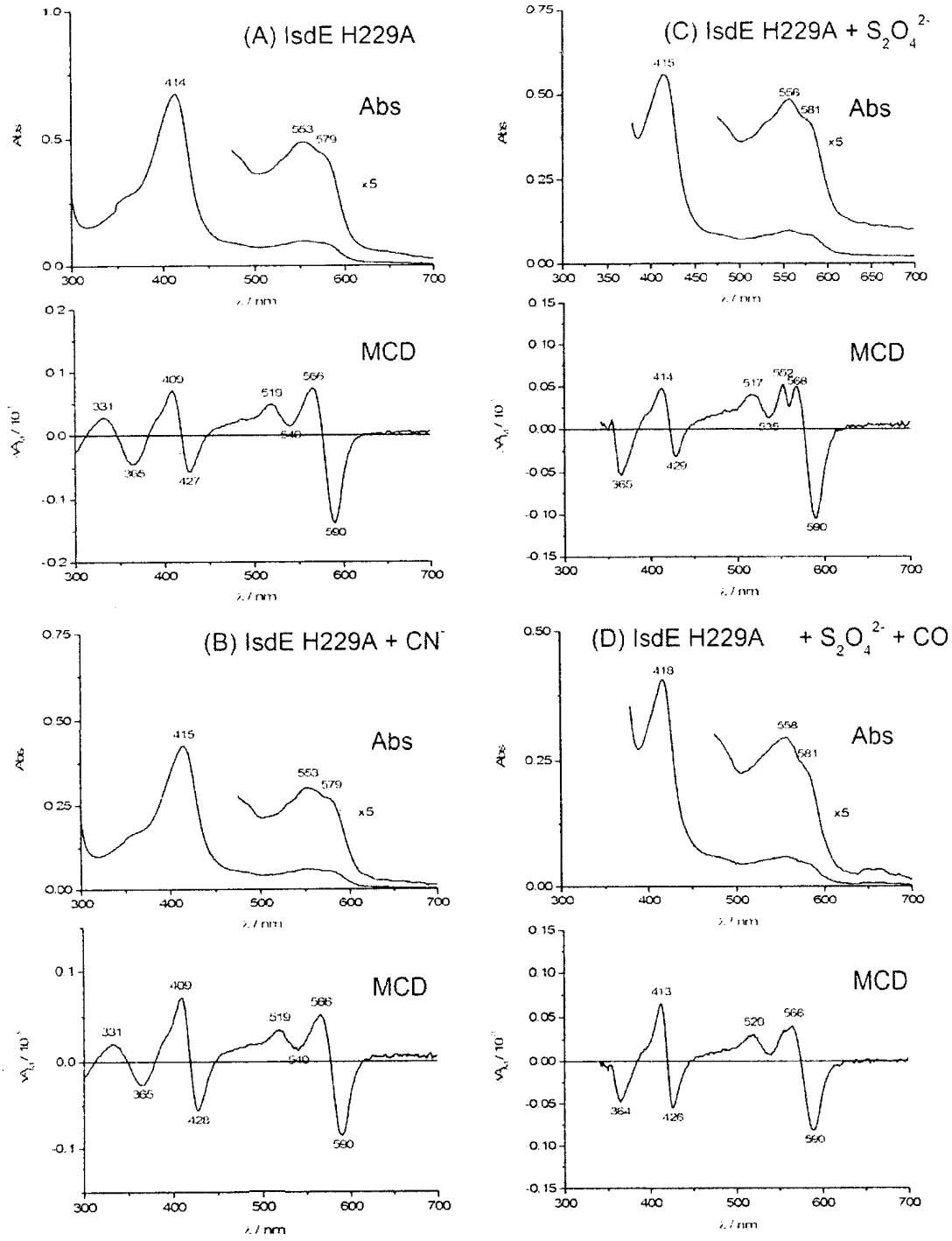

Figure 5.12. Absorption and MCD spectra of rIsdE H229A. (A) As it is purified from *E. coli*. (B) Following the addition of sodium cyanide. (C) Following the addition of sodium hydrosulfite. (D) Following the addition of sodium hydrosulfite and carbon monoxide.

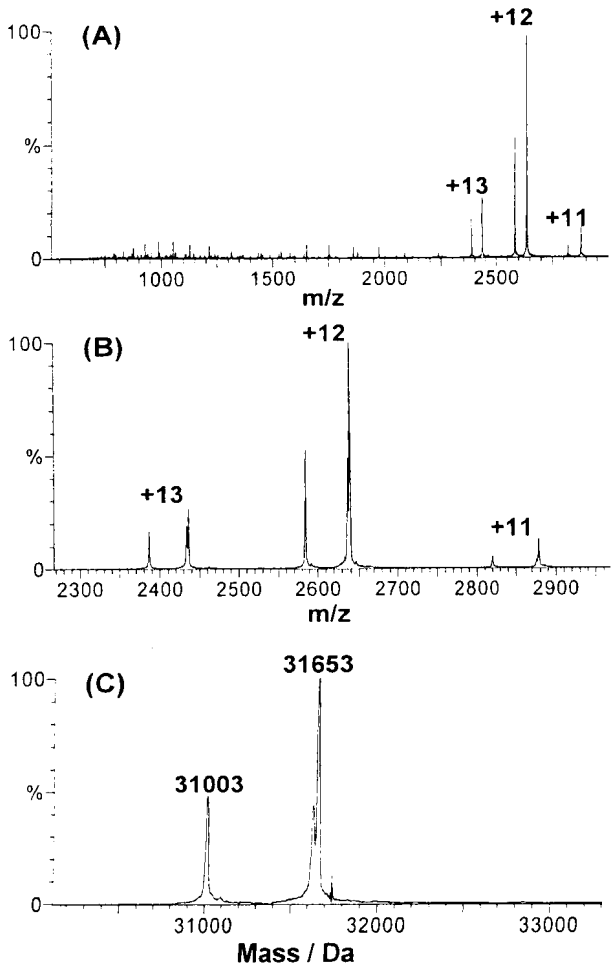

Figure 5.13. Charge state (A and B) and deconvoluted mass spectra of rIsdE Y61A/H229A.

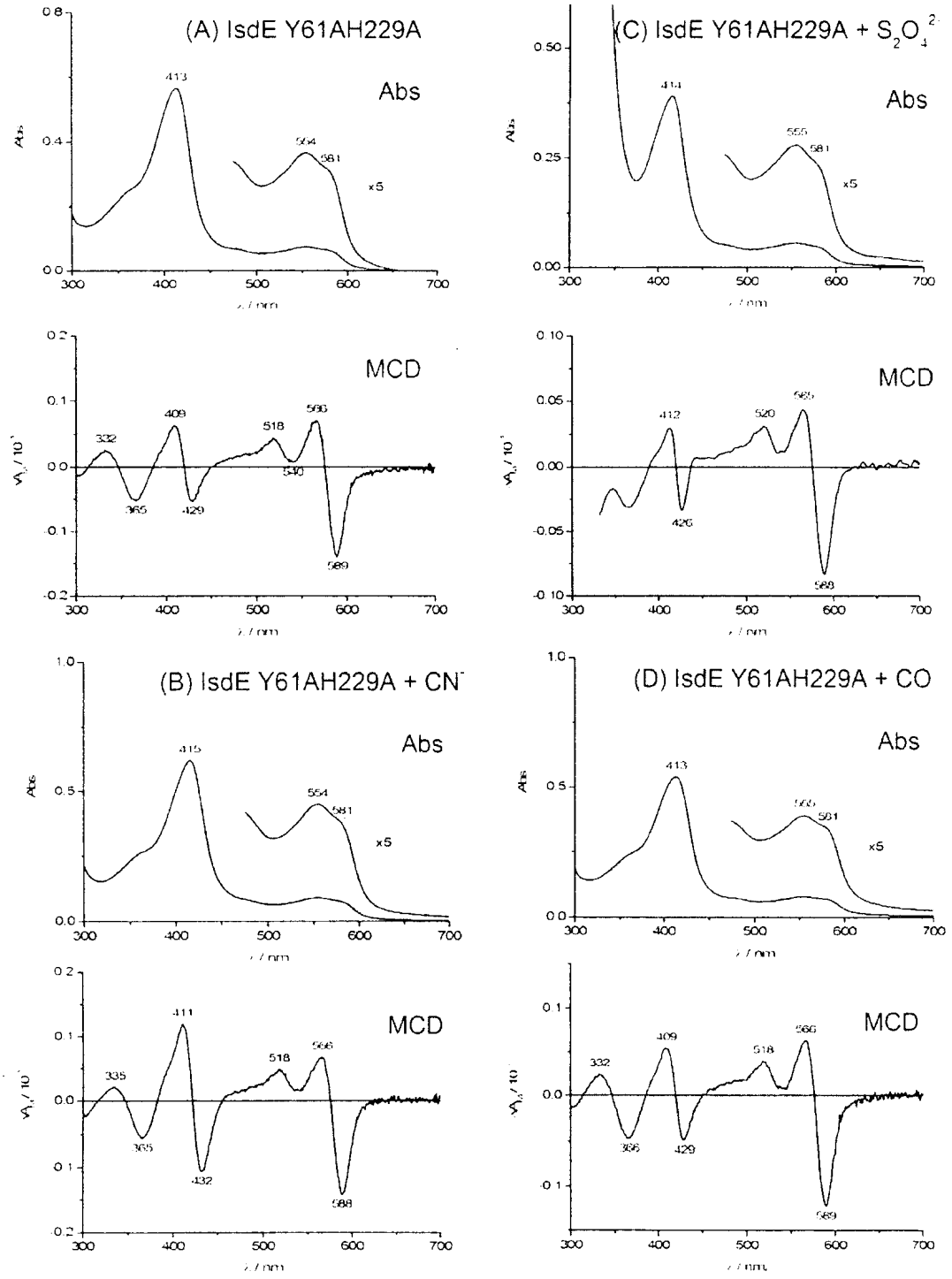

Figure 5.14. Absorption and MCD spectra of rIsdE Y61A/H229A. (A) As it is purified from *E. coli*. (B) Following the addition of sodium cyanide. (C) Following the addition of sodium hydrosulfite. (D) Following the addition of sodium hydrosulfite and carbon monoxide.

The data for rIsdE containing the Y61A and H229A mutations showed that only low-spin ferrous heme was bound. To investigate if ferric-heme could also bind in the ferrous-heme site, a strong oxidizing agent (ferricyanide) was added to samples of native rIsdE and rIsdE Y61A/H229A. Following addition of the oxidizing agent and purification on a G-25 size exclusion column, the charge state spectrum of oxidized rIsdE showed no change (Panels A and B of Figure 5.15). A strong single heme bound peak and a weak double heme bound peak were still present. In the rIsdE Y61A/H229A double mutant a marked reduction in the degree of heme binding was observed. Preceding ferricyanide addition (Figure 5.15C) approximately 60-70% of the protein was bound to heme. This value significantly dropped to less than 10% following oxidation (Figure 5.15D).

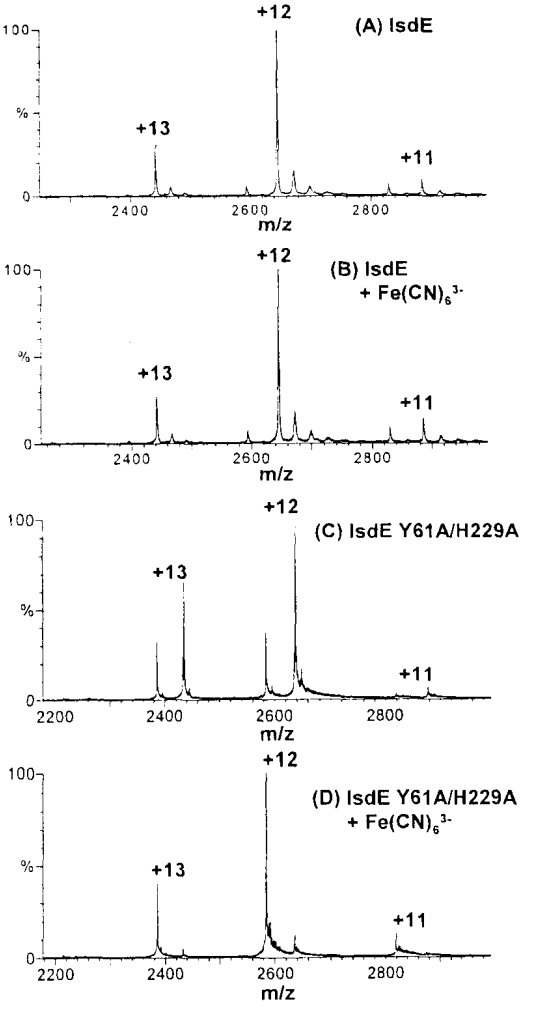

Figure 5.15. Charge state spectra of rIsdE and rIsdE Y61A/H229A preceding (A, C) and following (B, D) the addition of $Fe(CN)_6^{3-}$.

5.4 Discussion

The mass spectrum of rIsdE shows that it is capable of binding a single heme, an unidentified ligand, and possibly a second heme (Figure 5.3B). Mack *et al.* have reported that cell lysates containing over-expressed rIsdE showed signs of low-spin ferric and low-spin ferrous hemes (*2*). The MCD data of purified rIsdE presented in this chapter offers support for this conclusion and, furthermore, helps answer questions regarding the heme binding environments within the protein.

Due to a lack of charge transfer bands, the MCD spectra of low spin ferrous hemes are quite simple to analyze. Three features are observed: two A terms corresponding to the B and Q absorption bands and a positive peak to the blue of the Q band A term (*8*). The MCD spectrum of rIsdE (Figure 5.6A) follows this band pattern with only slight differences, suggesting that the predominant heme species present is low-spin ferrous heme. An abnormally large B:Q A-term intensity ratio and the appearance of overlapping bands in the visible region separate the MCD spectrum of rIsdE from those of other low-spin ferrous heme containing proteins. These anomalies can be explained by the presence of ferric heme. Ferric hemes contain numerous charge transfer bands in the visible region (*8, 15, 16*), which may explain the complex rIsdE MCD spectrum observed in this region. In myoglobin, carbon monoxide binding to ferrous heme gives a 2:1 B:Q band A term intensity ratio in the MCD spectrum (*8*). Oxygen binding gives an approximate 1:3 ratio. In rIsdE, the observed 5:1 intensity ratio is unlike any observed for low-spin ferrous hemes in the literature. Ferric heme A-terms show similar structure to those of low-spin ferrous hemes in the B region. Thus, the overlap between ferrous and ferric signals could result in the increased intensity observed.

The apparent dominance of the low-spin ferrous signal in the MCD spectrum suggests that the majority of heme present in a sample of rIsdE is low spin ferrous, while ferric heme is a minor component. The appearance of a double peak following the addition of sodium dithionite and carbon monoxide suggests that the ferrous heme in rIsdE is only partially accessible given that vigorous addition of carbon monoxide could not eliminate this feature. This is most likely a result of proximal and distal ligation by amino acid residues of the protein, as would be expected from the presence

of a low-spin ferrous iron. Protein bound ferrous hemes, containing water or an open distal position, show high-spin characteristics, as observed in myoglobin (*8, 13*). If the ferrous heme is coordinated in both the 5^{th} and 6^{th} positions to the protein, whereas ferric heme is only coordinated in one position, ferrous heme would be expected to coordinate tighter and therefore be the major component in rIsdE. H229 most likely coordinates in the proximal position of the ferric hemes. To date, however, the identities of the amino acids coordinating to the ferrous heme remain unknown.

Since the MCD spectrum of rIsdE is dominated by ferrous heme, analysis of the ferric heme becomes more difficult. The presence of ferric heme is hinted towards in the MCD spectrum of rIsdE. Further proof is shown in the MCD spectral changes observed following the addition of ligands (CN^- and CO) and a reducing agent ($Na_2S_2O_4$) (Figure 5.6). Cyanide coordinates much more strongly to ferric heme than to ferrous heme. The appearance of low-spin ferric heme signals following cyanide addition, therefore, suggest that ferric heme was initially present. Confirmation also comes from the changes observed following the addition of sodium hydrosulfite. If only ferrous heme were present, one would expect no change in the MCD spectrum, as in rIsdE Y61A/H229A. This, however, is not the case. The most notable change occurs in the B region of the MCD spectrum. Typical heme MCD spectra are dominated by symmetric A-terms in the B region, except for the case of high-spin ferrous heme (*8, 16-18*). In the case of reduced rIsdE, a very weak band is observed in the B region and a dominant A-term is seen in the Q region. The odd shape of the B band is believed to be a result of overlapping signals in this region. The question then becomes: what two signals would overlap to give the observed result? As seen in rIsdA, low-spin ferrous heme gives a B region A-term with a negative to positive transition with increasing energy. The signal for high-spin ferrous heme in this region is flipped, giving a positive to negative transition with increasing energy. This feature is exclusive to high-spin ferrous heme. If both high- and low-spin ferrous hemes were present, the overlap of their signals could cancel out their individual intensity and give the observed band in the MCD spectrum of reduced rIsdE. The model then becomes quite clear. The original ferric heme in rIsdE is reduced upon addition of sodium hydrosulfite, forming a high-spin ferrous heme. The low-spin ferrous heme, originally present in rIsdE, is

unaffected by the reducing agent and, thus, the signals of the two distinct heme molecules overlap to give the observed result. Cyanide addition was shown to coordinate the ferric heme, so when reduced to ferrous, coordination by a small ferrous binding ligand would still be expected to occur. Indeed, the addition of carbon monoxide to a reduced solution of rIsdE produces an MCD spectrum characteristic of low-spin ferrous heme (Figure 5.6D). The return of the intensity in the B region shows this. Thus, the high-spin ferrous heme present in reduced rIsdE, binds carbon monoxide, producing the low-spin ferrous state. The MCD signals from this species then overlap with those of the other low-spin ferrous heme, originally present, to give the observed spectrum. The overlapping signals observed in the Q region (as shown by the peaks at 562 and 572 nm) are believed to arise from the incomplete ligation of carbon monoxide.

The MCD spectrum of rIsdE (Figure 5.6A) suggests that ferric heme is only a minor component. In contrast, the intensity of the 572 nm peak relative to the 562 nm peak observed in the reduced, carbonmonoxy-rIsdE MCD spectrum (Figure 5.6D) suggests that the hemes are in comparable concentrations. This disagreement could be explained by the reduction of the intensity of the 562 nm peak by the positive portion of the band giving rise to the 572 nm negative band, so in fact, the ferric heme concentration may be significantly lower.

The MCD spectrum of rIsdE H229A (Figure 5.12A) clearly shows that the ferrous heme bound in rIsdE is low-spin. Analysis of the spin state of the ferric heme is, however, a more difficult task due to the dominance of the ferrous heme. The band appearing at 650 nm in the absorption spectra of rIsdE (Figure 5.6A) offers evidence of a high-spin ferric state. Heme bands this far to the red are rare, but have been observed in cytochrome c peroxidase (*11*). Yonetani *et al.* have assigned this band to a charge transfer transition in a high-spin ferric heme (*11*). A trend exists between the spin state of ferric hemes and the B:Q band A term intensity ratio. The more low spin character the heme iron possesses, the larger the ratio (*8*). Since the MCD spectrum of rIsdE is dominated by low-spin ferrous heme, ferric heme appears to be a minor component. For a minor ferric heme component to exert an influence in the B region it seems as though an intermediate-low spin ferric heme must be present. However, the possibility of having a larger ferric heme component, than as indicated by the rIsdE MCD

spectrum, makes the assignment of the ferric heme spin state difficult. By identifying the ferrous heme binding amino acid(s) and introducing mutations at those sites, the production of pure ferric-heme rIsdE would become possible. The assignment of the ferric heme spin state would then become trivial through MCD analysis.

The 650 nm peak appearing in the rIsdE absorption spectrum (Figure 5.6A) may arise from a high-spin ferric heme, however, bands in this region have also been observed for the products of PPIX photo-oxidation (*9, 10*). A third possibility is that the 650 nm band represents an electronic transition involving the unknown ligand. The MCD data of rIsdE shows that cyanide coordination to ferric heme does occur. As shown in cytochrome c peroxidase, ligation of cyanide to a high-spin ferric heme completely wipes out the 650 nm band (*11*). Its persistence in all of the rIsdE MCD spectra presented in Figure 5.6 suggests that high spin ferric heme is not the cause. For all of the rIsdE mass spectra recorded, peaks corresponding to PPIX (mass 562.7 Da) or bilirubin (mass 584.7 Da) (free in solution or bound to rIsdE) have never been observed. Although a 650 nm band could arise from photoxidation of PPIX, it does not appear to be the case in rIsdE. Support for the third proposal comes from the rIsdE H229A mutant absorption and mass spectral data. Elimination of H229 results in the inability of rIsdE to bind the unidentified ligand and possibly a second heme (ferric). This coincides with the elimination of the 650 nm band, as shown in Figure 5.12. This offers evidence that the unknown ligand causes the observed absorption at 650 nm. It could be argued that it arises from the ferric heme, since it too is absent, as shown by the rIsdE H229A MCD spectrum (Figure 5.12A) But, as previously mentioned, the persistence of this band following cyanide addition negates this possibility. Identification of the unknown ligand would help resolve this issue, however, future work is required to do so.

The theoretical model of rIsdE shows that H229 is located at the outer portion of the proposed heme binding pocket (Figure 5.2). Since mutation of this residue eliminates ferric heme binding, it can be concluded that H229 binds ferric heme near the edge of the heme binding pocket. This location would leave bound heme relatively exposed to the environment, which helps to explain the observed ligation of cyanide and carbon monoxide (when reduced). The ferrous heme, on the other hand appears, to be

buried deeper within the pocket, where it would be more concealed. As such, the inability to ligate the ferrous heme is not surprising.

The results indicate that both ferric and ferrous heme can coordinate in the rIsdE heme binding site. Coordination of ferric heme to the rIsdE containing the H229A mutation, however, does not occur. The charge state spectra of rIsdE shown in Figure 5.15 show that following the addition of an oxidizing agent, no change is observed. However, the charge state spectra of rIsdE Y61A/H229A show that heme binding is greatly reduced following the addition of ferricyanide. This result illustrates two points. Firstly, without H229 rIsdE cannot coordinate ferric heme. Secondly, the results support the conclusion that the ferrous heme is buried deep within the pocket and that the ferric heme is exposed. The presence of the unknown ligand appears to restrict access to the ferrous heme, preventing its oxidation.

When examining the data for rIsdA, rIsdC, and rIsdE, there are several common themes. One is the ability of each protein to bind heme. The other is the presence of a second ligand of approximately 300-320 Da in mass. This suggests that the Isd proteins are capable of binding and perhaps transporting a ligand other than heme, or that this molecule plays some role in the transport mechanism. Due to the multiple purification steps preceding mass spectral analysis, it is unlikely that any compound not bound to the protein would still be present. The mass spectrum of rIsdE at low pH (unfolded) clearly shows that only ligand-free protein is present, providing strong evidence that these unidentified peaks in the mass spectrum do not arise from a slightly heavier protein (this has been known to occur from imperfect cleavage, as seen in rIsdA). A protein heavier by 320 Da would be distinguishable from the charge states of rIsdE at pH 2.3. For example, rIsdE in the +22 charge state is observed at 1418 m/z. If present, a protein heavier by 320 Da would be observed at approximately 1430 m/z, however, no signal is observed in this region (Figure 5.16). Isolation and identification of this unknown ligand, would help to confirm its role in the Isd system.

In summary, rIsdE can bind both ferric- (spin state unknown) and low spin ferrous-hemes, and an unidentified ligand of approximately 320 Da. The ferric heme is held near the edge of the heme binding pocket by H229, and is accessible to small ligands. The ferrous heme is located deeper within the heme binding pocket and is

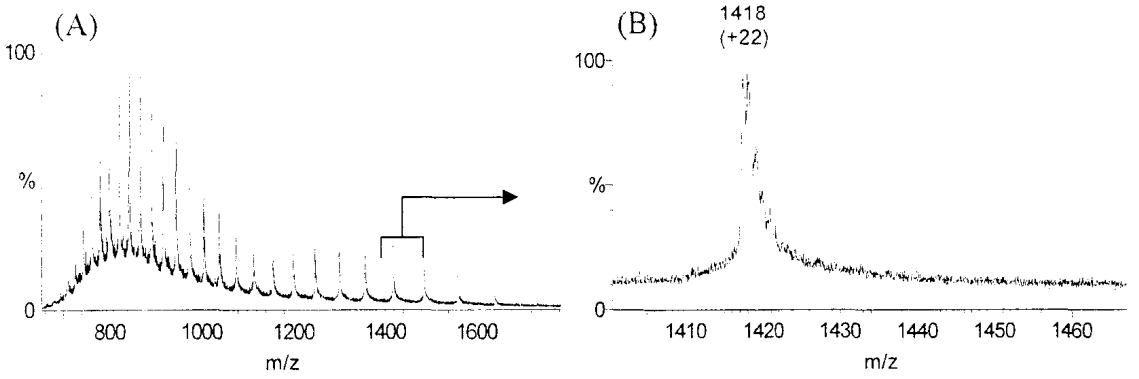

Figure 5.16. Charge state spectra of rIsdE at pH 2.3. (A) the entire scan range and (B) magnification of the area around the +22 charge state.

partially accessible to small ligands. The ferrous heme binding amino acid(s) and the spin state of the ferric heme require future work to decipher.

5.5 References

1. Mazmanian, S. K., Skarr, E. P., Gaspar, A. H., Humayun, M., Gornicki., P., Jelenska, J., Joachmiak, A., Missiakas, D. M., and Schneewind, O. (2003) Passage of heme-iron across the envelope of *Staphylococcus aureus*, *Science 299*, 906-909.
2. Mack, J., Vermeiren, C., Heinrichs, D. E., and Stillman, M. J. (2004) In vivo heme scavenging by *Staphylococcus aureus* IsdC and IsdE proteins, *Biochem. Biophys. Res. Comm. 320*, 781-788.
3. Carter, D. M., Miousse, I. R., Gagnon, J. N., Martinez, E., Clements, A., Lee, J., Hancock, M. A., Gagnon, H., Pawelek, P. D., and Coulton, J. W. (2006) Interactions between TonB from *Escherichia coli* and the periplasmic protein FhuD, *J. Biol. Chem. 281*, 35413-35424.
4. Skaar, E. P., and Schneewind, O. (2004) Iron-regulated surface determinant (Isd) of *Staphylococcus aureus*: stealing iron from heme, *Microb. Infect. 6*, 390-397.
5. Koster, W., and Braun, V. (1990) Iron (III) hydroxamate transport into *Escherichia coli*. Substrate binding to the periplasmic FhuD protein, *J. Biol. Chem. 265*, 21407-21410.
6. Cunsolo, V., Foti, S., Rosa, C. L., Saletti, R., Canters, G. W., and Verbeet, M. P. (2003) Monitoring of unfolding of metallo-proteins by electrospray ionization mass spectrometry, *J. Mass Spec. 38*, 502-509.
7. Konnermann, L., and Douglas, D. J. (1997) Acid-induced unfolding of cytochrome c at different methanol concentrations: Electrospray ionization mass spectrometry specifically monitors changes in the tertiary structure, *Biochemistry 36*, 12296-12302.
8. Vickery, L., Nozawa, T., and Sauer, K. (1976) Magnetic circular dichroism studies of myoglobin complexes. Correlations with heme spin state and axial ligation, *J. Am. Chem. Soc. 98*, 343-350.
9. Pluym, M., Vermeiren, C. L., Mack, J., Heinrichs, D. E., and Stillman, M. J. (2007) Protoporphyrin IX and heme binding properties of *Staphylococcus aureus* IsdC, *J. of Porphyrins and Phthalocyanines*. In press.

10. Ericson, M. B., Grapengiesser, S., Gudmundson, F., Wennberg, A.-M., Larko, O., Moan, J., and Rosen, A. (2003) A spectroscopic study of the photobleaching of protoporphyrin IX in solution, *Las. Med. Sci. 18*, 56-62.

11. Yonetani, T., Wilson, D. F., and Seamonds, B. (1966) Studies on cytochrome c peroxidase, *J. Biol. Chem. 241*, 5347-5352.

12. Housecroft, C. E., and Sharpe, A. G. (2005) *Inorganic chemistry*, Vol. 2, Pearson Education Limited, Essex, England.

13. Pluym, M. (2005) Characterizing the heme binding properties of Staphylococcus aureus iron-regulated surface determinant protein A., in *Chemistry* University of Western Ontario, London.

14. Greenberg, A. J., Bossenmaier, I., and Schwartz, S. (1971) Green Jaundice, *Dig. dis. sci. 16*, 873-880.

15. Browett, W. R., and Stillman, M. J. (1984) Temperature dependence in the absorption spectra of beef liver catalase, *Biophys. Chem. 19*, 311-320.

16. Browett, W. R., and Stillman, M. J. (1979) Magnetic circular dichroism studies of bovine liver catalase, *Biochim. Biophys. Acta. 577*, 291-306.

17. Sutherland, J. C. (1980) Magnetic circular dichroism of biological molecules, *Ann. Rev. Biophys. Bioeng. 9*, 293-326.

18. Springall, J., Stillman, M. J., and Thomson, A. J. (1976) Low temperature magnetic circular dichroism spectra of met- and myoglobin derivatives, *Biochim. Biophys. Acta. 453*, 494-501.

Chapter 6: Conclusions

6.1 Summary and Conclusions

S. aureus is only one among many multidrug resistant pathogens that are causing worldwide health and economic crises. Recent examples, such as the 2007 outbreaks of *Mycobacterium tuberculosis* in Russia *(1)* and *Clostridium difficile* in Mississauga, Ontario *(2)*, highlight our vulnerability to these antibiotic resistant "superbugs." In order to combat these threats, innovative new treatments need to be devised. These could include direct attack upon the organism itself, and thereby destroying the bacterial cell, or alternatively, by using approaches that hinder bacterial growth. Slowed growth would then allow the host's immune system to mount an attack on the invading pathogen and destroy it. The latter is the drive behind investigating the mechanism by which the Isd system serves to transport heme-iron into growing *S. aureus* cells. It has been shown that disruption of the Isd system, through gene knockout studies, greatly hinders bacterial growth in environments low in free iron (*1, 2*). If the overall system can be compromised through the use of some pharmaceutical agent, the lethality of *S. aureus* infection would be greatly reduced. However, before this can be accomplished, a detailed understanding of the Isd heme binding properties and overall heme transport mechanism is required.

Figure 6.1 provides a summary of the information currently available on the Isd proteins from both the literature (IsdB, HarA/IsdH, and IsdA) (*1, 3-8*) and this thesis (IsdA, IsdC, and IsdE). In particular it highlights the changes experienced by heme molecules as they are shuttled into the bacterial cytoplasm. The data presented in this thesis can now be added to the proposed Isd heme transport mechanism outline in section 1.3.

Both ferric and ferrous hemes were shown to bind to rIsdA and rIsdC so it appears that both ferric and ferrous heme could be scavenged by *S. aureus* from the direct environment. The experiments carried out in this thesis were performed under aerobic conditions, so it is not surprising that only ferric heme was observed for both rIsdA and rIsdC, given that heme is relatively exposed when bound.

The surface proteins then transfer the heme to IsdC through an unknown mechanism. An increased affinity for heme in IsdC could promote this proposed transfer, a hypothesis which could be investigated through determination of the heme binding

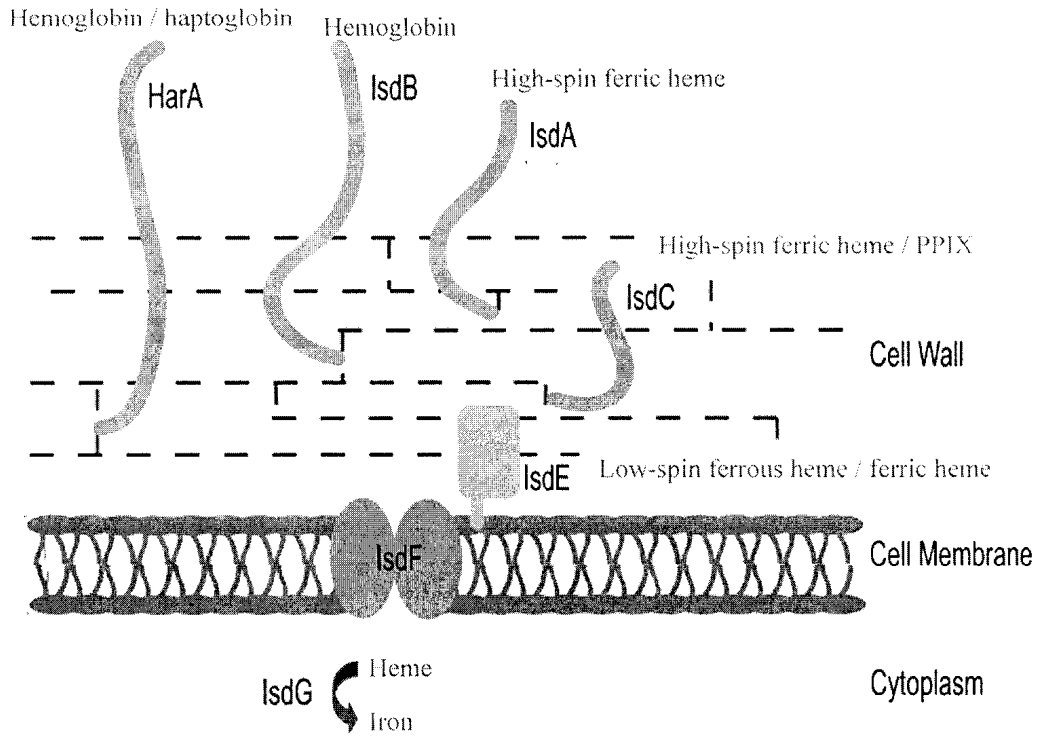

Figure 6.1. Overview of the Isd heme scavenging system highlighting the changes scavenged heme molecules experience at each stage.

constants for each of the proteins. Once the heme reaches the bacterial cell membrane, IsdE is believed to perform its function. The presence of ferrous heme in rIsdE, despite being analyzed in an aerobic (oxidizing) environment, suggests that the formation or existence of the 2+ oxidation state of iron plays some meaningful role. The fact that ferric heme did not bind to the ferrous heme binding site offers support that ferric heme may be reduced before transport across the cell membrane occurs. Ferric iron is extremely insoluble in aqueous solution at neutral pH and, conversely, ferrous iron is quite soluble. Upon cleavage of the PPIX ring by IsdG, iron is released into the bacterial cytoplasm, an aqueous environment. A reduction mechanism at some point along the pathway (intra- or extra-cellular) would, therefore, be expected so that ferric iron does not precipitate within the bacterial cell. Such mechanisms are known to occur in mammals following red blood cell turnover. Identification of the unknown ligand that was observed is both IsdC and IsdE may help answer this question. It is interesting to note that glutathione (Figure 6.2), a biological reducing agent, has a mass of 307 Da, very close to the mass of the unidentified peaks observed in rIsdC and rIsdE. Glutathione has

been shown to participate in the extra-cellular reduction of insoluble ferric iron to the soluble ferrous form (at neutral pH) in an iron transport system found in zoopathogenic fungi (*9*).

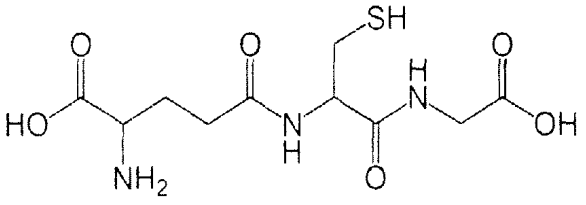

Figure 6.2. Structure of glutathione.

6.2 Future work

The heme binding characteristics of rIsdA, rIsdC, and rIsdE have now been characterized. A few grey areas, however, still exist. The spin state of the ferric heme in IsdE, the IsdE ferrous heme binding amino acid(s), and the heme binding constants for the Isd proteins still remain unknown. The type of studies performed throughout this thesis can also be directed towards the remaining Isd proteins; IsdB, IsdH/HarA, IsdD, and IsdF. To date, very little is known of the heme binding properties of these proteins.

Following heme binding characterization of the Isd proteins, investigations into the heme transport mechanism become more feasible. Depending on which Isd protein heme molecules are bound to, characteristic spectroscopic signatures are given, whether they are an absorption or MCD band. Therefore, a transfer from IsdC to IsdE, for example, could be monitored through the use of absorption or MCD spectroscopy. Alternatively, mass spectrometry could be used to monitor the rate of heme transfer between the Isd proteins. Furthermore, through charge state analysis, any major conformational changes that occur in heme transfer reactions could be studied.

The identity of the unknown ligand in rIsdC and rIsdE also warrants further investigation. The possibility that glutathione binds to the Isd proteins suggests an extra-cellular reduction of heme occurs. This opens the door to a large number of experiments involving the heme reduction mechanism along the Isd pathway.

Due to their recent discovery (in 2003) very little is known of the Isd heme-scavenging system. This leaves many opportunities open to those who wish to study specific aspects of the system. Furthermore, studies involving the inhibition of the Isd system are very appealing due to the public interest in finding alternatives to antibiotics in treating pathogenic bacterial infections.

6.3 References

1. Mazmanian, S. K., Skaar, E. P., Gaspar, A. H., Humayun, M., Gornicki., P., Jelenska, J., Joachmiak, A., Missiakas, D. M., and Schneewind, O. (2003) Passage of heme-iron across the envelope of *Staphylococcus aureus*, *Science 299*, 906-909.
2. Mazmanian, S. K., Ton-That, H., Su, K., and Schneewind, O. (2002) An iron-regulated sortase anchors a class of surface protein during *Staphylococcus aureus* pathogenesis, *Proc. Nat. Acad. Sci. U.S.A. 99*, 2293-2298.
3. Torres, V. J., Pishchany, G., Humayun, M., Schneewind, O., and Skaar, E. P. (2006) *Staphylococcus aureus* IsdB is a hemoglobin receptor required for heme iron utilization, *J. Bacteriol. 188*, 8421-8429.
4. Pilpa, R. M., Fadeev, E. A., Villareal, V. A., Wong, M. L., Phillips, M., and Clubb, R. T. (2006) Solution structure of the NEAT domain (NEAr Transporter) domain from IsdH/HarA: The human hemoglobin receptor in *Staphylococcus aureus*, *J. Mol. Biol. 360*, 435-447.
5. Skaar, E. P., Gaspar, A. H., and Schneewind, O. (2005) *Bacillus anthracis* IsdG, a Heme-Degrading Monooxygenase, *J. Bacteriol. 188*, 1071-1080.
6. Pluym, M. (2005) Characterizing the heme binding properties of Staphylococcus aureus iron-regulated surface determinant protein A., in *Chemistry* University of Western Ontario, London.
7. Skaar, E. P., and Schneewind, O. (2004) Iron-regulated surface determinant (Isd) of *Staphylococcus aureus*: stealing iron from heme, *Microb. Infect. 6*, 390-397.
8. Mack, J., Vermeiren, C., Heinrichs, D. E., and Stillman, M. J. (2004) In vivo heme scavenging by *Staphylococcus aureus* IsdC and IsdE proteins, *Biochem. Biophys. Res. Comm. 320*, 781-788.
9. Zarnowski, R., and Woods, J. P. (2005) Glutathione-dependant extracellular ferric reductase activities in dimorphic zoopathogenic fungi, *Microbiology 151*, 2233-2240.